Theses and Dissertations

2015

Characterization of Cryptosporidium parvum oocyst attachment to environmental biofilm surface

Xia Luo
Lehigh University

CHARACTERIZATION OF CRYPTOSPORDIUM PARVUM OOCYST
ATTACHMENT TO ENVIRONMENTAL BIOFILM SURFACE

By

Xia Luo

Presented to the Graduate and Research Committee
of Lehigh University
in Candidacy for the Degree of
Doctor of Philosophy

in
Environmental Engineering

Lehigh University
January 2016

DISSERTATION SIGNATURE SHEET

Approved and recommended for acceptance as a dissertation in partial fulfillment of the requirements for the degree of Doctor of Philosophy.

_____
Date

_____
Dr. Kristen L. Jellison, Dissertation Director

_____
Accepted Date

Committee Members:

_____
Dr. Derick Brown, Chair

_____
Dr. Arup K. Sengupta, Member

_____
Dr. John T. Fox, Member

_____
Dr. Sabrina Jedlicka, External Member

_____
Dr. Bruce R. Hargreaves, External Member

ACKNOWLEDGMENT

With immense pleasure I express my gratitude to my advisor Dr. Kristen L. Jellison for all her technical, moral and financial support throughout my research. She is the true embodiment of a mentor, who is very patient, supportive, knowledgeable, and encouraging. I am truly grateful to her. This thesis would not have come to an end successfully without her support and advice.

I would like to especially thank Dr. Sabrina Jedlicka for helping me in modeling and inspiring me in my research topic over the last three years. I would further like to thank Dr. Derick Brown, Dr. Arup Sengupta, Dr. John Fox, Dr. Sabrina Jedlicka and Dr. Bruce Hargreaves for their enormous help and suggestions as committee members. I am also thankful to the Department of Civil and Environmental Engineering, Lehigh University, for giving me an opportunity to pursue my Ph.D. degree.

I am grateful to work and share my life with decent colleagues whom I call life-time friends: Julie Napotnik, Kyle Doup, Danhong Luo, Natalie Tacka, Jenelle E. Fortunato, Dan Cannistraci, Lynal Albert, Cathy Fletcher and Michelle Fedun. Working with these friends has been a gift and expands the value of work.

Table of Contents

LIST OF TABLES

LIST OF FIGURES

ABSTRACT

Biofilms are communities of microorganisms that form on a solid surface. It has been shown previously that *Cryptosporidium parvum* is able to accumulate and survive in association with bacterial biofilms in aquatic environments. The long-term survival and sudden release of pathogenic microorganisms due to biofilm sloughing may lead to waterborne disease transmission. The fact that biofilms can immobilize *C. parvum* oocysts from the water column poses fundamental questions regarding interactions of oocysts with biofilm surfaces. Consequently, the main objectives of this study were to: 1) investigate the mechanisms that govern *C. parvum* oocyst attachment to environmental biofilms; 2) examine the role of light exposure, water chemistry, and wall shear stress on oocyst attachment to biofilms; and 3) identify *C. parvum* oocysts by scanning electron microscopy (SEM) using an immunogold labeling technique.

Mechanisms of *C. parvum* oocyst attachment to environmental biofilms grown on polycarbonate coupon surfaces were investigated. Biofilms were formed in rotating annular bioreactors using water and biomaterials collected from different streams in northeastern Pennsylvania with different water chemistries under conditions of dark or light exposure. Biofilm physical structure was characterized by optical microscopy for mean biofilm thickness and roughness, and by SEM for characterization of biofilm architecture. A calcium-mediated psudo-second-order kinetic model for *C. parvum* oocyst deposition was developed to derive kinetic parameters, such as total number of oocysts retained on biofilm surfaces at equilibrium and the initial deposition rate constant, based on oocyst deposition efficiency. The pseudo-second-order kinetic model for oocyst

deposition enabled correlation of water chemistry, hydrodynamic shear stress, and biofilm properties with the derived kinetic parameters. On mature environmental biofilm surfaces (150 days old), the adhesion of *C. parvum* oocysts was found to be independent of biofilm characteristics (*e.g.*, dry mass, organic mass, protein content, mean biofilm thickness and roughness), solution chemistry (*e.g.*, conductivity, alkalinity and hardness), and growth conditions (*e.g.*, light or dark). However, in this study, mature biofilms developed in bioreactors with the same hydrodynamic shear stress but with different environmental waters had similar surface roughness, suggesting that the range of the roughness coefficient in our bioreactors may have been too narrow to observe any impacts on oocyst attachment. Calcium was observed to play a significant role in oocyst attachment to biofilms.

In addition to water chemistry and growth conditions, the impact of wall shear stress on oocyst deposition was also investigated. Dense, compact and smooth biofilms formed under high wall shear stress, whereas fluffy, loose and rough biofilms developed under low wall shear stress. The initial attachment rate constant of *C. parvum* oocysts on the biofilm surface was found to increase as a function of wall shear stress, presumably due to enhanced mass transport between oocyst and surface; however, the value dropped when the wall shear exceeded a certain limit. The total number of oocysts retained on the biofilms decreased with increasing wall shear stress, possibly due to the smooth biofilm surface and increased drag force acting on the biofilm surface discouraging oocysts from adhering. Biomaterials collected from different seasons (i.e., summer and winter) resulted in different biofilms with respect to roughness, mean thickness and biomass, however

these differences were not observed to impact the effect of wall shear stress on oocyst deposition kinetics, suggesting that shear stress plays a critical role in oocyst deposition.

Progress was made on the development of an immunogold labeling technique to identify *C. parvum* oocysts in environmental biofilms by SEM. The performance of different fixatives (i.e., formalin, a mixture of paraformaldehyde and glutaraldehyde, and glutaraldehyde), two drying approaches (hexamethyldisilazane (HMDS) and critical point drying (CPD)), four coating materials (iridium, gold, gold palladium, and carbon), and four scanning electron microscopes (Environmental SEM, Hitachi 4300 4300 SEM, Zeiss 1550 1550 SEM, and FIB-SEM) were assessed to find the optimum settings for *C. parvum* oocyst and gold marker visualization. In our study, fixation by glutaraldehyde, dehydration by HMDS, and then coating with iridium was found to effectively preserve the specimen architecture. The best combination of coating, resolution and signal-to-noise ratio for a *C. parvum* oocyst positive specimen in our study was 5 kV beam voltage plus -1.5 kV beam receleration at a working distance of less than 3 nm with 1.7 nm iridium coating imaged with the FIB-SEM.

The overall goal of this study is an increased understanding of oocyst and biofilm interaction mechanisms. Understanding the mechanisms of oocyst attachment to biofilm surfaces, and how environmental conditions and biofilm surface topography influence oocyst-surface interactions, is critical to the development of anti-adhesive surfaces or materials and could enable enhanced removal of oocysts from surface water. Kinetic profiles obtained from this research will also enable more accurate predictions of *C. parvum* oocyst fate and transport in the environment. Additionally, the information

obtained from this work may be used to guide the engineering of biomimetic surfaces for oocyst detection in the environment.

Further research will focus on manufacturing a standardized biomimetic surface which can be used to detect oocysts quantitatively. The impact of factors like temperature and pH, as well as biofilm roughness and composition, will also be further investigated to confirm the oocyst adhesion kinetics obtained from this study. Viability of attached oocysts over time will also be considered in future work.

CHAPER 1

INTRODUCTION

1.1. Background

Cryptosporidium, a protozoan parasite, is considered an important cause of gastrointestinal disease in human patients and in animals worldwide (Ehsan *et al*, 2015) . *C. parvum* is one of the *Cryptosporidium* species most commonly identified to cause human infection (Ruecker *et al*, 2007; Tzipori & Griffiths, 1998). Infection by *C. parvum* due to oral ingestion may lead to cryptosporidiosis with vomiting, abdominal pain and prolonged watery diarrhea in immunodeficient persons, such as the elderly, young children, and AIDS patients, but in healthy individuals, the disease is usually self-limiting with a duration of less than one month (Bruce *et al*, 2000; Teunis, Medema, Kruidenier, & Havelaar, 1997). Outside the host, *C. parvum* exists as an oocyst (4 – 6 μm), i.e., a multilayered wall which protects four infectious sporozoites from a myriad of environmental conditions, including disinfection (Chatterjee *et al*, 2010; Fayer, Speer, & Dubey, 1990; Karaman, Pashley, Bustamante, & Shanker, 1999; Samuelson, Bushkin, Chatterjee, & Robbins, 2013); thus, removal of oocysts from water supplies typically depends on physical treatment processes (Dai & Hozalski, 2002). Harris and Petry (Harris & Petry, 1999) have reported the existence of three distinct layers of the oocyst wall by transmission electron microscopy. The outermost layer is 5-nm thick with variable electron density and sparse filamentous material, mainly composed of acidic glycoprotein, extending outward. Moving inward, there is an approximately 5-nm thick electron transparent space, followed by a 10-nm thick electron dense layer of filamentous

glycoprotein. The innermost layer is a rigid, complex lipid approximately 20-nm thick and somewhat less electron dense.

Due to the potential health threat, a great deal of research in the past decade has been conducted to evaluate the fate and transport of oocysts in the environment. Many of these studies focused on factors that affect oocyst aggregation in water or oocyst adhesion to organic and inorganic surfaces, including pH (Drozd & Schwartzbrod, 1996; Gao & Chorover, 2009), ionic strength (Drozd & Schwartzbrod, 1996; Gao & Chorover, 2009; Yuanyuan Liu, Janjaroen, Kuhlenschmidt, Kuhlenschmidt, & Nguyen, 2009), bivalent and trivalent salts (Iyer, Majumdar, Waskar, & Dagaonkar, 2013), surface functional groups (Butkus, Bays, & Labare, 2003), and adsorption of inorganic and organic matter from solution (Gao, Metge, Ray, Harvey, & Chorover, 2009). The role of biofilms on *C. parvum* oocyst deposition has received a lot of attention recently (Characklis, 1990; Dai & Hozalski, 2002; Searcy, Packman, Atwill, & Harter, 2006; Wolyniak, Hargreaves, & Jellison, 2009, 2010); DiCesare *et al* (DiCesare, Hargreaves, & Jellison, 2012) reported the percent oocyst retention to biofilms collected at three different streams over four different seasons was positively correlated with biofilm roughness because rougher surfaces provide a larger surface area for oocyst attachment and also protect oocysts from hydrodynamic shear.

In addition to physical properties of biofilms, water chemistry and microorganism surface chemistries, including surface charge, surface molecular structure, and hydrophobicity, also play a significant role in oocyst deposition. Multiple studies have shown that oocysts have a neutral or slightly negative surface charge at circumneutral pH (Brush, Walter, Anguish, & Ghiorse, 1998; Dai & Hozalski, 2002; Drozd &

6

Schwartzbrod, 1996), with an isoelectric point between 2 and 3 depending on solution ionic strength (Tufenkji, Dixon, Considine, & Drummond, 2006). Functional groups on the oocyst surface, such as amides, carboxylates, phosphates, and polysaccharides (Gao & Chorover, 2009; Karaman *et al*, 1999), contribute to a polar, charged oocyst surface in typical surface water conditions. Therefore, the destabilization and aggregation of charged oocysts includes compression of the double layer, charge neutralization, precipitate enmeshment, and interparticle bridging (Amirtharajah & O'melia, 1990). Dai and Hozalski (Dai & Hozalski, 2002) used bench-scale rapid filters to evaluate the effects of biofilms and natural organic matter (NOM) on removal of *C. parvum* oocysts and found that calcium improved oocyst aggregation by double layer compression. Iyer *et al* (Iyer *et al*, 2013) reported that the addition of divalent or trivalent salts enhanced aggregation due to the suppression of the surface charge of oocysts, resulting in a decrease in the energy of interaction between oocysts and a decrease in double layer thickness around the oocyts.

Specific effects of divalent ions on oocyst binding to carboxyl groups and NOM surfaces have also been investigated by others. Kalinichev and Kirkpatrick (Kalinichev & Kirkpatrick, 2007) used molecular simulation to explain the affinity of calcium and magnesium to carboxylate groups and suggested that the formation of metal-NOM complexes is strongly dependent on both the charge/radium ratio and the size of the cation. Their studies were confirmed by Janjaroen *et al* (Janjaroen, Liu, Kuhlenschmidt, Kuhlenschmidt, & Nguyen, 2010), who reported that the binding of Ca^{2+} to carboxylate groups leads to cation bridging between these NOM surfaces and enhances *C. parvum* oocyst deposition. In addition, binding of Mg^{2+} with carboxylate groups is likely to

neutralize charges on these NOM surfaces to promote oocyst deposition to NOM. The presence of exposed carboxylate groups on the extrapolymeric substances (EPS) of biofilms (Sutherland, 2001) and the oocyst wall (Gao *et al*, 2009; Karaman *et al*, 1999) appears to allow Ca^{2+} and Mg^{2+} to form inner-sphere and outer-sphere complexes, respectively. Because calcium (R_{Ca}=1.61 Å) is bigger than magnesium (R_{Mg}=0.92 Å), the hydration shell is much more easily released to form the inner-sphere surface complex. De Kerchove and Elimelech (De Kerchove & Elimelech, 2008) also reported a similar interaction between metal cations and carboxyl groups via both experimental and computational molecular modeling.

The abovementioned studies provide an initial understanding of how *C. parvum* oocyst surface chemistry and water chemistry affect the interaction between *C. parvum* oocysts and biofilms. However, further studies are essential in order to identify specific mechanisms of oocyst adhesion to biofilms and to develop a kinetic model of oocyst attachment to biofilms under varying conditions of water chemistry and hydrodynamics.

1.2. Objectives

The main objectives of this study were to:

- Investigate the mechanisms of *C. parvum* oocyst attachment to environmental biofilms (Chapter 2).
- Elucidate the effect of light exposure and water chemistry on the attachment of *C. parvum* oocysts to environmental biofilms (Chapter 2).
- Identify the effect of hydrodynamic shear stress on *C. parvum* oocyst attachment to biofilms (Chapter 3).

- Develop an immunogold labeling technique for identification of *C. parvum* oocysts in biofilms by scanning electron microscopy (Chapter 4).

1.3. References

Amirtharajah, Appiah, & O'melia, Charles R. (1990). Coagulation processes: destabilization, mixing, and flocculation. *MCGRAW-HILL, INC.,(USA). 1194*, 1990.

Bruce, Beau B, Blass, Mitchell A, Blumberg, Henry M, Lennox, Jeffrey L, del Rio, Carlos, & Horsburgh, C Robert. (2000). Risk of *Cryptosporidium* parvum transmission between hospital roommates. *Clinical infectious diseases, 31*(4), 947-950.

Brush, Charles F, Walter, Michael F, Anguish, Lynne J, & Ghiorse, William C. (1998). Influence of pretreatment and experimental conditions on electrophoretic mobility and hydrophobicity of *Cryptosporidium* parvum oocysts. *Applied and Environmental Microbiology, 64*(11), 4439-4445.

Butkus, Michael A, Bays, J Timothy, & Labare, Michael P. (2003). Influence of surface characteristics on the stability of *Cryptosporidium* parvum oocysts. *Applied and environmental microbiology, 69*(7), 3819-3825.

Characklis, WG. (1990). Biofilms: a basis for an interdisciplinary approach. 3–15. WG Characklis and KC Marshall (ed.) Biofilms: Wiley-Interscience, New York.

Chatterjee, Anirban, Banerjee, Sulagna, Steffen, Martin, O'Connor, Roberta M, Ward, Honorine D, Robbins, Phillips W, & Samuelson, John. (2010). Evidence for

mucin-like glycoproteins that tether sporozoites of *Cryptosporidium* parvum to

the inner surface of the oocyst wall. *Eukaryotic cell, 9*(1), 84-96.

Dai, Xiaojun, & Hozalski, Raymond M. (2002). Effect of NOM and biofilm on the

removal of *Cryptosporidium* parvum oocysts in rapid filters. *Water Research,

36*(14), 3523-3532.

De Kerchove, Alexis J, & Elimelech, Menachem. (2008). Calcium and magnesium

cations enhance the adhesion of motile and nonmotile Pseudomonas aeruginosa

on alginate films. *Langmuir, 24*(7), 3392-3399.

DiCesare, EA Wolyniak, Hargreaves, BR, & Jellison, KL. (2012). Biofilm roughness

determines *Cryptosporidium* parvum retention in environmental biofilms. *Applied

and environmental microbiology, 78*(12), 4187-4193.

Drozd, C, & Schwartzbrod, J. (1996). Hydrophobic and electrostatic cell surface

properties of *Cryptosporidium* parvum. *Applied and Environmental Microbiology,

62*(4), 1227-1232.

Ehsan, Amimul, Geurden, Thomas, Casaert, Stijn, Paulussen, Jef, De Coster, Lut,

Schoemaker, Toon, . . . Claerebout, Edwin. (2015). Occurrence and potential

health risk of *Cryptosporidium* and Giardia in different water catchments in

Belgium. *Environmental monitoring and assessment, 187*(2), 1-12.

Fayer, Ronald, Speer, CA, & Dubey, JP. (1990). General biology of *Cryptosporidium*.

Cryptosporidiosis of man and animals., 1-29.

Gao, Xiaodong, & Chorover, Jon. (2009). In-situ monitoring of *Cryptosporidium* parvum

oocyst surface adhesion using ATR-FTIR spectroscopy. *Colloids and Surfaces B:

Biointerfaces, 71*(2), 169-176.

Gao, Xiaodong, Metge, David W, Ray, Chittaranjan, Harvey, Ronald W, & Chorover, Jon. (2009). Surface complexation of carboxylate adheres *Cryptosporidium* parvum Oocysts to the hematite− water interface. *Environmental science & technology, 43*(19), 7423-7429.

Harris, J Robin, & Petry, Franz. (1999). *Cryptosporidium* parvum: structural components of the oocyst wall. *The Journal of parasitology*, 839-849.

Iyer, Venkatesh Shankar, Majumdar, Udayan, Waskar, Morris, & Dagaonkar, Manoj V. (2013). Aggregation kinetics of *Cryptosporidium* parvum oocysts. *Journal of Environmental Chemical Engineering, 1*(3), 504-509.

Janjaroen, Dao, Liu, Yuanyuan, Kuhlenschmidt, Mark S, Kuhlenschmidt, Theresa B, & Nguyen, Thanh H. (2010). Role of divalent cations on deposition of *Cryptosporidium* parvum oocysts on natural organic matter surfaces. *Environmental science & technology, 44*(12), 4519-4524.

Kalinichev, AG, & Kirkpatrick, RJ. (2007). Molecular dynamics simulation of cationic complexation with natural organic matter. *European Journal of Soil Science, 58*(4), 909-917.

Karaman, Marilyn E, Pashley, Richard M, Bustamante, Heriberto, & Shanker, S Raj. (1999). Microelectrophoresis of *Cryptosporidium* parvum oocysts in aqueous solutions of inorganic and surfactant cations. *Colloids and Surfaces A: Physicochemical and Engineering Aspects, 146*(1), 217-225.

Liu, Yuanyuan, Janjaroen, Dao, Kuhlenschmidt, Mark S, Kuhlenschmidt, Theresa B, & Nguyen, Thanh H. (2009). Deposition of *Cryptosporidium* parvum oocysts on

natural organic matter surfaces: microscopic evidence for secondary minimum deposition in a radial stagnation point flow cell. *Langmuir, 25*(3), 1594-1605.

Ruecker, Norma J, Braithwaite, Shannon L, Topp, Edward, Edge, Thomas, Lapen, David R, Wilkes, Graham, . . . Neumann, Norman F. (2007). Tracking host sources of *Cryptosporidium* spp. in raw water for improved health risk assessment. *Applied and environmental microbiology, 73*(12), 3945-3957.

Samuelson, John, Bushkin, G Guy, Chatterjee, Aparajita, & Robbins, Phillips W. (2013). Strategies to discover the structural components of cyst and oocyst walls. *Eukaryotic cell, 12*(12), 1578-1587.

Searcy, Kristin E, Packman, Aaron I, Atwill, Edward R, & Harter, Thomas. (2006). Deposition of *Cryptosporidium* oocysts in streambeds. *Applied and environmental microbiology, 72*(3), 1810-1816.

Sutherland, Ian W. (2001). Biofilm exopolysaccharides: a strong and sticky framework. *Microbiology, 147*(1), 3-9.

Teunis, PFM, Medema, GJ, Kruidenier, L, & Havelaar, AH. (1997). Assessment of the risk of infection by *Cryptosporidium* or Giardia in drinking water from a surface water source. *Water Research, 31*(6), 1333-1346.

Tufenkji, Nathalie, Dixon, David R, Considine, Robert, & Drummond, Calum J. (2006). Multi-scale *Cryptosporidium*/sand interactions in water treatment. *Water research, 40*(18), 3315-3331.

Tzipori, Saul, & Griffiths, Jeffrey K. (1998). Natural history and biology of *Cryptosporidium* parvum. *Adv Parasitol, 40*, 5-36.

Wolyniak, EA, Hargreaves, BR, & Jellison, KL. (2009). Retention and release of

    Cryptosporidium parvum oocysts by experimental biofilms composed of a natural

    stream microbial community. *Applied and environmental microbiology, 75*(13),

    4624-4626.

Wolyniak, EA, Hargreaves, BR, & Jellison, KL. (2010). Seasonal retention and release of

    Cryptosporidium parvum oocysts by environmental biofilms in the laboratory.

    Applied and environmental microbiology, 76(4), 1021-1027.

CHAPTER 2

PSEUDO-SECOND ORDER CALCIUM-MEDIATED *CRYPTOSPORIDIUM PARVUM* OOCYST ATTACHMENT TO ENVIRONMENTAL BIOFILMS

2.1. Abstract

Cryptosporidium parvum oocysts are able to infect a wide range of mammals, including humans, via fecal-oral transmission. The remobilization of biofilm-associated C. parvum oocysts back into the water column by biofilm sloughing or bulk erosion poses a threat to public health and may be responsible for waterborne outbreaks; thus, the investigation of C. parvum attachment mechanisms to biofilms, particularly the physical and chemical factors controlling oocyst attachment to biofilms, is essential to predict the behavior of oocysts in the environment. In our study, biofilms were grown in rotating annular bioreactors using prefiltered stream water (filters passed particles smaller than 0.2 µm) and rock biofilms (filters passed particles smaller than 6 µm retention) until the mean biofilm thickness reached steady-state. Oocyst deposition followed a calcium-mediated pseudo-second-order kinetic model. Kinetic parameters (i.e., initial oocyst deposition rate constant and total number of oocysts adhered to biofilms at equilibrium) from the model were then used to evaluate the impact of biofilm characteristics (including protein, biomass, mean thickness and roughness) and water chemistry (including conductivity and alkalinity) on the attachment of oocysts to biofilms. Oocyst deposition was found to be independent of solution chemistry and biofilm properties; instead, the presence of calcium enhanced oocyst attachment as demonstrated by deposition tests. Calcium was identified as the predominant factor that bridges the carboxylic functional groups on biofilm and oocyst surfaces to cause attachment. The

pseudo-second-order kinetic profile was determined to fit all experimental conditions, regardless of water chemistry and/or lighting conditions.

2.2. Introduction

Cryptosporidium parvum is a protozoan pathogen that can infect a wide range of mammals, including humans, through either direct contact or ingestion of contaminated food and/or water (Donnelly & Stentiford, 1997). It can cause a severe diarrheal disease called cryptosporidiosis, which lasts one to two weeks for immunocompetent people but could be fatal for the elderly, infants or immunocompromised people. Contamination of source water is potentially a major source for massive outbreaks of infection, therefore, developing methods for assessing the levels of *Cryptosporidium* in source waters is of increasing interest to the environmental engineering community.

To facilitate the development of methodology to assess levels of *Cryptosporidium* in source waters, a number of studies have been performed to assess the conditions under which *Cryptosporidium* can be selectively removed and subsequently detected. A wide variety of different surfaces and filter media have been assessed. For example, the attachment of oocysts to different surfaces (i.e., clean glass beads and biofilm-coated glass beads) in the presence of natural organic matter (Dai & Hozalski, 2002), or under different electrolyte concentrations (Iyer *et al*, 2013; Janjaroen *et al*, 2010; Kim, Walker, & Bradford, 2010), has been investigated at length. Multiple studies have shown that oocysts have a neutral or slightly negative surface charge at circumneutral pH (Brush *et al*, 1998; Dai & Hozalski, 2002; Drozd & Schwartzbrod, 1996), with an isoelectric point between $2 - 3$ depending on solution ionic strength (Tufenkji *et al*, 2006). Dai *et al* (Dai & Hozalski, 2002) proposed that applying alum as a coagulant at a proper dosage appears

to effectively neutralize the electrostatic repulsion between oocysts and a negatively

charged surface so as to improve oocysts removal efficiency in the filter bed. Lyer *et al*

(Iyer *et al*, 2013) found the addition of a bivalent or trivalent salt with stirring condition

could promote C. parvum oocyst aggregation due to the suppression of the oocyst surface

charge, causing a decrease in the interaction energy between oocysts, a decline in double

layer thickness around the oocysts, and a significant improvement in the oocyst removal

efficiency from untreated drinking water.

A number of research studies have shown that the presence of biofilms in natural

and engineered systems may facilitate the retention of C. parvum oocysts (Dai &

Hozalski, 2002; Searcy *et al*, 2006; Wolyniak *et al*, 2009, 2010). Biofilms, loosely

described as microbial assemblages in an extracellular polymeric matrix, are known to

form on surfaces in virtually all aquatic ecosystems supporting microbial growth, such as

soil, plants, rock, sediments as well as filter media (Sussman, Denyer, & Gorman, 1993).

Generally, the biofilms are composed of water (85-95% wet weight), exopolysaccharides

(EPS, 1-2% wet weight) (Characklis, 1990), and polypeptide polymers. The extracellular

polymeric substance (EPS) consists of both polysaccharides and proteins which can

anchor bacteria to surfaces (Characklis, 1990). This extensive polymer network has also

been shown to be highly reactive and is capable of selectively binding non-metallic

elements, such as Ca, F, and P (Leme, Koo, Bellato, Bedi, & Cury, 2006; Shiraishi,

Bissett, de Beer, Reimer, & Arp, 2008), or metals (Nelson, Lion, Shuler, & Ghiorse, 1999)

from the environment. Furthermore, functional groups on the EPS and the cell wall of

microorganisms may bind elements and control the interaction between planktonic cells

and biofilms. For example, divalent cations can form bridges between negatively charged

groups on cell surfaces and the material supporting the biofilm, in addition to bridging cell surfaces and EPS (Schmidt & Ahring, 1994). A similar phenomenon may be relevant to *Cryptosporidium* binding to biofilm surfaces.

Biofilm structure has been demonstrated to play a role in *Cryptosporidium* binding efficiency. This structure and biofilm microbial composition may change in relation to nutrient levels (Lawrence *et al*, 2004; Paul Stoodley, Dodds, Boyle, & Lappin-Scott, 1999), dissolved oxygen concentration (Lawrence *et al*, 2004; Yun *et al*, 2006), the presence of light (Romaní *et al*, 2014; Ylla, Borrego, Romaní, & Sabater, 2009), as well as flow regimens (i.e., laminar and turbulent) (Purevdorj, Costerton, & Stoodley, 2002). For example, Stoodley *et al* (Paul Stoodley *et al*, 1999) found that increasing carbon and nitrogen by a factor of 10 increased biofilm thickness, surface coverage and biomass. Ripples grown on initial biofilms disappeared, the cluster and streamers grew larger, and many of them even merged to form a porous structure. In addition, Ylla *et al* (Ylla *et al*, 2009) showed that artificial biofilms grown by simulated river water under light had abundant algal filaments, resembling those of the freshwater algae Stigeoclonium tenue and diatoms such as Achnanthidium minutissimum and Melosira varians. However, biofilms grown in dark conditions revealed mixed bacterial communities comprised of mostly either Actinobacteria and α- and β-proteobacteria. In another study, Li *et al* (Li, Lei, & Lou, 2012) also found that light enhances the production of EPS, resulting in a sticky biofilm. EPS is able to alter the physicochemical characteristics of the surface, including hydrophobicity, charge and polymeric properties (Neu & Marshall, 1990; Rijnaarts, Norde, Bouwer, Lyklema, & Zehnder, 1993); a study from Tsuneda *et al* (Tsuneda, Aikawa, Hayashi, Yuasa, & Hirata, 2003) has shown a positive correlation

between EPS and cell adhesiveness and concluded that the high-molecular-mass polysaccharides in EPS could serve as polyelectrolytes to promote cell adhesion by polymeric interaction. Azeredo and Oliveira (Azeredo, Visser, & Oliveira, 1999) reported that the exopolymer bound to glass and the exopolymer present at the surface of the Sphingomonas paucimoilis bound together to overcome the energy barrier created by the negative charge of both surfaces.

This study examined C. parvum oocyst deposition under two different lighting conditions using biofilms grown from collected environmental biofilm samples. The biofilms were grown on polycarbonate surfaces, in water with variable chemistry (i.e., ionic strength, pH, divalent ions, the presence of nutrients, etc.). Biofilm development was monitored, and upon reaching steady-state thickness, C. parvum oocysts were introduced to determine deposition efficiency. A calcium-mediated, pseudo-second order kinetic profile was determined to fit all conditions, regardless of water chemistry and/or lighting conditions.

2.3. Materials and methods

2.3.1. Bioreactor operation and calculation of shear stress

The bioreactor was comprised of a sterile glass beaker, with a rotating drum which housed 12 removable polycarbonate coupons (Figure 2.1). Biofilms were formed on the surface of polycarbonate coupons (11.2 × 1.1 cm) (Sheffield Plastics Inc., Sheffield, MA, USA). A total of eight bioreactors were run in parallel to determine the effects of water chemistry and illumination on biofilm formation and oocyst retention. Four reactors were

run in a dark box with water collected from four local streams to simulate underground

conditions, whereas the remaining four reactors were run with the same water, but in the

presence of sunlight to simulate conditions of a natural stream.
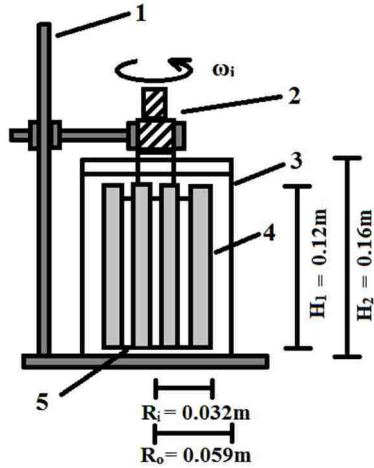
Figure 2. 1. Schematic of the annular rotating bioreactor.

1, clamp stand; 2,1/50 hp AC Dayton gear motor (Model 5VXU1, Dayton Electric

Manufacturing Co., Chicago, IL); 3, 1L glass beaker; 4, polycarbonate coupon; 5, inner

rotational cylinder. R_i and R_o are the radii (m) of the inner and outer cylinder,

respectively; H_1 and H_2 are the height (m) of inner and outer cylinder, respectively

The bioreactor flow was modeled as Taylor-Couette flow between concentric

rotating cylinders, where the inner cylinder is rotating and the outer cylinder is fixed.

Fokoua *et al* (Fokoua, Gabillet, & Colin, 2013) showed that the inner wall shear stress of

the bioreactor was determined according to the viscous torque (G) (Equations 2.1-2.2),

which is a function of the Reynolds number. The Reynolds number of the flow (Re) is

defined as: $R_e = \frac{\omega_i R_i (R_o - R_i)}{\upsilon}$, where ω_i is the angular velocity of the rotating inner

cylinder (rad/s), R_i and R_o are the radius (m) of the inner and outer cylinder, respectively,

and υ is the kinetic viscosity of water (1 x 10^{-6} m^2/s). The wall shear stress at the inner

cylinder (τ_i) was then deduced from the dimensionless torque G: $\tau_i = \frac{\rho\upsilon^2 G}{2\pi R_i^2}$, in which ρ is

the water density (999.97 kg/m^3).

$$G = 1.45 \times \frac{\eta^{1.5}}{(1-\eta)^{1.75}} Re^{1.5} \text{ for } 400 \le Re \le 10000 \qquad \text{Equation 2. 1}$$

$$\eta = \frac{R_i}{R_o} \qquad\qquad\qquad\qquad\qquad\qquad\qquad\qquad \text{Equation 2. 2}$$

Therefore, the shear stress in each reactor can be controlled by either adjusting the

rotational speed or changing the distance between the inner and outer cylinders; in these

experiments, shear stress was controlled by adjusting the rotational speed of the inner

cylinder. Water in each reactor was exposed to air to allow for aerobic microbial growth.

The shear stress in each bioreactor was equal to 0.11 Pa, and the corresponding Reynolds

number was 4478.

The reach-averaged shear stress method was used to estimate the mean bed shear

stress for open-channel flow studies (Babaeyan-Koopaei, Ervine, Carling, & Cao, 2002).

It serves as an index of the total resistance by all frictional influences on the flow

(particle-, bedform-, bar-, and planform-scale effects). The bed shear stress is given as:

$$\tau_0 = \gamma R_h S_f \qquad\qquad\qquad\qquad\qquad\qquad\qquad \text{Equation 2. 3}$$

where: τ_0 = boundary shear stress, lb/ft^2 = 47.88Pa;

γ = specific weight of the fluid, γ = 9,806 N/m^3 (62.4 lb/ft^3);

R_h = hydraulic radius, ft;

S_f = friction slope

The hydraulic radius (R_h) for a rectangular channel (similar to the basin topography of the streams where we collected biomaterial for the bioreactor studies) can be computed as:

$$R_h = \frac{By}{B+2y}$$ **Equation 2. 4**

where B = channel bottom width, ft

y = flow depth, ft

When B >> y, equation 2.4 can be written as

$$R_h = y$$ **Equation 2. 5**

Equation 2.3 can be then computed as

$$\tau_0 = \gamma y S_f$$ **Equation 2. 6**

According to Manning's equation

$$\upsilon = \frac{1.49}{n} R_h^{2/3} S_f^{1/2} = \frac{1.49}{n} y^{2/3} S_f^{1/2}$$ **Equation 2. 7**

where υ = flow rate (ft/sec) and n = Manning's coefficient (dimensionless, n = 0.03 for clean, straight, full stage, no rifts or deep pools) (Te Chow, 1959).

Substituting Equation 2.7 into Equation 6 yields:

$$\tau_0 = \gamma y \left(\frac{\upsilon}{\frac{1.49}{n} y^{\frac{2}{3}}} \right)^2$$ **Equation 2. 8**

These equations assume that 1) the flow is one-dimensional, steady flow; 2) the bed and bank shear are equal; 3) the velocity coefficients are constant over the reach; 4) shear along the water surface is negligible; and 5) there is a small channel slope ($\tan\theta \approx \sin\theta$) in

the derivation of Equation 2.3 (Bruner, 2008; Finnemore & Franzini, 2002; Henderson, 1996). The shear stresses in the four streams of northeastern Pennsylvania from which we collected biomaterials for the bioreactor experiments, computed by Equation 2.8, are shown in Table 2.1

Table 2. 1. Calculated shear stress of four streams

Dataset	N*	Shear stress (Pa)		
		Range	Mean	One standard deviation
Hokenduagua Creek	10	0.036 - 0.22	0.083	0.056
Indian Creek	10	0.0028 - 0.60	0.096	0.2
Little Lehigh River	10	0.0017 - 0.038	0.15	0.15
Monocacy Creek	11	0.073 - 2.79	0.72	0.83

*N is the number of measurements in the stream at the same day.

2.3.2 Development of biofilms and monitoring of biofilm growth

Four stream water types with different characteristics were used in the experiments. Creek water along with the biofilm scrapings from the four streams were collected in the summer and stored as described by (Wolyniak *et al*, 2010). Stream water was filtered to remove particulate matter, and an aliquot of 4 x 10^7 cells of the biofilm culture (from stream rock scrapings) was introduced into each bioreactor. The inner rotating drum with 12 removable coupons was aseptically introduced into the inoculated medium in the bioreactors.

To obtain steady-state growth phase biofilms, a semi-continuous mode of biofilm growth was employed; i.e., water in the bioreactors was removed and replaced with an equal amount of fresh, bacteria-inoculated water every four days. Every eighth day, one to two coupons were retrieved from the inoculated medium for average biofilm thickness measurements using an optical microscope (Nikon ECLIPSE 50i, Melville, NY) (Luo, Jellison, Huynh, & Widmer, 2015), and the drained water was analyzed for water nutrients and chemical parameters, including pH and conductivity (Oakton Ion 510 benchtop meter, Vernon Hills, IL, USA); turbidity (HACH 2100AN turbidimeter, Loveland, CO, USA); hardness (HACH Method 8204); alkalinity (HACH Method 8203); nitrate-N, nitrite-N, and ammonia-N (HACH Method 8171, 8507, and 8155, respectively); phosphorus (HACH Method 8048); and dissolved oxygen (YSI 5000 benchtop meter, YSI Inc., OH, USA). All experiments were carried out in batch mode under aerobic conditions at room temperature.

Two experiments were performed. In the first experiment, the attachment of oocysts to mature biofilms was quantified using bioreactors run with different water

chemistries (from four different streams) and different operating conditions (i.e., dark and natural light). In the follow-up experiment, the impact of calcium and magnesium on oocyst deposition onto environmental biofilms (grown in bioreactors using water and scraped biomaterials from Monocacy Creek, PA) was further investigated.

2.3.3 Spiking test

Once biofilms reached steady-state thickness, one of the twelve coupons in each bioreactor was removed and cut into small pieces (~2.5 × 1.1 cm each) for scanning electron microscopy (SEM) prior to spiking. The coupon removed from the bioreactor was replaced with a sterile clean coupon to maintain the shear condition, and the inner rotating cylinder containing all 12 coupons was removed and inserted into a clean beaker (outer cylinder) for the spiking tests. Oocysts (10^5) were spiked into 700 mL prefiltered stream water (0.2 μm retention size) in each bioreactor. At each time point (ranging from 0.083h to 96h), five (5) ml spiked water was removed from the reactor for immunomagnetic separation (IMS) to purify oocysts and an immunofluorescent assay (IFA) to quantify the number of oocysts remaining suspended in water. An equal volume of fresh water was added back to each bioreactor to maintain the reactor volume. The total number of oocysts attached to the entire bioreactor surface (i.e., coupons and walls of the reactor) was calculated by subtracting the number of oocysts remaining suspended in the bioreactor at different time points from the total number of oocysts (i.e., 10^5 oocysts) added to the bioreactor.

2.3.4 Determination of the effects of calcium and magnesium on oocyst retention

In the follow-up experiment, ion exchange was coupled with the spiking test to further assess the role of calcium and magnesium on oocyst attachment to biofilms (Figure 2.2). Calcium and magnesium were removed from Monocacy Creek water by ion exchange, oocysts were spiked into this treated water in the bioreactor (as described previously), and then calcium and magnesium were added back to each bioreactor after 96 h in concentrations equal to the original respective cation concentrations in Monocacy Creek. Slightly different from the first experiment, before the spiking test, one of the twelve coupons in each bioreactor was removed for IMS as a control, and a sterile clean coupon was then put back into each bioreactor to maintain the shear condition. Additionally, at each sampling point (ranging from 0.5 – 96 h), 5 mL of spiked water was sampled and the number of oocysts suspended in the water was enumerated only by IFA (i.e., no IMS was performed) due to the low turbidity in the spiked water (i.e., < 4 NTU).
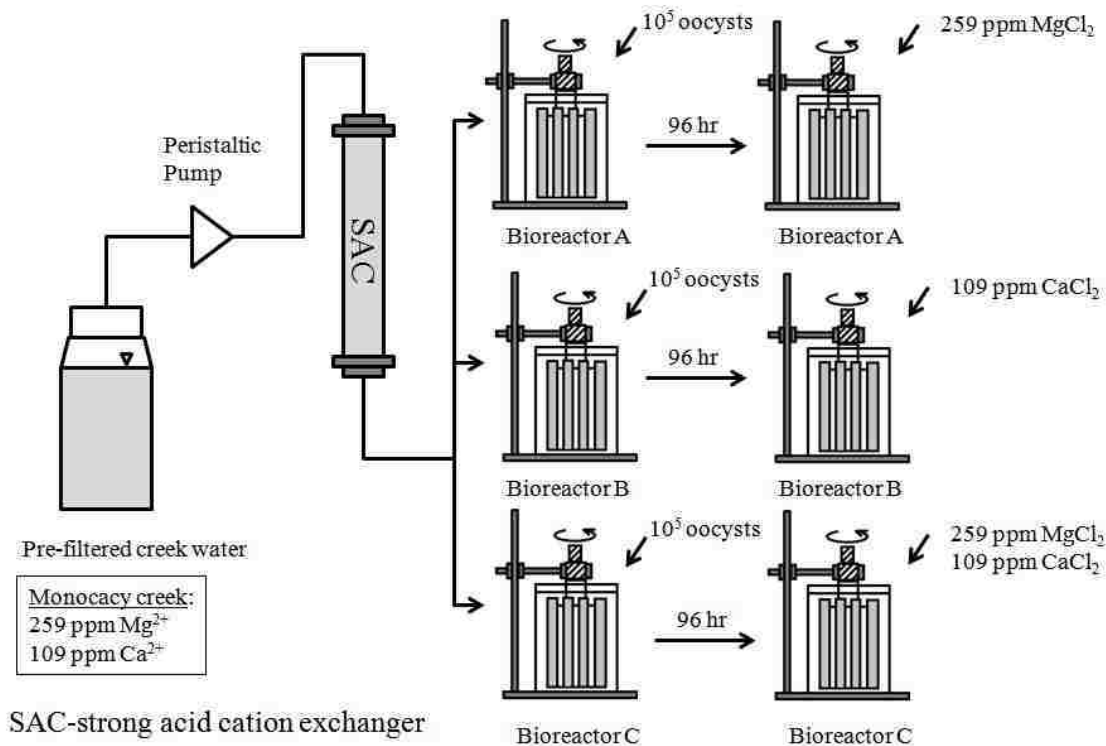
Figure 2. 2. Schematic diagram of coupling ion exchange with the spiking test.

2.3.5 Preparation and use of ion exchange columns as pretreatment method

For investigation of the impact of calcium and magnesium on oocyst deposition, cation exchange was used to remove these ions from the source water, using a strong acid cation (SAC) resin (Purolite C145™, Purolite Co., Bala Cynwyd, PA). SAC resins operate over a very wide pH range because the sulfonate group, being strongly acidic, is ionized throughout the pH range (1 to 14). Equation 2.9 is the standard ion exchange softening reaction in which sodium ions are exchanged for the hardness ions Ca^{2+} and Mg^{2+}.

$$2\overline{RSO_3^-Na^+} + \left.\begin{matrix}Ca\\Mg\end{matrix}\right\}\left\{\begin{matrix}(HCO_3)_2\\SO_4\\Cl_2\end{matrix}\right. \leftrightarrow \overline{(RSO_3^-)_2}\left\{\begin{matrix}Ca^{2+}\\Mg^{2+}\end{matrix}\right. + Na_2\left\{\begin{matrix}(HCO_3)_2\\SO_4\\Cl_2\end{matrix}\right. \qquad \textbf{Equation 2. 9}$$
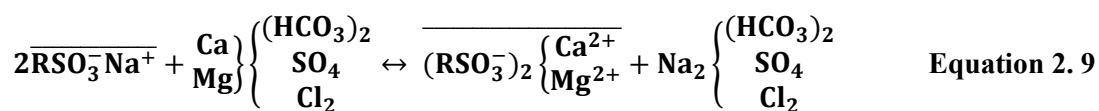
In these reactions, R denotes the resin matrix, and the overbar indicates the solid (resin) phase. To ensure consistent volume measurements, the resin was settled for one hour before processing. The ion exchange resins were dosed volumetrically by measuring the volume of wet settled resin using a graduated cylinder. The system was operated at room temperature with a feed rate of 10 mL/min, corresponding to an empty bed contact time (EBCT) of 8 min, until complete breakthrough of those two ions had occurred. Before use, 1 M NaCl was passed through the polypropylene column packed with SAC resin, and rinsed with deionized water to ensure the resin was in sodium form.

2.3.6 Analysis of water

Cations, including calcium, magnesium, and sodium, were analyzed using an atomic absorption spectrophotometer (Spech AA-200, Varian, Victoria, Australia) according to the manufacturer's instructions. Duplicate tests were performed at each sampling time point for the follow-up experiment.

2.3.7 Coupon processing

At the end of the spiking test, one of the eleven coupons with mature biofilms was removed and cut into small pieces (~2.5 × 1.1 cm each) for SEM. Two coupons with mature biofilms were removed for Chlorophyll a test (only in the first experiment); another two coupons were removed for dry weight (DW), ash-free dry weight, organic mass, and water content analysis; and two coupons were used for protein micro-assay (kit II, cat #: 500-0002, Bio-Rad Inc., Hercules, CA). The remaining four coupons with mature biofilms, along with the inner rotating cylinder, were scraped using a sterile Falcon^R cell scraper (Handle: 18cm; Blazer: 1.8cm, Fisher Scientific, Pittsburg, PA); the scraped biomaterial was resuspended in ultra-pure water, the sample was centrifuged at

1100 x g for 15 min, the supernatant was removed, the pellet was mixed vigorously to homogenize, and the homogenized pellet was processed through IMS and IFA. The total number of oocysts attached to the biofilms was calculated by multiplying the number of oocysts in the pellet divided by the sampled area times the total area of the bioreactor with mature biofilms. The clean coupon used to maintain shear in the reactor, along with the new outer beaker, were scraped with another sterile Falcon[R] cell scraper; the scraped biomaterial was resuspended in ultra-pure water, and a 5-10 mL well-mixed sample was removed for IMS and IFA. The number of oocysts recovered from biofilms matched the number of oocysts calculated at the end of spiking test (within 15% for the first experiment and the follow-up experiment).

2.3.8 Chlorophyll a test

Biofilms from two coupons were scraped into two separate 15-mL sterile centrifuge tubes. Four (4) mL methanol was added into each tube and vortexed with the scraped biomaterial. The well-mixed samples were then stored at -20°C for a day or two to extract *Chl* a from biofilms. The frozen samples were left open in the -20°C freezer to allow the methonal to be evaporated, the remaining samples were thawed by freeze-drying and centrifuged at 2000 x *g* for 15 min. The clear supernatant was transferred to a test tube and the extract fluorescence was measured using a Turner Design Model 10-AU digital fluorometer (Sunnyvale, CA).

2.3.9 Protein micro-assay

Three to five dilutions of the BSA protein standard (the linear range of the assay for BSA is 1.2 to 10 µg/mL) were prepared. Each standard and recovered biofilm sample solution (800 µL each) were pipetted into a separate clean, dry 1.5-mL microcentrifuge

tube (protein standard solutions were assayed in duplicate). Dye reagent concentrate (200

µL) was then added to each microcentrifuge tube, and the tubes were vortexed and

incubated at room temperature for at least five minutes but no more than one hour.

Absorbance at 595 nm of the samples along with the protein standards was then measured

using a GeneQuant pro spectrophotometer (Amersham Biosciences, NJ).

2.3.10 Dry weight and ashed weight

The biofilm organic matter content was determined by subtracting ashed weight

(500°C, 3h) from dry weight (105°C, overnight) (Amalfitano *et al*, 2008). The water

content was calculated by subtracting dry weight from saturated biofilms.

Dry weight (DW) =
Biofilms dried at 105°C, overnight   **Equation 2. 10**

Ashed weight (AW) =
Biofilms burned at 500°C for 3hr   **Equation 2. 11**

Water content (%) = $\frac{W_{biofilm} - DW}{W_{biofilm}} \times$
100%   **Equation 2. 12**

Organic matter content = DW −
AW   **Equation 2. 13**

2.3.11 SEM study

To investigate the morphology and topography of the steady-state biofilms after

spiking with *C. parvum* oocysts for 4 days, a coupon was removed from each bioreactor

and analyzed by SEM. Biofilms were fixed by rinsing the coupons with sterile phosphate

buffered saline (PBS) solution to remove the dead and loosely attached bacteria, followed

by treatment with a mixture of 1% paraformadehyde and 1% glutaraldehye in 0.05M

piperazine-N,N'-bis(2-ethanesulfonic acid (PIPES) at pH 7.4, overnight at 4°C. The

specimen was then rinsed with 0.01M PIPES + 0.001M $CaCl_2$ to remove excess fixative, dehydrated in a series of ethanol baths (35 - 100%), and treated with hexamethyldisilazane (HMDS) to dehydrate the specimen. Specimens were coated with gold palladium (Au-Pd) using a sputtering diode, and viewed under a Zeiss SEM (Oberkochen, Germany).

2.3.12 Statistical analysis

Correlation analysis was used to evaluate the potential relationships between the analyzed variables. Physical and chemical parameters of water samples from each bioreactor were analyzed by independent-sample t-test to check the stability of those parameters during the experiment and to identify any differences among those parameters due to illumination, water chemistry, and storage. All statistical analyses were performed using Microsoft Office Excel 2007, SPSS (ver. 22, SPSS Inc., 2013) or the OriginPro (ver. 8.6, OriginLab, 2011) software package for Windows.

2.4 Results

2.4.1 Physical and chemical conditions in the bioreactor

General water quality parameters of stored water, analyzed every two weeks, remained steady. Dissolved oxygen and pH in stored water were significantly higher than in bioreactor water (t-test, $p < 0.01$ for dissolved oxygen; $p < 0.03$ for pH), indicating a high demand for oxygen, and a transitory occurrence of acid intermediates, due to biofilm propagation. Nutrient levels, especially phosphorus, depleted in each 4-day period in bioreactors (data not shown), suggesting that water replacement every four days was reasonable to maintain necessary nutrients for biofilm growth throughout the study period.

Turbidity within bioreactors differed significantly from the stored water as a result of the sloughing and erosion of biofilm communities. The temperature in dark bioreactors was significantly higher than the temperature in light bioreactors (t-test, $p < 0.01$), likely due to the confinement of the bioreactors in a box to eliminate light, therefore impeding heat dissipation. Besides temperature, Table S2.1 shows a summary of the statistical analyses obtained from the t-tests performed on other water quality parameters among bioreactors operated in dark and light, and stored water. Mean water physical and chemical parameters are summarized in Table S2.2.

2.4.2 Biofilm development

In the approximately 150 days of biofilm development, biofilms were changing from bacterial clusters to discrete biofilms. The mean thickness and heterogeneity of biofilms increased with time when analyzed by optical microscopy. Regardless of the variety of the water chemistry or light, the biofilm growth curves were sigmoidal, with a lag phase, a linear growth phase, and a steady-state phase. The biofilms grew markedly slow during the initial two-three weeks of lag phase (Figure 2.3). During the exponential phase, the depth of biofilms increased significantly (Figure 2.3). Upon reaching steady-state, the biofilm thickness eventually became stable (although more sloughing was observed in biofilms grown under dark conditions). Assuming the biofilm formation in each phase is linear over time, the specific growth rate k for the linear growth phase represents the slope of the line, thus, calculated by equation 2.14:

$$\overline{L_f} = k \times t + \overline{L_0} \hspace{3cm} \textbf{Equation 2. 14}$$

with $\overline{L_f}$ the mean biofilm thickness over time, and the $\overline{L_0}$ the mean biofilm thickness at the beginning of the phase. The time range and the specific growth rate k, representing the mean biofilm thickness increase in µm per hour, are given for the exponential phase in Table S2.3. Statistical analysis suggests that biofilm developed under dark has a slightly greater specific growth rate than formed under light, but the difference is not significant (paired t-test, $p = 0.14$).
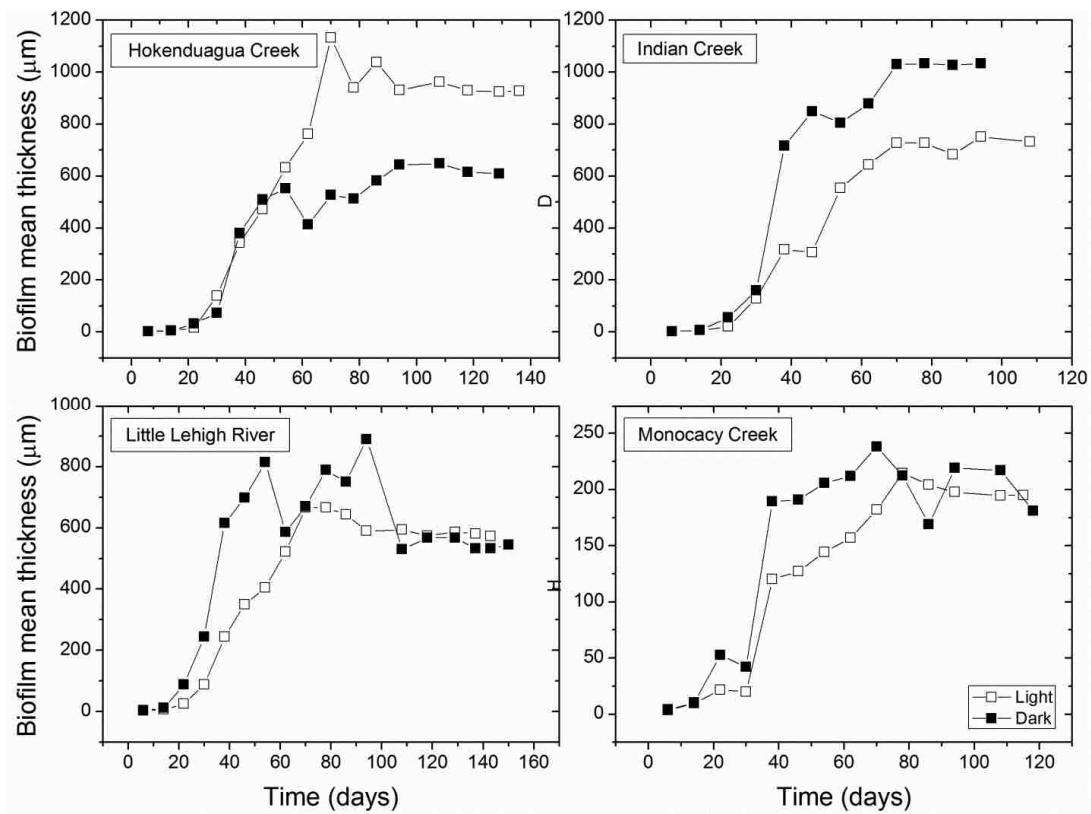
Figure 2. 3. Development of biofilms in bioreactors with water from different streams under light and under dark condition.

DO content was the limiting reactant when biofilms grew rapidly with nearly linear kinetics, as demonstrated by a marked drop in DO concentration during this phase of growth. However, DO concentration stabilized once the biofilms reached steady state

(Figure S2.1). The depth of steady-state light biofilms ranged from $201.2 - 973.1 \mu m$, while the depth of mature dark biofilms ranged from $206.8 - 1030.7$ μm. The mean thickness of dark and light mature biofilms was not significantly different (paired t-test, $p = 0.47$), indicating that illumination was not related to the depth of stabilized biofilms. No correlation was found between water chemistry and biofilm growth rate or stabilized thickness.

Biofilm roughness decreased with biofilm maturity and approached a similar value in all eight conditions, suggesting that shear stress is a primary attribute in the formation of the porous and heterogeneous conditioning layers. This result is in agreement with the observation of Battin *et al* (Battin, Kaplan, Newbold, Cheng, & Hansen, 2003), who postulated that the enhanced transport of particles and substrates between neighboring protuberances would successively reduce biofilm surface roughness. Fluctuations in the roughness coefficients can be attributed to cell detachment and regrowth. In general, thicker biofilms were smoother, especially for biofilms grown in light (Pearson's r = - 0.999, $p < 0.01$).

2.4.3 The effect of light exposure and water chemistry on biofilm characteristics

The characteristics of established biofilms under different streams and growth conditions are shown in Table S2.4. Overall, no significant differences ($p < 0.05$) between illumination/water chemistry and biofilm protein/dry mass/organic mass levels were observed. Chlorophyll a levels in biofilms developed under light exposure condition were higher than those formed under dark condition, but the difference was not significant (paired t-test, $p = 0.090$). This is most likely due to the fact that although the

bioreactor was exposed to sun for at least 7 h a day, due to the relatively narrow coupon surface area (12.25 cm) as well as the spinning of the inner rotating cylinder, direct illumination time was minimized. On the other hand, the algae and grazer in biofilm suspension scraped from stream rocks has been pre-filtered by a 6-μm-pore-size cellulose filter paper, because the algae would not survive in the absence of sunlight in laboratory experiments, and the grazers can disturb the biofilm structure and consume oocysts (Wolyniak *et al*, 2010).SEM images (Figure S2.2) showed that a dense biofilm has been formed on the polycarbonate coupon surface as the biofilm reached to equilibrium.

2.4.4 Deposition of C. parvum oocyst onto environmental biofilms

The impact of water chemistry, specifically hardness, alkalinity and conductivity, and illumination on C. parvum oocyst deposition were studied by measuring the efficiencies of attachment of oocysts onto well established or pseudo-equilibrium biofilms over time to perform valid comparisons (Figure 2.4). The different water conditions did result in different final numbers of oocysts attaching to biofilm surfaces, specifically in water with higher conductivity levels and ionic strength, indicating that conductivity and/or ionic strength may play roles in oocyst adhesion.. Although the impact of ionic strength on oocyst deposition efficiency is not evident, loss of calcium and magnesium levels were noticed in this study. The consumptions of calcium ranged from 7.33 – 35.85% and 12.41 – 70.55% for bioreactors operated under light and dark conditions, respectively. Results of the calcium and magnesium consumption are presented in Table S2.5. In support of this finding, a follow-up experiment was performed in order to investigate the effects of calcium and magnesium on oocysts adhesion, and also to assess the mechanisms used to describe the adhesion kinetics.
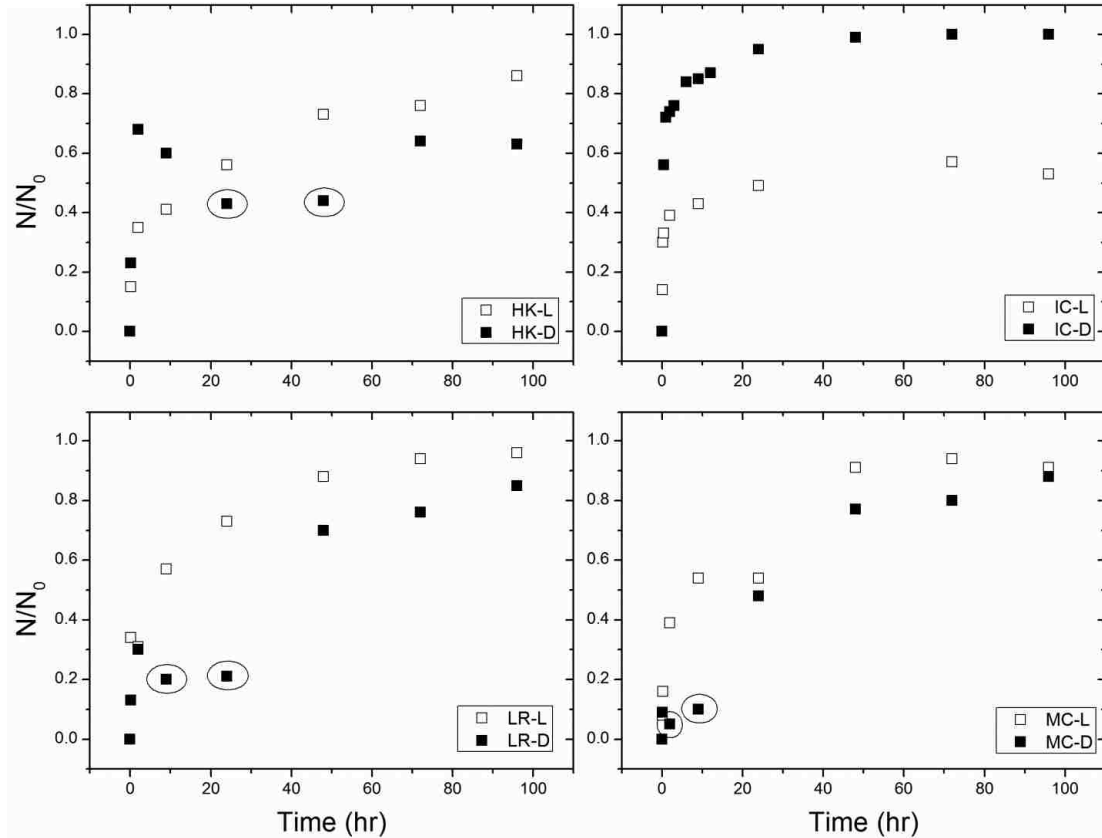
Figure 2. 4. Deposition efficiencies of C. parvum oocyst onto environmental biofilms under different water chemistry and environmental conditions (light (L) versus dark (D)) as a function of time.

Data points circled indicate the releasing of attached oocysts back to water column due to biofilm sloughing. HK-Hokendauqua Creek; IC - Indian Creek; LR - Little Lehigh River; MC - Monocacy Creek.

2.4.5 Effect of calcium and magnesium on C. parvum oocyst deposition efficiency

The reduction of calcium and magnesium in the bioreactor water after oocyst introduction indicates that calcium and magnesium may play a critical role in oocyst deposition. Thus, the concentration of calcium and magnesium were decreased significantly in the bioreactor water by SAC treatment and re-introduced at a concentration consistent with natural stream water at different phases of oocyst spiking.

Figure 2.5 shows the impact of those two cations on oocyst deposition efficiency as a function of time. It shows the deposition efficiencies of C. parvum oocysts onto environmental biofilms when the calcium and magnesium concentration of the bioreactor water is reduced is roughly 50%, significantly less than efficiences observed in the presence of a normal stream concentration of calcium and magnesium. It is worthwhile noting that the SAC treated water still had low circulating levels of calcium and magnesium (see below) which may have contributed to the initial binding of oocysts at the 50% efficiency. When magnesium alone was added back to the bioreactor, the oocyst deposition efficiency fluctuated and increased by around 20% at the end. However, when calcium was added back to the bioreactors, oocysts deposition efficiency increased steadily, reaching nearly 100%. When both ions were added back to the bioreactors, the deposition efficiency was similar to that of calcium alone, suggesting calcium is the predominant factor for oocyst deposition.
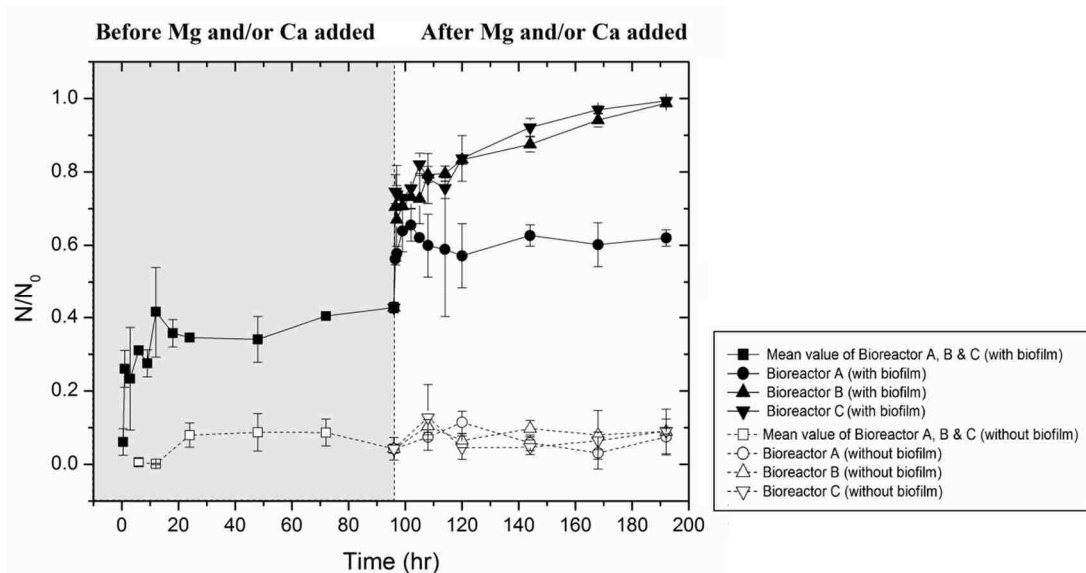
Figure 2. 5. Deposition efficiency of C. parvum oocysts on to polycarbonate coupon with (solid curve, closed symbol) and without (dashed curve, open symbol) biofilms in the presence of CaCl₂ and/or MgCl₂. Error bar indicates one standard deviation of at least duplicate tests.

Figure 2.6 shows the concentration of calcium, magnesium and sodium within each bioreactor before and after the addition of the same amount of those cations as they presented in the stream water. Interestingly, the background concentrations of calcium and magnesium in the SAC treated stream water (not shown) were at or below 0.5 ppm, but the concentration of calcium and magnesium SAC treated water within the bioreactors was 13.71 ppm (n = 3, SD = 2.04) and 12.27 ppm (n = 3, SD = 3.06), likely due to the leaching of these ions from the biofilms back into the circulating water. After adding calcium and magnesium back to the bioreactors after 96h of running, Figure 2.6 (a) showed that the calcium level in the Bioreactor B and C declined considerably, reaching 57.73% and 36.68% of the added calcium at the end of the experiment, respectively, calcium consumption within bioreactors mostly resulted from the interaction of calcium ions with newly developed carbonate and exopolysaccharide polymers on biofilm surface, or the binding of calcium ions with negatively charged carboxyl and phosphate groups on oocyst surface. The consumption of calcium increased the attachment of oocyst as shown in Figure 2.5. In contrast to the pronounced calcium uptake observed in bioreactor B and C , only 12.53% of the added magnesium was consumed in bioreactor A, minor consumption of magnesium was observed in the bioreactor C(Figure 2.6 (b)) . The reduction of magnesium in bioreactor A contributed to 20% increasing in oocyst attachment efficiency (Figure 2.5). Concentration of sodium in all three bioreactor remained nearly constant and even slightly increased as a result of water evaporation (Figure 2.6 (c). For the cations changes in the bioreactors in the absence of biofilms (Figure 2.6 (d-f)), a decrease in calcium level after they were added back to bioreactor B and C was observed, however, magnesium and sodium concentrations kept constant.

From these results, we conclude that (i) the binding pattern of C. parvum oocysts onto

biofilm surfaces in the presence of calcium and magnesium may be different. (ii) Rather

than magnesium or sodium, the C. parvum oocyst is more likely to use calcium to

enhance adhesion.
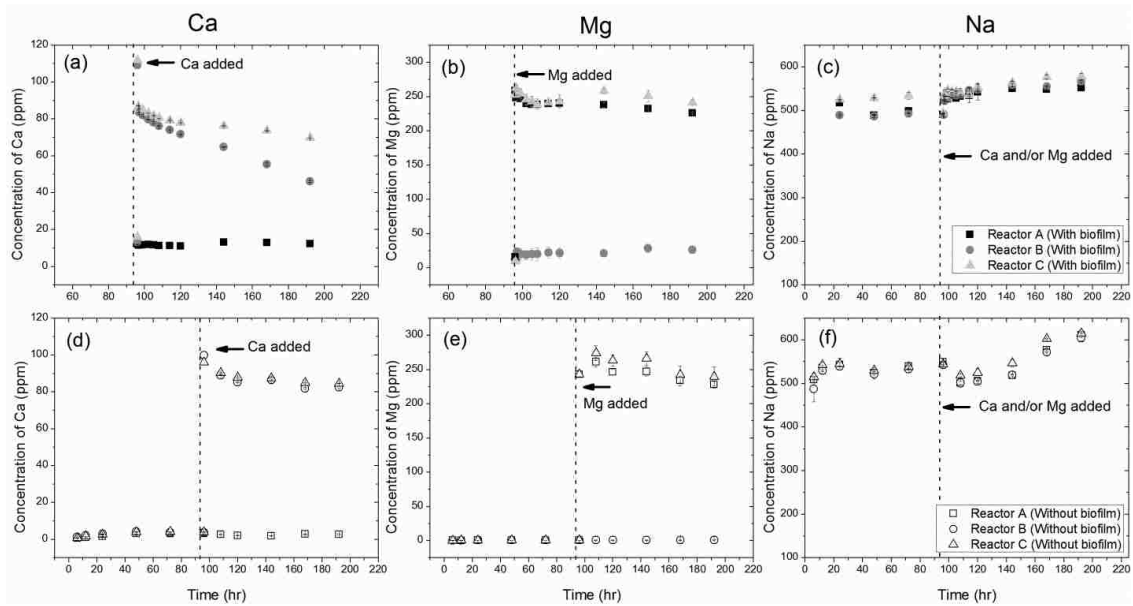
Figure 2. 6. Concentration of calcium, magnesium and sodium as a function of time in each bioreactor.

243 ppm $MgCl_2$, 96 ppm $CaCl_2$, and a mix of 243 ppm $MgCl_2$ and 96 ppm $CaCl_2$ was added into bioreactor A, B and C after a 96-h of running, respectively (Dash line).

2.5 Discussion

2.5.1 Water chemistry within bioreactors

Nutrient uptake in streams is partially the result of specific bacterial processes, such

as nitrification (i.e. oxidization of NH_4^+ to NO_3^-) and denitrification (i.e. respiratory

process reducing NO_3^- to N_2) (Ribot *et al*, 2013). Thus, the observed fluctuation in

nitrogen levels in reactor water would be expected during biofilm growth. For

phosphorus level in the bioreactors, within a four-day operation period, phosphorus

concentration in some bioreactors decreased due to the phosphorus taken up by biofilms,

whereas the phosphorus concentration in some bioreactors increased. One possibility, as

described by Falkentoft *et al* (Falkentoft, Harremoes, & Mosbaek, 1999), are in an

anaerobic condition, phosphate accumulating organisms (PAOs) adsorb and store easily

degradable organic matter, mainly as polyhydroxybuturate (PHB), while they could

release phosphate; in aerobic or anoxic conditions, PAOs will degrade the stored organic

matter while taking up phosphate and storing it as poly-phosphate. Since the deep part of

the biofilms is constantly anaerobic (Falkentoft *et al*, 1999), while the upper part of the

biofilms contacted with flow and are aerobic, thus, the phosphorus levels in bioreactors is

related with the uptake rate of biofilm upper layers and the releasing rate of biofilm

bottom layers.

2.5.2 Biofilm development

The initial delay in biofilm formation that is observed can be explained by the

properties of the EPS producing cells, which possess poor adhesion efficiency under

dynamic flow conditions (Habimana, Meyrand, Meylheuc, Kulakauskas, & Briandet,

2009). Deposition of cell and bacteria to a solid surface is governed by two stages (Zobell,

1943): 1) initial interactions dominated by long-range, physical forces between the cell

and the substrate; 2) biological or specific interactions (short-range force) that require

longer time to enable cellular rearrangement or adaptation. Derjaguin-Laudau-Vervewy-

Overbeek (DLVO) theory is commonly used to interpret collector surface and colloidal

particle interaction. This interaction contributes to the total Gibbs energy which is a

function of the separation distance between the cell and the substratum (Rijnaarts, Norde,

Bouwer, Lyklema, & Zehnder, 1995). We would expect for a given fluid shear, the biofilm thickness would increase with ionic strength according to the DLVO theory, which has been widely used to explain the effect of electrolyte concentration on the bacteria approaching to a charged surface (M. C. van Loosdrecht, Lyklema, Norde, & Zehnder, 1989).DLVO theory indicates that as ionic strength increases, the depth of the energy wall which leads to repulsion between the bacterial surface and the solid surface will be reduced. As a consequence, more cells are expected to attach to the charged surface. Converse to this theory, the biofilm thickness did not appear to be influenced by the changes in ionic strength at given shear force, suggesting that forces other than electrostatic forces are influencing adhesion of bacteria to the growing biofilm surface. One possible reason is biofilm mass contains extra-cellular polymeric substance (EPS), lipids, water, cells etc, thus using the classic DLVO model to describe the interaction between biofilm surface and oocysts cell wall is an oversimplification. Another possible explanation is that the cells suspended into the bioreactors are a combination of motile and non-motile microbes, in which cell motion may aid in attaching and detaching cells from a surface. McClaine and Ford (McClaine & Ford, 2002) have found that motile bacterium appeared to be unaffected by ionic strength because i) bacteria swimming would help cells to get closer to the surface or ii) tumbling acted as an anchor would cause one or more flagella to attach to the surface. Additionally, the adhesion and detachment of bacterial cells within biofilms may be caused by the metabolism of bacterial cells and the production of surface-active compounds (Neu, 1996).

2.5.3 Kinetics of C. parvum oocyst adhesion to biofilm surfaces

The experimental system was originally developed to investigate the water chemistry and light exposure on the deposition kinetics of C. parvum oocyst onto environmental biofilms. A first order kinetic has been derived initially to model oocyst association with environmental biofilm, since this kinetic has been widely used to model the cell deposition onto different surfaces (Vunjak‐Novakovic *et al*, 1998; Walters, Schwarzwälder, Rutschmann, Müller, & Horn, 2014; Yuan, Pham, & Nguyen, 2008). Details of the model have been described as below:

It has been assumed that the adhesion of oocysts to the semi-batch annular rotating bioreactor can be characterized as:

$$\text{oocysts} + \text{biofilm} \overset{k_1}{\underset{k_2}{\rightleftharpoons}} \text{oocysts} \equiv \text{biofilm}$$
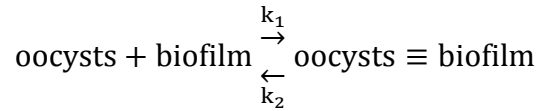
Assuming first-order attachment and detachment kinetics, the change in oocyst concentration in the bulk suspension can be modeled as:

$$-\frac{dC}{dt} = k_1 C - k_2 C_f \qquad\qquad \textbf{Equation 2. 15}$$

in which C is the concentration of suspended oocysts at time t in the bulk suspension, C_f is the concentration of attached (fixed) oocysts at time t (i.e., the number of oocysts transferred from the liquid phase to the biofilm per unit volume of liquid), and k_1 and k_2 are the first-order adhesion and desorption rate constants, respectively. A mass balance of oocysts in each bioreactor is described as:

$$C_0 = C_f + C \qquad\qquad \textbf{Equation 2. 16}$$

in which C_0 is initial concentration of oocysts spiked into the bioreactor. When oocyst attachment reaches equilibrium, Eq. 2.16 becomes:

$$C_0 = C_{fe} + C_e \qquad\qquad \text{Equation 2. 17}$$

in which C_{fe} and C_e are the concentrations of the attached oocysts and suspended

oocysts at equilibrium, respectively. In addition, at steady state Eq. 2.15 is equal to 0 and

$$k_2 C_{fe} = k_1 C_e \qquad\qquad \text{Equation 2. 18}$$

Substituting Eq. 2.16 – 2.18 into Eq. 2.15 yields

$$-\frac{dC}{dt} = (k_1 + k_2)(C - C_e) \qquad\qquad \text{Equation 2. 19}$$

Integrating Eq. 2.19 yields

$$\ln\frac{C_0 - C_e}{C - C_e} = kt \qquad\qquad \text{Equation 2. 20}$$

where $k = k_1 + k_2$ is termed the overall adhesion rate of oocysts (time^{-1}).

Substituting Eqs. 2.16 – 2.17 into Eq. 2.20 yields

$$C_f = C_{fe}(1 - e^{-kt}) \qquad\qquad \text{Equation 2. 21}$$

Multiplying Eq. 2.21 by the bulk volume in the bioreactor and dividing by the

available coupon surface area yields a general model to describe the attachment of

oocysts to the coupon surface over time:

$$N = N_{eq}(1 - e^{-kt}) \qquad\qquad \text{Equation 2. 22}$$

where N is the number of oocysts attached to the biofilm per unit coupon surface

area at time t, and N_{max} is the specific adhesion capacity at the adhesion equilibrium per

unit coupon surface area. Based on this model, the overall adhesion rate constant will be

determined as a function of biofilm characteristics (i.e., mean thickness, roughness

coefficient, protein mass, dry mass and organic mass) and water chemistry using the experimental results.

Unexpectedly, it was found the experimental results did not fit into the pseudo-first order kinetic, instead a reduction in calcium and magnesium levels were noticed, implying the interaction of soluble divalent cations with either biofilm/oocyst surface may make the pseudo-first order model inappropriate for this study.

It has been shown that cations, including calcium and magnesium, can bind to carboxyl and other chemical functional groups to inhibit calcium and/or magnesium carbonate precipitation in freshly produced EPS (Braissant *et al*, 2007; Dupraz & Visscher, 2005). The oocysts possess a thick wall, containing glycolipids and phospholipids (Robertson, Campbell, & Smith, 1993), amide, carboxylate, phosphate, and polysaccharide functional groups (Gao & Chorover, 2009; Karaman *et al*, 1999). These functional groups, in the absence of further modification, would lead to an overall polar, charged (histidine positive charge, carboxylate/phosphate negative charge) oocyst surface in typical surface water conditions. The presence of those charged functional groups will lead to electrosteric repulsion, significantly hindering oocyst deposition (Kuznar & Elimelech, 2004). Increasing ionic strength in our study did not improve the oocyst deposition efficiency effectively, however, the addition of the calcium enhanced the oocyst deposition considerably. The presence of exposed carboxylate groups on the EPS of biofilms (Sutherland, 2001) and oocyst wall appear to allow Ca^{2+} and Mg^{2+} to form inner-sphere and outer-sphere complexation, respectively. Kalinichev and Kirkpartrick (2007) used a molecular simulation study to explain the affinitie of calcium

and magnesium to carboxylate groups, and suggested that the tendency of forming metal-NOM complexation is strongly dependent on both the charge/radium ratio and the size of the cation. Their studies were confirmed by Janjaroen et al (Janjaroen et al, 2010), who have reported that the binding of Ca^{2+} to carboxylate groups will form cation bridging between these surfaces and enhance C. parvum oocyst deposition. On the other hand, the weakly associates of Mg^{2+} with carboxylate groups are likely to neutralize charges on these surfaces to promote oocyst deposition. Because calcium (R_{Ca}=1.61 Å) is bigger than magnesium (R_{Mg}=0.92 Å), thus the hydration shell is much more easily to be released to form the inner sphere surface complex. De Kerchove and Elimelech (2008) also reported a similar interaction between metal cations and carboxyl groups via both experimental and computational molecular modeling. Therefore, the electrostatic binding between calcium and negatively charged functional groups via complex formation could effectively neutralize the surface charge of biofilms/oocysts and accounts for the discreprency of classic DLVO theory in our study.

In this subsection, we attempted to model the experimental data using chemical kinetics. We took advantage of previously reported case that calcium is able to bridge the carboxylic group to address this question. Deposition kinetics were analyzed using a pseudo-second order model (Figure 2.7) in which the calcium mediated the interaction between biofilm surface and the C. parvum oocyst. The overall exchange reaction of carboxylic group bound by divalent ions (i.e., Ca^{2+}) in the solution which can be written:

$$Ca^{2+} + RCOO^- \rightarrow [Ca^+(RCOO)] \qquad\qquad\qquad \text{Step 1}$$

$$[Ca^+(RCOO)] + OocCOO^- \underset{k_2}{\overset{k_1}{\leftrightarrow}} (RCOO)Ca(OocCOO) \qquad\qquad\qquad \text{Step 2}$$
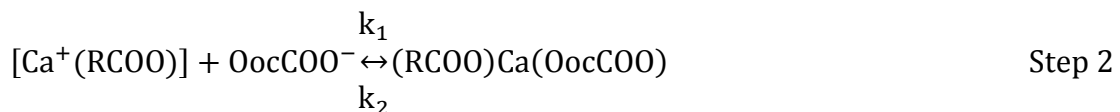
Step 1 happens really fast, whereas Step 2 is slow thus it is the rate limiting step, the expression of Step 2 can be written as:

$$\frac{d[RCOO]_t}{dt} = k_1[Ca^+(RCOO)][OocCOO] - k_2[(RCOO)Ca(OocCOO)] = k_1[Ca][RCOO]_r^2 - k_2[Ca(RCOO)(OocCOO)]$$

Equation 2. 23

$[RCOO]_t$ is the number of carboxyl active sites binding by oocysts carboxyl active sites at time t, $[RCOO]_r$ represents the unbounded carboxyl active sites on biofilm. Model assumptions included that calcium and carboxylic groups are excess, and the detachment of the oocysts is so small that can be negligible comparing to the attachment. The kinetic order is two with respect to the number $([RCOO]_{eq} - [RCOO]_t)$ of available sites for the exchange. With these simplifications, the change in the number of carboxyl active sites bounded can be expressed as

$$\frac{d[RCOO]_t}{dt} = k_1[RCOO]_r^2 = k_1([RCOO]_{eq} - [RCOO]_t)^2$$

Equation 2. 24

where $[RCOO]_{eq}$ is the total number of available carboxyl active binding sites at equilibrium. The driving force $([RCOO]_{eq} - [RCOO]_t)$, is proportional to the available fraction of active binding sites, thus the differential equation 2.24 can be rewritten as

$$\frac{dN_t}{dt} = k_1(N_{eq} - N_t)^2$$

Equation 2. 25

where N_t is the number of oocysts attached to biofilm at time t, N_{eq} is the amount of oocysts attached at equilibrium. Integration of equation 2.25 for the boundary conditions $t = 0$ to $t = t$, and $N_t = 0$ to $N_t = N_t$, to get a linear form

$$\frac{t}{N_t} = \frac{1}{k_1 N_{eq}^2} + \frac{t}{N_{eq}}$$

Equation 2. 26

where $k_1 N_{eq}^2$ is the initial adhesion rate (#·hr^{-1}) as $\frac{t}{N_t}$ approaches 0. The pseudo-second-order model constants can be then determined by plotting $\frac{t}{N_t}$ against t for our experimental data.

The kinetic data for oocyst deposition in experiment 1 and the follow-up experiment were plotted in Figure 2.8 and Figure 2.9 in linear form according to the pseudo-second-order kinetic model, respectively. The results of the kinetic parameters from those two experiments are calculated and shown in Table 2.2 and Table 2.3. The adjusted data in Table 2.2 indicates the circled dots in Figure 2.3 has been eliminated due to biofilm sloughing. The χ^2, which indicates the difference between model values and experimental values of equilibrium adhesion, was found to be really small (less than 1.00E-7) for the adjusted data in experiment 1 and the follow-up experiment where there were SAC treated or calcium added, suggesting that pseudo-second-order kinetics sufficiently described the adhesion of C. parvum oocyst onto biofilm surface. Moreover, the correlation coefficient values, r^2, were all higher than 0.94. In the follow-up experiment, a similar trend in the pseudo-second-order plots were observed for the SAC treated, 109 ppm calcium and a mix of 259 ppm magnesium and 109 ppm calcium water (Figure 2.6), however, a deviation from the straight line can be noticed after 6 hr of magnesium addition in the bioreactor A. This may signify that magnesium does not influence deposition in the same way that calcium does. From Table 2.3, the values of the initial rate constant, $k_1 N_{eq}^2$, was found to increase with the addition of calcium in bioreactor B and C. Comparing with adding calcium alone, there was an increase in the initial deposition rate constant, while adding both magnesium and calcium. In addition,

the number of oocyst retained to biofilm at equilibrium, N_{eq}, with the addition of both

calcium and magnesium is almost equal to the equilibrium value with the addition of

calcium alone. This can be attributed to the fact that magnesium could facilitate the

adhesion of oocyst, but the calcium still play a predominant role in oocyst deposition

kinetics.
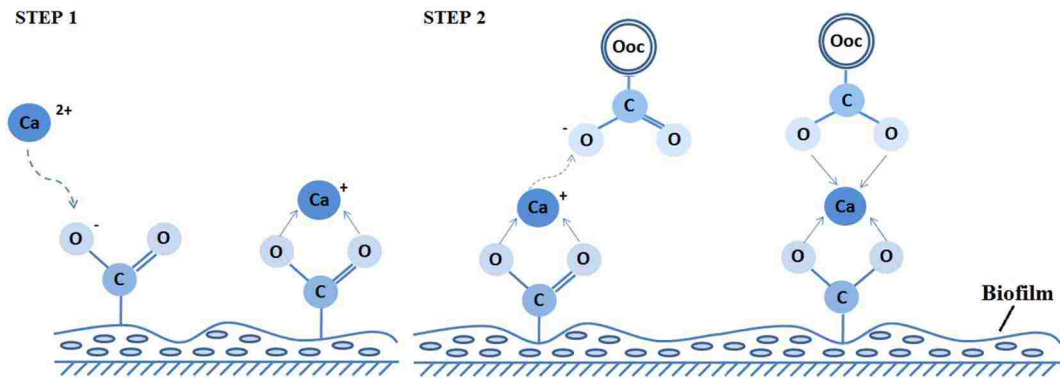
Figure 2. 7. Conceptual model of oocyst deposition onto biofilm due to calcium bridging with carboxylate groups. Ooc indicates the C. parvum oocyst.
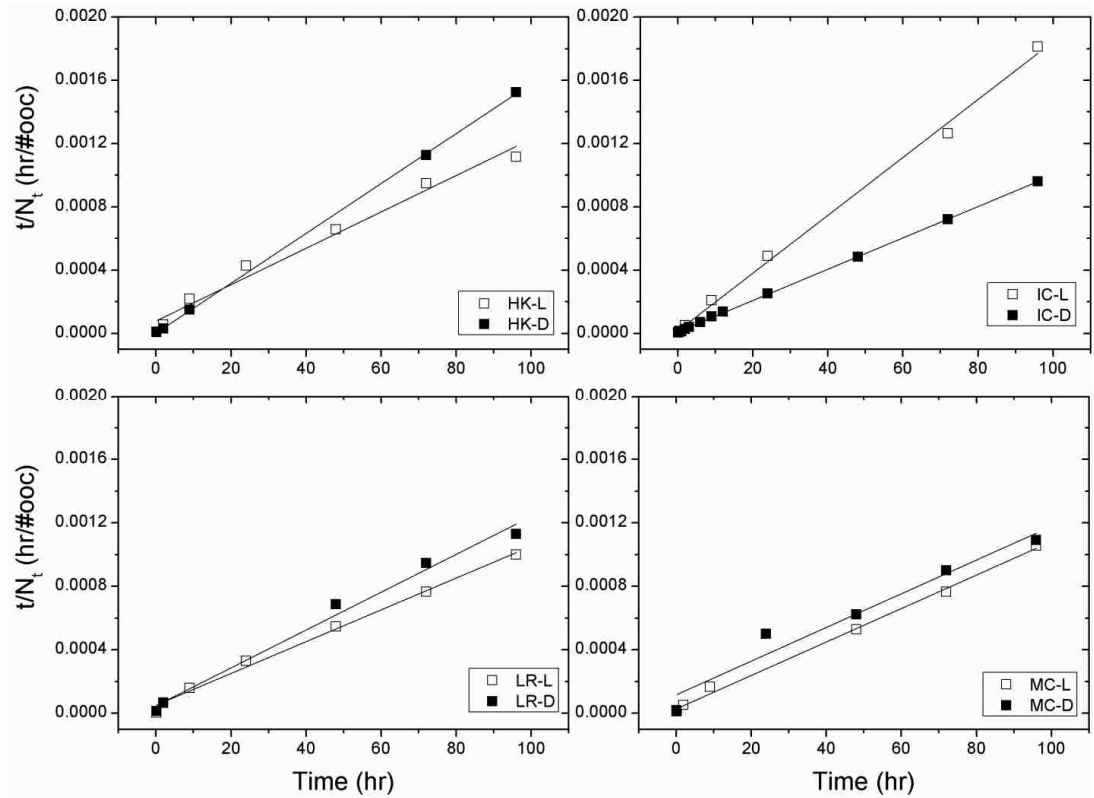
Figure 2. 8. Pseudo-second order rate model for C. parvum oocyst deposition onto different biofilms in the experiment 1. The theoretical values (—) were calculated from eq x by using the parameters determined from the equilibrium adhesion isotherm. The data points (□, ■) were obtained from experiments.
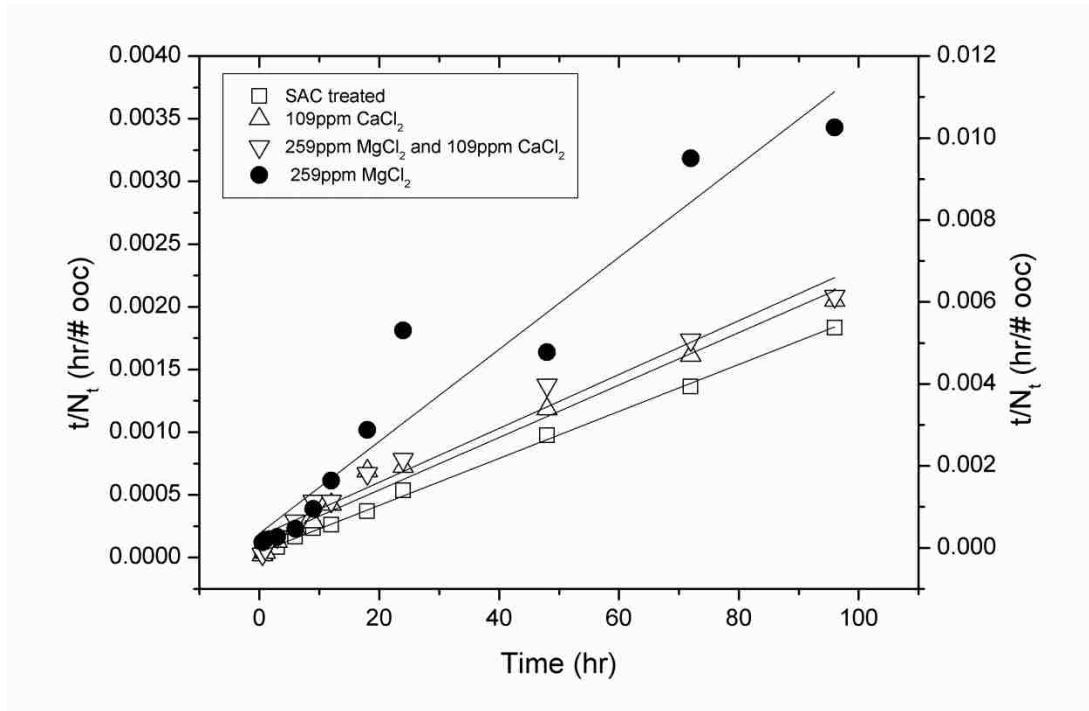
Figure 2. 9. Pseudo-second order rate model for C. parvum oocyst in the presence of CaCl₂ and/or MgCl₂ in the follow-up experiment. Y-axis of the open dots is on the left side, y-axis of the closed dots is on the right side.

Table 2. 2. Pseudo-second-order parameters for C. parvum oocyst deposition in the Experiment 1

	Parameters	HK-L	HK-D*	IC-L	IC-D	LR-L	LR-D*	MC-L	MC-D*
Adjusted[a]	$k_1 N_{eq}^2$ (#ooc·hr⁻¹)	1.27E+04	4.15E+05	6.24E+04	9.45E+04	2.03E+04	2.07E+04	1.91E+04	8.57E+03
	N_{eq} (#ooc)	8.70E+04	6.35E+04	5.47E+04	1.01E+05	9.96E+04	8.39E+04	9.60E+04	9.42E+04
	r^2	0.9782	0.9998	0.9969	0.9997	0.9938	0.9853	0.9707	0.9430
	χ^2	2.04E-08	2.77E-10	8.84E-09	2.45E-10	4.34E-09	1.14E-08	3.20E-09	2.89E-08
Unadjusted	$k_1 N_{eq}^2$ (#ooc·hr⁻¹)	1.27E+04	1.49E+04	6.24E+04	9.45E+04	2.03E+04	3.56E+03	1.91E+04	2.70E+03
	N_{eq} (#ooc)	8.70E+04	6.25E+04	5.47E+04	1.01E+05	9.96E+04	1.02E+05	9.60E+04	1.36E+05
	r^2	0.9782	0.9440	0.9969	0.9997	0.9938	0.5179	0.9707	0.4732
	χ^2	2.04E-08	1.05E-07	8.84E-09	2.45E-10	4.34E-09	5.41E-07	3.20E-09	3.52E-07

[a] Certain data points were eliminated due to biofilm sloughing prior to data analysis

* Data was modified due to biofilm sloughing

Table 2. 3. Pesudo-second-order parameters for C. parvum oocyst deposition in the follow-up experiment

Model	Parameters	SAC treated	259 ppm MgCl₂	109 ppm CaCl₂	109 ppm CaCl₂ and 259 ppm MgCl₂
Pseudo-second order kinetic	kN_{eq}^2 (#ooc·hr⁻¹)	2.44E+04	1.40E+05	2.70E+04	3.72E+04
	N_{eq} (#ooc)	5.34E+04	6.23E+04	9.99E+04	1.01E+05
	r^2	0.9981	0.9277	0.9714	0.9789
	χ^2	6.17E-09	9.00E-06	1.25E-07	8.68E-08

2.5.4 Measurements of free calcium and magnesium in the water with atomic absorption

Spectrophotometry showed that there was a release of those two cations in the presence of environmental biofilms. For the control sets, where there was no biofilm formed, the releasing of those cations can be negligible, suggesting that biofilms are responsible for the releasing of those cations. Braissant *et al* (Braissant *et al*, 2009) have showed that two different calcium pools may present on biofilms. One loosely bound that could be exchanged by dialysis or by moderate changes in pH, and one tightly bound that forms cross-linking EPS functional groups so that could not be exchanges. The decrease of calcium (Figure 2.5) may be involved in calcium binding to the various functional groups of newly produced EPS. Alternatively, calcium binds to oocyst wall and bridging the carboxylic groups between different oocysts and biofilm surface. The releasing of the calcium and magnesium is likely to account for the adhesion of C. parvum oocyst during the first 96-h of operation.

2.6 Conclusions

In this study, we have demonstrated that adhesion of C. parvum oocyst to biofilms is calcium mediated, and the pseudo-second-order kinetic appears to be the better-fitting model because it has a higher coefficient of determination, r^2, and nonlinear Chi-square values, χ^2. There are several lines of evidence that adhesion of C. parvum oocyst to biofilm surface depends on calcium/chemical functional group interaction. (i) Pretreatment of creek water with SAC did reduce the adhesion of oocyst, supporting the previous suggestion that calcium and magnesium play some role in oocyst adhesion. With the addition of magnesium, the binding of oocyst was only increased by approximately 20%, however, the binding of oocyst with the addition of calcium was spiked by 100%. Therefore, the effect of magnesium in adhesion of oocysts to biofilm surfaces appears to be minor compared to the role of calcium/chemical functional group interaction. (ii) Concentration of calcium was decreasing with the adhesion of oocysts, whereas the concentration of magnesium remains relatively constant during the course of the experiment. (iii) In the absence of the biofilms, the changes of oocyst concentrations in the suspension are negligible, but the oocysts clumped together with the addition of calcium (Figure 2.10), in the meanwhile, the evident dropping of calcium levels in bioreactor suggests the calcium loss contributed to the oocyst clustering. The kinetic parameters derived from the pseudo-second-order model could be used to correlate with various environmental conditions, such as flow rates, water temperature, pH, in future.
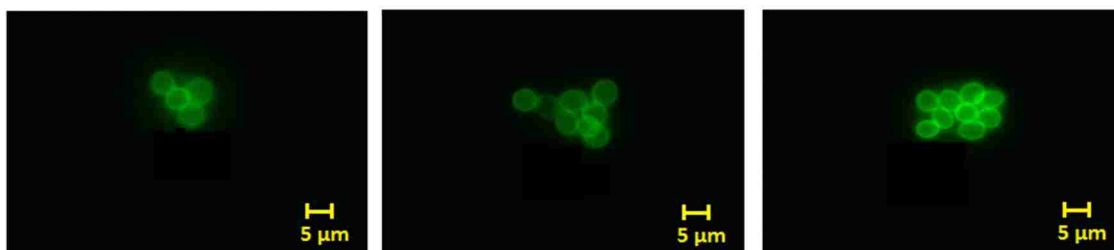
Figure 2. 10. Fluorescence image of *Cryptosporidium* parvum oocysts in control set after the addition of 194.4 mg CaCl₂ (without biofilm).

2.6 Acknowledgements

Table S2. 1. Differences between light, dark and stored water samples

P* value	Temp	pH	Conductivity (μs/cm)	Hardness (mg/L as CaCO₃)	Alkalinity (mg/L as CaCO₃)	Phosphorus (mg/L as P)	Nitrate-N (mg/L as N)	Nitrite-N (mg/L as N)	Ammonia-N (mg/L as N)	DO (mg/L)	Turbidity (NTU)
HK-L vs HK-D	**0.000**	0.768	**0.004**	0.998	0.698	0.744	**0.005**	0.977	**0.026**	0.591	0.387
Stored vs HK-L	**0.000**	**0.006**	0.062	**0.013**	0.081	0.331	**0.047**	0.191	**0.022**	**0.000**	**0.000**
Stored vs HK-D	**0.000**	**0.023**	0.384	**0.031**	0.137	0.218	0.298	0.343	0.843	**0.000**	**0.000**
IC-L vs IC-D	**0.002**	0.845	0.098	0.559	0.369	0.922	0.645	0.616	1.000	0.305	0.719
Stored vs IC-L	**0.000**	**0.003**	0.076	0.195	0.185	**0.034**	**0.013**	0.625	0.869	**0.000**	**0.029**
Stored vs IC-D	**0.000**	**0.012**	0.962	0.261	0.478	0.139	**0.037**	0.731	0.834	**0.000**	**0.000**
LR-L vs LR-D	**0.000**	0.156	0.077	0.053	0.428	0.837	0.398	0.218	0.158	0.822	0.902
Stored vs LR-L	**0.029**	**0.002**	**0.000**	**0.001**	**0.010**	0.799	**0.033**	0.132	0.096	**0.000**	**0.002**
Stored vs LR-D	**0.000**	**0.027**	0.256	**0.019**	**0.030**	0.990	0.259	**0.005**	**0.041**	**0.000**	**0.001**
MC-L vs MC-D	**0.000**	0.453	0.783	0.239	0.812	0.090	0.175	0.165	0.241	0.793	0.167
Stored vs MC-L	**0.023**	**0.000**	0.989	0.831	0.707	0.283	0.114	0.243	0.583	**0.009**	**0.000**
Stored vs MC-D	**0.006**	**0.000**	0.784	0.104	0.556	0.386	0.672	0.324	0.181	**0.008**	**0.000**

* The independent t-test was used to test for significance of water quality parameters within different bioreactors and the stored water. Bold-faced values represent differ significantly ($p < 0.05$)
HK – Hokendauqua Creek; IC – Indian Creek; LR – Little Lehigh River; MC – Monocacy Creek.

Table S2. 2. Mean water quality data

Parameters	HK-L	HK-D	IC-L	IC-D	LR-L	LR-D	MC-L	MC-D
Temperature (°C)	21.57 ± 0.61	22.37 ± 0.38	21.61 ± 0.56	22.32 ± 0.44	21.39 ± 0.55	22.68 ± 0.43	21.65 ± 0.48	22.54 ± 0.37
pH	7.37 ± 0.27	7.40 ± 0.3	7.52 ± 0.18	7.54 ± 0.24	7.89 ± 0.23	8.00 ± 0.23	8.08± 0.11	8.11 ± 0.11
Conductivity (μs/cm)	210.30 ± 14.8	195.28 ± 12.4	320.67 ± 23.8	307.03 ± 23.8	493.56 ± 23.3	470.68 ± 49.8	654.33 ± 70.1	661.02 ± 63.8
Hardness (mg/L as $CaCO_3$)	48.32 ± 5.9	48.31 ± 3.3	82.63 ± 9.1	80.85 ± 5.9	128.82 ± 19.9	117.87 ± 14	151.60 ± 25.0	142.20 ± 18.20
Alkalinity (mg/L as $CaCO_3$)	41.44 ± 10.0	40.13 ± 9.2	68.14 ± 17.2	62.65 ± 13.1	140.63 ± 17.8	136.3 ± 16	161.13 ± 19.1	159.50 ± 18.80
Phosphorus (mg/L as P)	0.049 ± 0.028	0.046 ± 0.027	0.039 ± 0.024	0.041 ± 0.039	0.11 ± 0.16	0.010 ± 0.24	0.056 ± 0.037	0.036 ± 0.023
Nitrate-N (mg/L as N)	0.82 ± 0.92	2.02 ± 1.33	1.17 ± 1.2	1.39 ± 1.23	3.64 ± 2.16	3.05 ± 2.16	3.16 ± 1.67	2.39 ± 0.72
Nitrite-N (mg/L as N)	0.032 ± 0.08	0.031 ± 0.083	0.014 ± 0.036	0.035 ± 0.053	0.042 ± 0.062	0.090 ± 0.17	0.19 ± 0.44	0.019 ± 0.033
Ammonia-N (mg/L as N)	0.014 ± 0.012	0.0056 ± 0.008	0.0087 ± 0.015	0.0085 ± 0.011	0.16 ± 0.36	0.048 ± 0.062	0.018 ± 0.053	0.096 ± 0.25
DO (mg/L)	7.58 ± 0.84	7.42 ± 0.86	7.24 ± 1.05	6.59 ± 1.97	6.88 ± 1.19	6.97 ± 1.31	7.26 ± 0.79	7.19 ± 0.75
Turbidity (NTU)	5.02 ± 3.52	4.15 ± 1.88	4.33 ± 4.41	4.88 ± 3.18	10.00 ± 10.21	9.60 ± 10.05	3.41 ± 2.21	2.35 ± 1.60

Values are reported as mean water quality data ± SD

HK – Hokendauqua Creek; IC – Indian Creek; LR – Little Lehigh River; MC – Monocacy Creek.

Table S2. 3. Biofilm sepcific growth rate of the observed linear phase

Bioreactor I.D.	Light				Dark			
	Duration (Days)	Specific growth rate (μm/day)	r^2	*P* value	Duration (Days)	Specific growth rate (μm/day)	r^2	*P* value
Hokendauqua Creek	40	19.67	0.996	< 0.001	40	16.26	0.916	0.003
Indian Creek	56	14.00	0.966	< 0.001	56	19.86	0.876	< 0.001
Little Lehigh River	56	11.52	0.981	< 0.001	40	19.21	0.885	0.005
Monocacy Creek	65	3.55	0.920	< 0.001	24	6.22	0.854	0.008

Table S2. 4. Effect of illumination and water chemistry on biofilm characteristics

Reactor I.D./Parameters		Mean results ± SD (n = 2)			
		Protein (mg/cm^2)	Dry mass (mg/cm^2)	Organic mass (mg/cm^2)	Chl a (µg/kg dry mass)
Light	Hokendauqua Creek	44.38 ± 1.00	0.46 ± 0.13	0.28 ± 0.13	30.23 ± 3.39
	Indian Creek	26.30 ± 14.57	0.48 ± 0.07	0.47 ± 0.07	22.79 ± 3.97
	Little Lehigh River	73.30 ± 1.75	1.02 ± 0.24	0.91 ± 0.27	8.98 ± 5.75
	Monocacy Creek	16.16 ± 4.24	1.92 ± 0.13	0.93 ± 0.67	13.15 ± 1.93
Dark	Hokendauqua Creek	17.46 ± 0.75	0.14 ± 0.0038	0.14 ± 0.0038	13.76 ± 2.07
	Indian Creek	45.09 ± 5.58	0.69 ± 0.41	0.65 ± 0.37	0.17 ± 0.03
	Little Lehigh River	10.69 ± 0.063	0.15 ± 0.035	0.11 ± 0.042	7.09 ± 0.32
	Monocacy Creek	11.62 ± 4.30	0.87 ± 0.13	0.30 ± 0.083	1.18 ± 0.04

Table S2. 5. Calcium and magnesium loss in bioreactors

Reactor I.D./Parameters		Mean results ± SD (n = 2)	
		Calcium loss (%)	Magnesium loss (%)
Light	Hokendauqua Creek	31.4 ± 15.89	9.28 ± 0.57
	Indian Creek	7.33 ± 0.11	4.71 ± 3.92
	Little Lehigh River	23.04 ± 2.54	27.54 ± 0.65
	Monocacy Creek	35.85 ± 1.94	4.08 ± 2.42
Dark	Hokendauqua Creek	12.41 ± 1.43	10.4 ± 5.73
	Indian Creek	32.41 ± 15.98	13.81 ± 9.67
	Little Lehigh River	23.26 ± 3.04	28.70 ± 0.36
	Monocacy Creek	70.55 ± 0.58	6.05 ± 2.95
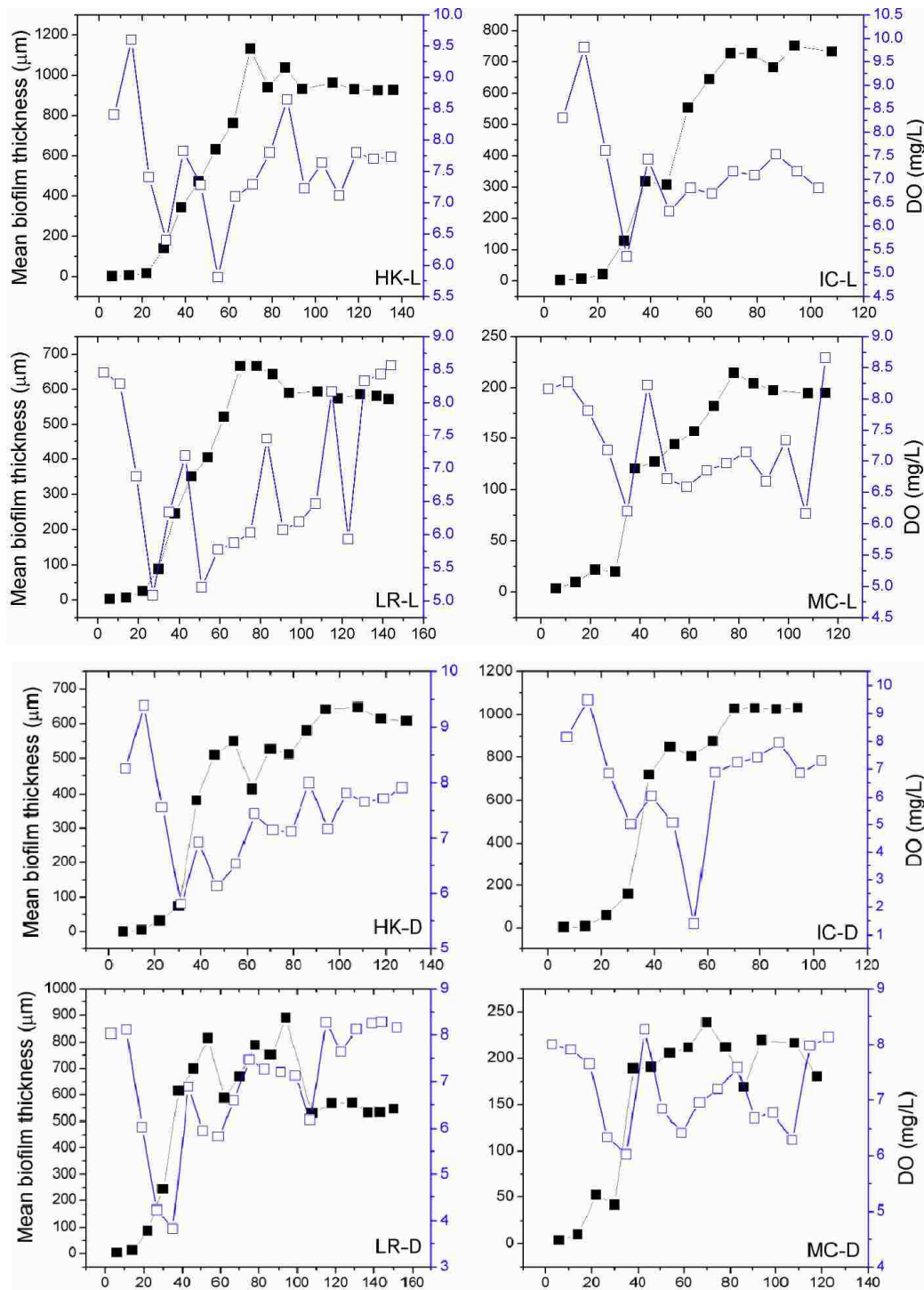
Figure S2. 1. The relationship between biofilm development and DO levels in each bioreactor under dark (D) and light (L) conditions.

HK-Hokendauqua Creek; IC - Indian Creek; LR - Little Lehigh River; MC - Monocacy Creek.
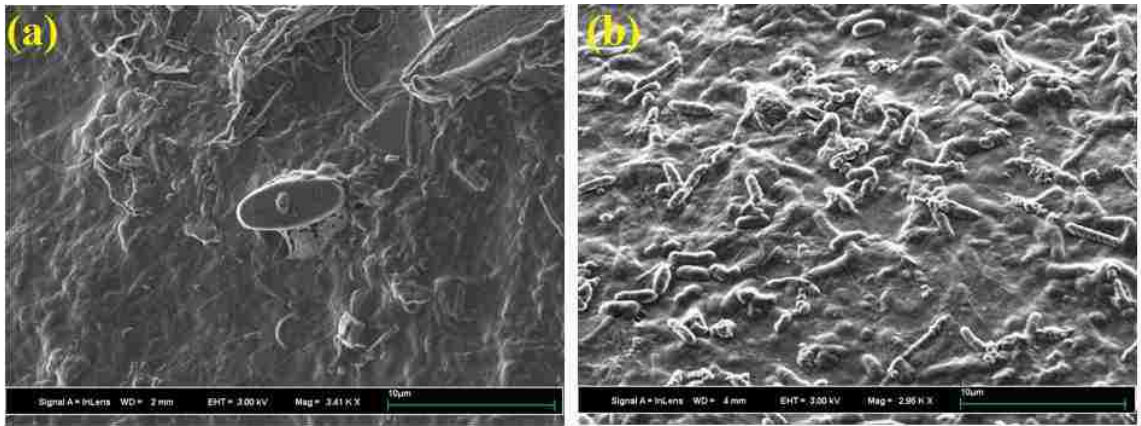
Figure S2. 2. SEM microphotographs of biofilm developed by Hokendauqua Creek water in light (a) and dark (b) conditions.

CHAPTER 3

ROLE OF SHEAR STRESS ON *CRYPTOSPORIDIUM PARVUM* OOCYST ATTACHMENT TO ENVIRONMENTAL BIOFILMS

3.1 Abstract

Hydrodynamic conditions affect microbial attachment and sloughing from biofilms. This study investigated *Cryptosporidium parvum* oocyst deposition on biofilms as a function of shear stress under laminar or turbulent flow. Annular rotating bioreactors were used to grow stabilized stream biofilms at shear stresses ranging from 0.038 to 0.46 Pa. Smooth, dense, and stable biofilms formed at high shear stress, compared to rough, loose and fluffy biofilms at low shear stress. The steady-state biofilms developed under different shear stress were then used to assess the impact of hydrodynamic condition on *Cryptosporidium* attachment. *Cryptosporidium* deposition onto biofilms followed a pseudo second-order model under both laminar (after a lag phase) and turbulent flows. Hydrodynamic conditions played a dual role of enhancing transport rates, but also inhibiting oocyst attachment efficiency due to enhancing lift and drag forces. Specifically, the total number of oocysts attached to the biofilm at steady state decreased as the hydrodynamic wall shear stress increased. The oocyst deposition rate constant increased with shear stress but dropped when the shear was too high (i.e., 0.46 Pa), suggesting that increasing wall shear stress results in faster attachment of *Cryptosporidium* due to higher mass transport until the wall shear exceeds a critical limit which prevents oocyst attachment.

3.2 Introduction

Cryptosporidium spp. are protozoan pathogens commonly present in surface water that are capable of infecting a wide range of wildlife and domesticated animals (Gomez-Bautista, Ortega-Mora, Tabares, Lopez-Rodas, & Costas, 2000; Medema, Bahar, & Schets, 1997). Several species of *Cryptosporidium* have been associated with cryptosporidiosis in humans, a gastrointestinal disease which can be life threatening for infants, the elderly, and immunosuppressed people (Thielman & Guerrant, 2004). *C. parvum* completes its life cycle within the intestine of the host and is commonly transmitted via the faeces of infected mammalian hosts as environmentally-resistant oocysts (Mawdsley, Bardgett, Merry, Pain, & Theodorou, 1995; Roefer, Monscvitz, & Rexing, 1996; Smith, 1992). As recent studies have shown that *C. parvum* oocysts readily attach to biofilms (Wolyniak *et al*, 2009, 2010), the sudden sloughing of oocysts from their associated biofilms is of great concern for water quality and human exposure to waterborne cryptosporidiosis.

The influence of hydrodynamic conditions on microbial attachment and the physical structure of biofilms has been studied (Fonseca & Sousa, 2007; Lynch & Ten Cate, 2006; P Stoodley, Cargo, Rupp, Wilson, & Klapper, 2002). An increase in hydrodynamic shear stress can cause the detachment of cells and also a decrease in bacterial activity for microorganisms not highly resistant to shear (Arrojo *et al*, 2008; Azevedo *et al*, 2006). High shear forces also enhance mass transfer between the bulk liquid and the biofilm and can therefore result in thicker biofilm growth (Fernández *et al*, 2014; Vieira *et al*, 1993).

Temperature also has an effect on bacterial activity and has been documented to impact rapid changes in aquatic microbial community composition. Adams *et al* (2010)

found that psychrophilic and psychrotolerant bacteria dominated under different temperature conditions, suggesting that bacterial populations within the biofilm matrixhad different temperature optima. Ylla *et al* (2014) found that just a 3 °C increase in water temperature led to a consequent increase of extracellular enzyme activities and organic matter decomposition ability in stream biofilms. .

To our knowledge, little is known about the effect of shear stress on the attachment of particular pathogens like *C. parvum* to environmental biofilms. In the present study, four different reactors operating under either laminar or turbulent flow were used to develop biofilms over a range of shear stresses. The main objectives of this study were to investigate (1) biofilm development under different hydrodynamic shear strengths and (2) the impact of shear stress on the mechanisms mediating *C. parvum* oocyst attachment to biofilms. Experiments were repeated using biofilms grown from winter versus summer microbial assemblages from local streams to also investigate whether biofilm development and oocyst attachment varied for different temperature-adapted biofilm communities. We developed a pseudo second-order model for oocyst deposition under different flow conditions, and then used the model to derive the initial deposition rate constant and total number of oocysts retained at equilibrium for each experiment. The results presented here permit the development of reliable predictions of oocyst attachment to environmental biofilms grown under different hydrodynamic conditions.

3.3 Materials and methods

3.3.1 Bioreactor operation and calculation of shear stress

The bioreactor consisted of a rotating drum, housing 12 removable polycarbonate coupons (11.2 × 1.1 cm) (Sheffield Plastics Inc., Sheffield, MA, USA), hanging in a sterile glass beaker filled with local stream water (Little Lehigh River, PA, USA) (Figure 3.1). Each bioreactor was exposed to air to create aerobic growth conditions, and biofilms formed on the surface of the polycarbonate coupons. A total of four bioreactors were set up to determine the effects of hydrodynamic force on biofilm formation, as well as the retention of oocysts under different flow conditions. Reactors were run simultaneously under certain constant shear stresses (achieved by adjusting the rotational speed of the drum) to simulate the flow conditions in local streams. Hydrodynamic conditions within the bioreactor were modeled as Taylor-Couette flow between concentric rotating cylinders, where the inner cylinder is rotating and the outer cylinder is fixed to generate an annular flow between those two coaxial cylinders. The equations of Fokous *et al* (Fokoua *et al*, 2013), based on the theoretical concept of Wendt (Wendt, 1933), were used since they were built using an annular reactor configuration close to the present bioreactor. Fokoua *et al* (Fokoua *et al*, 2013) showed that the inner wall shear stress of the bioreactor (τ_i) was determined according to the viscous torque (G), which is a function of the Reynolds number (Re):

$$R_e = \frac{\omega_i R_i (R_o - R_i)}{\upsilon} \hspace{4cm} \text{Equation 3. 1}$$

$$G = 1.45 \times \frac{\eta^{1.5}}{(1-\eta)^{1.75}} Re^{1.5} \text{ for } 400 \leq Re \leq 10000 \hspace{1cm} \text{Equation 3. 2}$$

$$\eta = \frac{R_i}{R_o} \hspace{4cm} \text{Equation 3. 3}$$

$$\tau_i = \frac{\rho \upsilon^2 G}{2\pi R_i^2} \hspace{4cm} \text{Equation 3. 4}$$

In these equations, ω_i is the angular velocity of the rotating inner cylinder (rad/s); R_i and R_o are the radius of the inner and outer cylinder, respectively (m); υ is the kinetic viscosity of water (1×10^{-6} m^2/s); and ρ is the water density (999.97 kg/m^3).
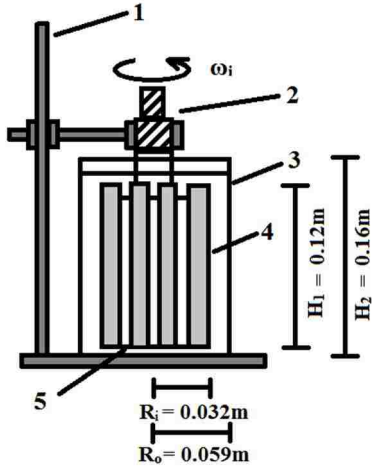
Figure 3. 1. Schematic of the annular rotating bioreactor.

1, clamp stand; 2,1/50 hp AC Dayton gear motor (Model 5VXU1, Dayton Electric Manufacturing Co., Chicago, IL); 3, 1L glass beaker; 4, polycarbonate coupon; 5, inner rotational cylinder. R_i and R_o are the radii (m) of the inner and outer cylinder, respectively; H_1 and H_2 are the height (m) of inner and outer cylinder, respectively

The shear stress in each reactor can be controlled by either adjusting the rotational speed or changing the distance between the inner and outer cylinders; in these experiments, the distance between the inner and outer cylinders was fixed, and all adjustments were made to the rotational speed of the inner cylinder. The rotational speed of the inner cylinder of each bioreactor was controlled at 25, 70, 100, and 130 rpm, respectively, resulting in wall shear stresses of 0.04, 0.18, 0.30 and 0.46 Pa, respectively, and Reynolds numbers of 2239 (laminar flow), 6269 (turbulent flow), 8956 (turbulent

flow) and 11642 (turbulent flow), respectively. These bioreactor shear stresses were similar to those calculated for typical local streams; local stream shear stresses range from 0.083 to 0.72 Pa, calculated by the conventional Reach-averaged shear stress method (Babaeyan-Koopaei *et al*, 2002).

3.3.2 Development of biofilms and monitoring of biofilm growth

Water and benthic rock biofilms in the Little Lehigh River (PA, USA) were collected in the winter (i.e., February) and summer (i.e., June) of 2015 and stored as described by Wolyniak *et al* (2010). An aliquot of 3 x 10^8 cells of the stream rock biofilm culture was introduced into 800 mL of the filtered stream water (0.45 μm retention size) in each bioreactor to improve and accelerate microbial colonization of the polycarbonate coupons. The inner rotating drum housing 12 removable polycarbonate coupons was aseptically introduced into the inoculated medium in the bioreactor. A semi-continuous mode of biofilm growth was employed, i.e., the bioreactor was emptied and replaced with an equal volume of a fresh inoculated medium every four days. Every eighth day, one to two coupons in each bioreactor were randomly selected and retrieved for average thickness measurements using an optical microscope (Nikon ECLIPSE 50i, Melville, NY) as previously described (Luo *et al*, 2015), and the drained water was analyzed for physical and chemical parameters, including pH and conductivity (Oakton Ion 510 benchtop meter, Vernon Hills, IL, USA); turbidity (HACH 2100AN turbidimeter, Loveland, CO, USA); hardness (HACH Method 8204); alkalinity (HACH Method 8203); nitrate-N, nitrite-N, and ammonia-N (HACH Method 8171, 8507, and 8155, respectively); phosphorus (HACH Method 8048); and dissolved oxygen (YSI 5000

benchtop meter, YSI Inc., OH, USA). The biofilm roughness coefficient (R) was measured using equation 5, as described by Searcy *et al* (2006):

$$R = \frac{1}{N}\sum_{i=1}^{N}\frac{|L_i - \bar{L}|}{\bar{L}}$$ **Equation 3. 5**

where N is the number of thickness measurements (N=50 for each measured R value), L_i is the ith individual thickness, and $\bar{L}$ is the mean biofilm thickness. All experiments were carried out in batch mode under aerobic conditions at room temperature.

3.3.3 Determination of biofilm average specific growth rate

Biofilm growth curves, representing the mean biofilm thickness of 50 readings across the transect of the polycarbonate coupon as a function of time, were used to determine biofilm growth rates. A least-squares regression was performed on the exponential stage of the growth curve to ascertain the biofilm growth rate according to Wentland *et al* (Wentland, Stewart, Huang, & McFeters, 1996). The slope of the regressed line was taken as the biofilm specific growth rate (day^{-1}).

3.3.4 Spiking test

Once biofilms reached steady-state thickness, one of the twelve coupons in each bioreactor was removed, scraped using a sterile Falcon® cell scraper (Handle: 18cm; Blazer: 1.8cm, Fisher Scientific, Pittsburgh, PA), and resuspended in 10 mL Milli-Q water (Millii – pore, Bedford, MS). Five (5) mL of well-mixed sample was centrifuged at $1100 \times g$ for 15 min, and the pellet (~0.5 mL) was processed through immunomagnetic separation (IMS) according to manufacturer's recommendations (Dynabeads anti-*Cryptosporidium*; Dynal A.S., Oslo, Norway) and an immunofluorescent assay (IFA, as

described below) to quantify oocysts in the sample and confirm that no *Cryptosporidium* spp. were present in the mature bioreactor biofilms. A sterile clean coupon was inserted into each bioreactor to replace the IMS-processed coupon and maintain the shear condition at the surface of the inner cylinder. For each bioreactor, the inner rotating cylinder (with all twelve polycarbonate coupons) was removed and placed into a new sterile beaker containing 10^5 oocysts spiked into 800 mL of prefiltered stream water (0.45 µm retention size). Rotational speed of the inner cylinder in the new beaker was maintained to match the rotational speed in the original beaker during the biofilm growth phase. At each time point (0.5, 1, 3, 6, 9, 12, 18, 24, 48, 72, 96 and120 h), 5 ml of spiked water was removed from the bioreactor and an equal volume of prefiltered stream water was added back to ensure that the total volume of water in the bioreactor was maintained at 800 mL. The 5-mL sample removed at each time point was centrifuged at $1100 \times g$ for 15 min, and the concentrate obtained (~100 µL) was processed by IFA to quantify the oocysts remaining suspended in water. The total number of oocysts attached to surfaces within the bioreactor system at each time point was calculated by subtracting the number of oocysts remaining suspended in the bioreactor water from the total (i.e., 10^5 oocysts) added to the bioreactor.

3.3.5 Coupon processing

At the end of the spiking test, one of the eleven coupons with mature biofilms was removed and cut into small pieces (~2.5 × 1.1 cm each) for analysis by confocal laser scanning microscopy; two coupons with mature biofilms were removed and scraped with a sterile Falcon® cell scraper for dry weight (DW), ash-free DW, organic mass, and water content analyses; and two coupons with mature biofilms were removed and scraped

for protein quantification (Protein Assay Kit II, cat #: 500-0002, Bio-Rad Inc., Hercules, CA) and cell enumeration by DAPI staining (only for the summer biofilms). Biomaterials on five additional coupons and the inner rotating cylinder were scraped and vortexed in 100 mL Milli-Q water. Five (5) mL of the well-mixed sample was centrifuged at $1100 \times g$ for 15 min, the supernatant was reduced to approximately 1 mL, and the pellet (~0.5 mL) was mixed vigorously to homogenize. *C. parvum* oocysts in the homogenized pellet were recovered by IMS, and purified oocysts were then enumerated by IFA (as described below). The number of oocysts per unit surface area of biofilm was calculated by dividing the number of oocysts quantified in the pellet by the scraped surface area (i.e., 330.05 cm^2); the total number of oocysts retained in biofilms in the bioreactor was calculated by multiplying this value by the total area of the bioreactor with mature biofilms (i.e., 403.55 cm^2).

The clean coupon used to maintain the shear condition at the surface of the inner cylinder, along with the new beaker surface, was scraped with a sterile Falcon® cell scraper. The scraped biomaterial was resuspended in 15 mL Milli-Q water and centrifuged at $1100 \times g$ for 15 min. The supernatant was reduced to approximately 1 mL, the pellet (~0.5 mL) was mixed vigorously to homogenize, and the homogenized pellet was processed by IMS and IFA to quantify the number of oocysts attached. The number of oocysts attached to scraped surfaces in the reactor (i.e., mature biofilms and clean surfaces) was compared to the number of oocysts calculated to be attached to biofilms according to mass balance calculations at the final time point of the spiking tests.

3.3.6 Quantification of *Cryptosporidium* oocysts by the immunofluorescence assay (IFA)

Oocysts were enumerated by immunofluorescence microscopy as follows. Fifty (50) µL of the 100-µL IMS product, or 10 µL of purified oocyst stock (10^4 oocysts/mL) (Waterborne Inc., New Orleans, LA) plus 40 µL of Milli-Q water, was placed into a 1.5-mL polypropylene tube. Oocysts were stained using the Crypt-a-Glo fluorescent antibody staining kit (Waterborne Inc., New Orleans, LA) in accordance with the manufacturer's recommendations. Microscopic examination was performed with a Nikon ECLIPSE 50i epifluorescence microscope (Melville, NY). The oocysts stained with the fluorescein isothiocyanate (FITC)-conjugated antibody were observed using a FITC filter cube with an excitation band of 465 - 490 nm and an emission band of 515 – 555 nm.

3.3.7 Protein micro-assay

Scraped biomaterials from two coupon surfaces were resuspended in Milli-Q water (8 mL for each coupon). Protein quantification was performed using the Protein Assay Kit II (Bio-Rad). Three to five dilutions of the BSA protein standard (the linear range of the assay for BSA is 1.2 to 10 µg/mL) were prepared. An 800-µL aliquot of each standard and well-mixed biofilm sample suspension was transferred into a separate clean, dry 1.5-mL microcentrifuge tube (protein standard solutions were assayed in duplicate), and 200 µL of dye reagent concentrate was added to each tube. The tubes were vortexed and incubated at room temperature (for at least 5 minutes but no more than one hour). For each sample and standard, absorbance at 595 nm was measured using a GeneQuant pro spectrophotometer (Amersham Biosciences, NJ).

3.3.8 Biofilm cells enumeration

Biofilm samples recovered from the coupon surface were incubated with 5 µg/ml proteinase K at 37 °C for 1 h to decompose the EPS without damaging the DNA of cells that may bind to these compounds (Wu & Xi, 2009). Biofilm samples were then fixed by adding three volumes of filtered (0.2 µm pore size), freshly prepared 3-4% glutaraldehyde (Sigma, Deisenhofen, Germany) in phosphate-buffered saline (PBS; 10 mM NaPO$_4$ [pH 7.2], 120 mM NaCl) to one volume of bacterial suspension, and the samples were incubated overnight at 4 °C (Amann *et al*, 1990). Cell counts were determined by 4'6-diamidino-2-phenylindole (DAPI) staining according to the protocol of Porter and Feig (Porter & Feig, 1980).

3.3.7 Dry weight and ashed weight

Scraped biofilms were collected in a preweighed 50-mL pretreated glass beaker (i.e., heated to 500°C for 3h and cooled down to room temperature). The beaker with biofilms was weighed, and the saturated biofilm weight (W$_{biofilm}$) was calculated by subtracting the empty beaker weight from this weight. The beaker with biofilms was dried at 105°C in a drying oven overnight and reweighed; the dry weight (W$_{DW}$) was calculated by subtracting the empty beaker weight from this weight. The dried biofilms along with the glass beaker were ashed for 3 h at 500°C, and the ashed weight (W$_{AW}$) was calculated by subtracting the empty beaker weight from this weight. The biofilm organic matter content was determined by subtracting the ash-free dry weight from the dry weight (Amalfitano *et al*, 2008; APHA 1989). The water content was calculated by subtracting the dry weight from the saturated biofilm weight.

$$\text{Water content } (\%) = \frac{W_{\text{biofilm}} - W_{\text{DW}}}{W_{\text{biofilm}}} \times 100\% \qquad \text{Equation 3. 6}$$

$$(\text{Organic matter content} = W_{\text{DW}} - W_{\text{AW}} \qquad \text{Equation 3. 7}$$

3.3.8 Confocal laser scanning microscopy

Coupons containing biofilms with attached *C. parvum* oocysts were incubated in 5% fetal bovine serum (FBS; Hyclone, Logan, Utah) in PBS for 30 min at 37 °C to block any non-specific binding of antibodies. Coupons were washed twice with 1×PBS (with 50 mM glycine) for 5 min and then incubated with 25 µg/mL of anti-*C. parvum* sporozoite immunoglobulin M (IgM) monoclonal antibody conjugated with the fluorochrome Cy3 (Crypt-a-Glo, Waterborne Inc, New Orleans, LA) for 1 h at 37 °C in the dark to stain the attached *C. parvum* oocysts. The specimen was gently washed twice with 1×PBS (with 50 mM glycine) for 5 min, and then 20 µM SYTO 9 (Invitrogen, Molecular Probes, Eugene, OR) was added to stain the environmental biofilms. Fluorescence was observed by a Zeiss LSM 510 META laser scanning microscope, using an argon laser (458-nm, 477-nm, 488-nm, and 514-nm excitation wavelengths) and a HeNe1 laser (543-nm excitation wavelength).

3.4 Results

3.4.1 Water

No significant changes occurred in the water quality within each bioreactor and the stored water during the course of the two experiments with winter and summer biofilms, respectively (ANOVA; $P > 0.9$; Table S3.1). In addition, ANOVA analyses for the four

bioreactors operated under different shear stresses revealed that hydrodynamic force did not impact the water quality within bioreactors ($p > 0.1$ for both the winter and summer water). The stored summer stream water had significantly higher pH (t-test, $p = 0.016$) and alkalinity (t-test, $p = 0.016$), but significantly lower concentration of nitrates (t-test, $p = 0.0058$), than the winter stream water; however, other water quality parameters did not differ significantly between seasons (t-test, $p > 0.05$). Significant differences were noted for conductivity and alkalinity levels within bioreactor run by different water. The data show that conductivity levels within each bioreactor operated with winter water were significant higher than those operated with summer water (t-test, $p < 0.05$), whereas the alkalinity levels within each bioreactor operated with winter water were significant lower than those operated with summer water (t-test, $p < 0.05$). The phenomena were probably due to the higher conductivity (t-test, $p = 0.052$) and significant lower alkalinity (t-test, $p = 0.016$) levels in winter water.

3.4.2 Biofilm development

Figure 3.2 shows the thickness of biofilms grown with winter and summer stream water and biomaterial. Depending on shear stress, steady-state biofilm thickness at the end of the experiments ranged from 175 to 1689 µm for biomaterials collected in winter, and from 182 to 572 µm for biomaterials collected in summer. For the winter bioreactors, the thickest biofilm developed at a shear stress of 0.18 Pa, whereas for the summer bioreactors, the thickest biofilm developed at a shear stress of 0.46 Pa. For summer biofilms, thickness increased significantly with increases in wall shear stress (Pearson's r $= 0.969$, $p = 0.031$); this trend was not observed for the winter biofilms.

Steady-state mean biofilm thickness was reached after 126 and 64 days of growth for winter and summer biofilms, respectively. Regardless of the season, after an initial lag phase (approximately 48 and 10 days for winter and summer biofilms, respectively), biofilm thickness increased rapidly and entered a phase of linear growth. The biofilm growth rates during the linear stage indicated in Figure 3.2 are summarized in Table S3.2.
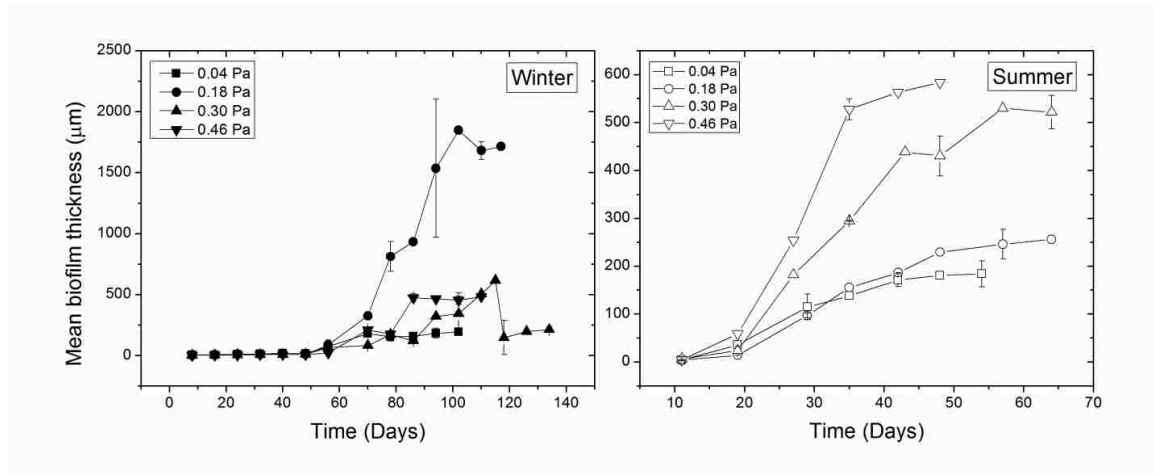
Figure 3. 2. Biofilm thickness over time in different bioreactors grown from winter (left panel) and summer (right panel) stream water and microbiota.

Data are the average thickness of two coupons from each bioreactor; error bars are the standard deviation.

3.4.4 Biofilm characteristics

3.4.4.1 Protein, dry, and organic mass in biofilms

Enhanced microbial growth associated with increasing the wall shear stress (0.04Pa to 0.46Pa) was observed by an increase in the protein, dry, and organic mass per unit surface area in both winter and summer biofilms (Figure 3.3A-3.3C)). Protein ($p < 0.12$ summer, $p < 0.032$ winter), dry ($p < 0.068$ summer, $p < 0.019$ winter), and organic mass

(p<0.078 summer, p<0.072 winter) increased with increasing wall shear stress. No significant difference in protein, dry, and organic mass was observed between winter and summer biofilms (paired t-test, $p \geq 0.058$).
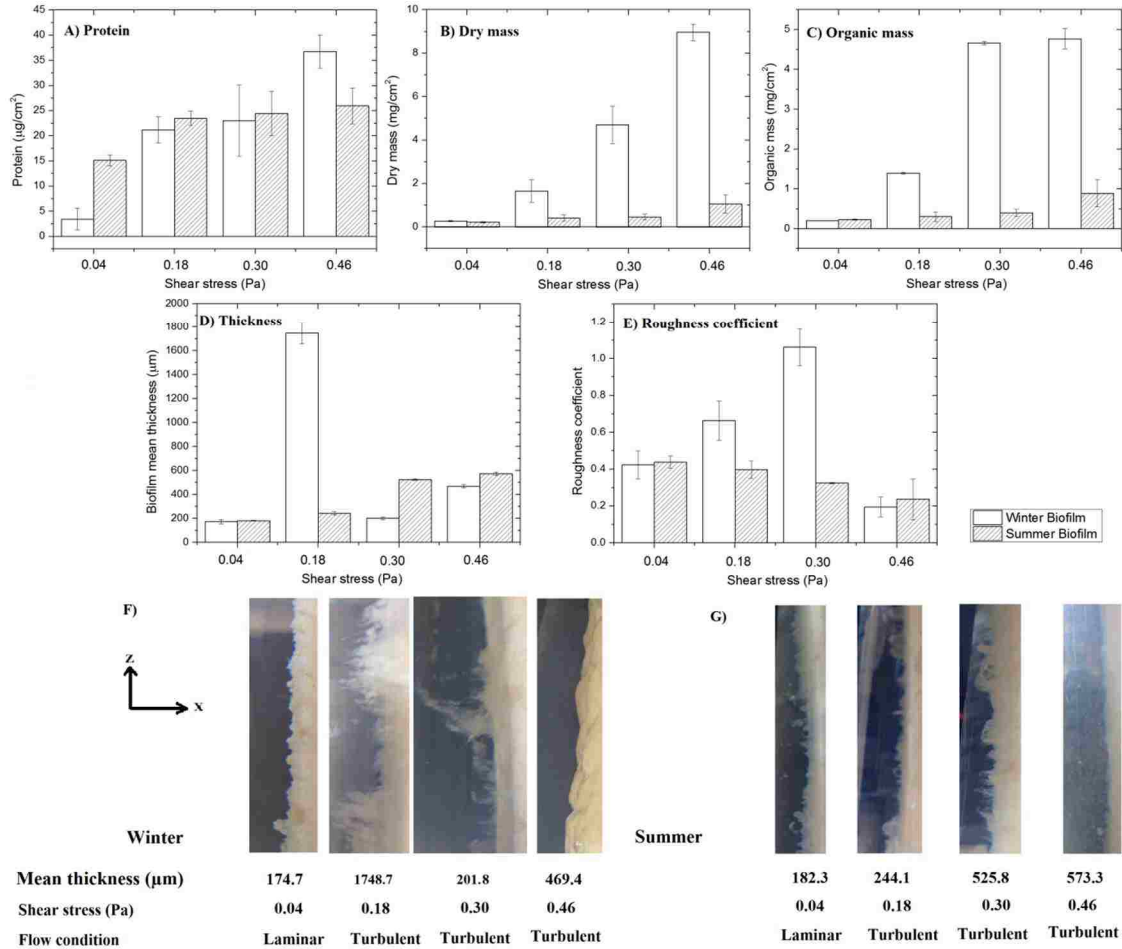
Figure 3. 3. Steady state biofilm characteristics, including the protein mass (A), dry mass (B), organic mass (C), thickness (D), and roughness coefficient (E).

Error bars indicate one standard deviation (n = 2). Panels F and G show the morphology of biofilms developed on the coupon surface as captured by a digital camera.

3.4.4.2 Biofilm thickness

At steady state, the geometric mean thicknesses of winter biofilms developed under wall shear stresses of 0.04, 0.18, 0.30, and 0.46 Pa were 174.7 (n=5, s.d.=16.92), 1748.7 (n=3, s.d.=87.92), 201.8 (n=3, s.d.=10.12), and 469.4 μm (n=4, s.d.=12.53), respectively; steady-state geometric mean thicknesses of summer biofilms developed under the same wall shear stresses were 182.3 (n=2, s.d.=2.24), 244.1 (n=3, s.d.=13.44), 525.8 (n=2, s.d.=5.79), and 573.3 μm (n=2, s.d.=14.54), respectively. No significant difference was observed between the steady state mean thickness of summer and winter biofilms (paired t-test, $p = 0.28$). For the summer biofilms, mean biofilm thickness at steady state increased with shear stress ($p = 0.06$); this trend did not hold for winter biofilms (Figure 3.3D).

3.4.4.3 Biofilm roughness coefficient

Figure 3.3E shows that biofilm roughness decreased significantly with shear stress for summer biofilms (Pearson's r = 0.991, $p = 0.0094$). However, for winter biofilms, roughness increased with shear up to 0.30 Pa and then dropped significantly at the highest shear tested of 0.46 Pa. Statistical analysis indicates that winter biofilms differed significantly from summer biofilms with respect to the roughness coefficient when bioreactors operated under 0.18 and 0.30 Pa (t-test, $p < 0.05$). These data show that the highest wall shear stress yielded the smoothest biofilms, and the lowest shear formed a relatively rougher biofilm. Moreover, Figures 3.3F and 3.3G show a visually smoother biofilm under high shear stress and a highly heterogeneous biofilm, with many protuberances and pores, at low shear stress.

3.4.4.4 Cell density

64

For the summer biofilms, the average wet biofilm bacterial cell count per unit coupon surface area was calculated to compare the average spatial concentration of biofilm cells under different hydrodynamic forces. No correlation was observed between cell density and hydrodynamic shear stress (Figure S3.1).

3.4.5 Mass balance

A mass balance was performed to verify oocyst recoveries during the spiking tests (Table 3.1). Recovery efficiency of C. parvum oocysts by IMS and IFA for scraped biofilm samples (based on controls consisting of 104 oocysts in Milli-Q water) ranged from 53 – 72.3% for the winter biofilm experiment and 71.98 – 85.44% for the summer biofilm experiment. Recovery efficiency of C. parvum oocysts by IFA for the suspension sampled at different time points (based on controls consisting of 200 oocysts in Milli-Q water) ranged from 47.52 – 79.12 % for the winter biofilm experiment and 72.44 – 75.95% for the summer biofilm experiment. Experimental oocyst losses during processing, based on mass balance calculations, ranged from -4.94 – 3.41% for winter biofilms and 2.33 – 10.32% for summer biofilms (Table 3.1).

Table 3 1. Oocyst retention and mass balance evaluation*

	% Oocysts							
	Winter				Summer			
Shear stress (Pa)	0.04	0.18	0.3	0.46	0.04	0.18	0.3	0.46
Oocyst Mass Balance Based on Suspension Analysis								
A. In suspension at end of experiment (measured)	22.86	38.10	55.24	58.04	17.97	37.94	51.72	62.85
B. Not in suspension at end of experiment (calculated; = 100-A)	77.14	61.90	44.76	41.96	82.03	62.06	48.28	37.15
Oocyst Mass Balance Based on Scraped Biofilm Analysis								
C. In scraped biofilms at end of experiment (measured)	64.00	53.46	40.18	30.15	66.27	42.14	34.91	17.60
D. In scraped biomaterial from bioreactor wall and clean coupon (measured)	0.54	0.15	0.65	0.59	2.68	2.67	2.87	2.81
E. Removed from suspension due to sampling at different time points (measured)	9.19	7.25	8.86	9.29	7.13	6.93	8.17	9.69
F. Not in suspension at end of experiment (calculated; = C+D+E)	73.73	60.86	49.69	40.03	76.08	51.74	45.95	30.10
Oocyst Losses (=B-F)	3.41	1.04	-4.93	1.93	5.95	10.32	2.33	7.05

*The table presents a summary of the proportion of oocysts attached to bioreactor surfaces, removed during sampling, and remaining in suspension at the end of the spiking experiment (120 h). Percentages were calculated by dividing the number of oocysts recovered from each sample by the total number of oocysts (10^5) spiked into each bioreactor.

3.4.6 Effect of shear stress on *C. parvum* oocyst adhesion efficiency

Scatter plots of *C. parvum* oocyst attachment to environmental biofilms as a function of time are shown in Figure 3.4 for winter and summer biofilms. A marked effect of shear stress on the adhesion kinetics of *C. parvum* oocysts was observed. Higher wall shear stress resulted in lower oocyst deposition efficiency. A lag phase was observed for oocyst deposition under laminar flow (i.e., 0.04 Pa; Figure 3.4 inset), which was shorter in the summer biofilm as compared to the winter biofilm (i.e., 1 h versus 6 h, respectively).
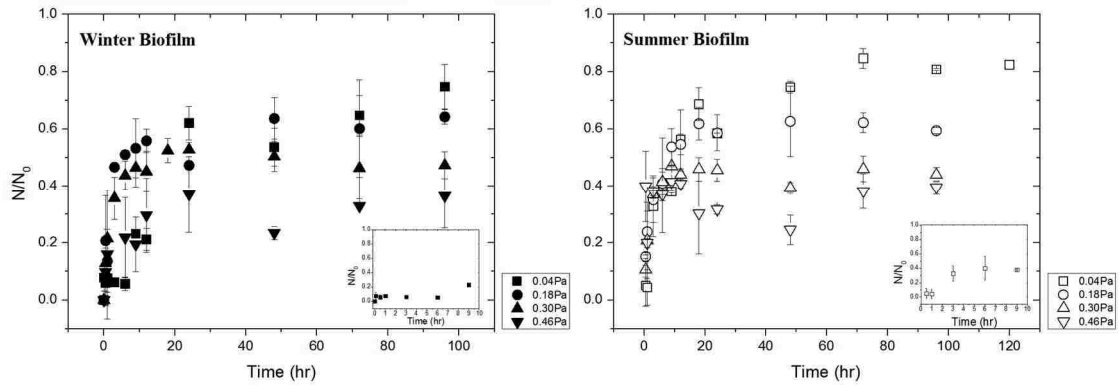
Figure 3. 4. Deposition efficiency of *C. parvum* oocysts on summer and winter biofilm surfaces as a function of time.

Error bars indicate one standard deviation of duplicate measurements at each time point. Inset shows the oocyst deposition efficiency during the first 9 hours in the bioreactor operated under laminar flow (i.e., 0.04 Pa).

3.5 Discussion

There are extensive studies concerning the shear stress on the formation of biofilms (Percival *et al*, 1999; Ollos *et al*, 2003; Lehtola *et al*, 2006; Brugnoni *et al*, 2011; Lemos *et al*, 2015), however, to our understanding, there is no systematic study investigating the effects of hydrodynamic forces on the kinetics of certain bacteria retained to well developed biofilms to date.

3.5.1 Biofilm development

Results from this study confirm previous work showing that shear stress appears to have no impact on biofilm thickness (Peyton, 1996). Although increases in the biofilm mean thickness and specific growth rate were observed with increasing shear for the summer biofilms, these same trends were not observed for the winter biofilms (Figure 3.3; Table S3.2). Presumably, bacteria collected from summer microbial stream

assemblages were able to adapt and take better advantage of increased shear forces than bacteria collected during the winter. Although we expected to see thicker biofilms develop under lower shear (and especially laminar flow) conditions due to reduced scouring and the absence of turbulent eddies (Pereira, Kuehn, Wuertz, Neu, & Melo, 2002), in reality, the biofilms developed in laminar flow were relatively thinner than those grown in turbulent flow. Howsam (Howsam, 1995) reported that turbulent flow enhances chemical nucleation as well as nutrient uptake at the biofilm surface to promote biofilm growth. Additionally, in lotic ecosystems, environmental conditions impacting microbial activity and biofilm growth, such as nutrient levels and temperature, change considerably with the season (Iriberri, Ayo, Unanue, Barcina, & Egea, 1993). Chénier *et al* (Chénier *et al*, 2003) showed that biofilms developed from river water collected at different times of the year had different microbial activities and community compositions, suggesting that microbial populations within biofilms vary significantly over the course of a year. These variations among microbial biofilm populations in different seasons may explain the lack of observed correlation between biofilm thickness and an environmental stressor like shear.

3.5.2 Biofilm structure

Smoothest biofilms were observed in bioreactors with the highest shear stress (Figure 2E). van Loosdrecht *et al* (M. Van Loosdrecht, Heijnen, Eberl, Kreft, & Picioreanu, 2002) reported that biofilms, grown at very high flow rates with large shear forces, adapt by becoming less porous and more smooth. By contrast, porous and heterogeneous biofilms predominate at lower shear forces due to mass transfer limitations and low detachment forces. They explained this phenomenon by the fact that biofilms

become more compact (i.e., less growth occurs in the outer filamentous biofilms and more in the base biofilms) at higher shear forces because filamentous structures and protrusions are detached before they can grow out. By contrast, low shear stress conditions yield a rougher biofilm as a result of biofilm erosion and the sloughing of microbial communities into the water when the biofilm reaches sufficient thickness.

3.5.3 Biofilm biomass and cell density

To further investigate the impact of wall shear stress on biofilm formation, protein, dry mass, and the organic mass of mature biofilms were measured. In agreement with previous studies (Feng *et al*, 2015; Yu Liu & Tay, 2002; M. Van Loosdrecht *et al*, 2002), we observed that biofilm biomass, including protein content, dry mass and organic mass, increased with an increase in wall shear stress (Figure 3.3). Liu and Tay (Yu Liu & Tay, 2002)reported that high shear force enabled to induce the biofilms to secrete more exopolysaccharides (EPS), which are the main composition of biofilm matrix, thus made biofilms denser. In addition to biofilm total biomass, areal cell density was measured for the summer biofilms, Figure S3.1 has shown that cell density in summer biofilms was independent of shear stress in bioreactor. In biofilm matrix, toal biofilm biomass can be divided into an EPS fraction and cell biomass, cell biomass usually accounts for $10 - 90\%$ of the organic matter ((Nielsen, Jahn, & Palmgren, 1997)). Therefore, the cell density may vary largely in different biofilms.

3.5.2 Wall shear stress on *C. parvum* oocyst deposition

Deposition efficiency curves for *C. parvum* oocsts to biofilms (Figure 3.4) are similar for both summer and winter biofilms and include an initial rapid attachment

phase, followed by a phase of slower oocyst attachment and ultimately a stable oocyst

attachment efficiency. Oocyst deposition efficiency decreased with increasing shear;

high wall shear stress likely hindered oocyst deposition efficiency as a result of the

increased drag force imposed by fluid flow. By contrast, decreasing wall shear stress was

associated with greater numbers of attached oocysts, likely due to the reduced frictional

force between the oocyst and the biofilm surface.

It is worth noting that for bioreactors operated under laminar flow (Figure 3.4

inset), a short lag phase in oocyst deposition was observed; this lag phase may be

explained by the hydrodynamic boundary layer on the biofilm surface. Turbulence

influences the thickness of the boundary layer, and subsequently the transfer resistance of

a substrate (e.g., a microorganism) from the bulk liquid into the biofilm (Chen, Ling, &

Blancheton, 2006; De Beer, Stoodley, & Lewandowski, 1996). As microbial cells

approach a surface, they must overcome the hydrodynamic boundary layer and repulsive

forces (Fletcher, 1996). Depending on the pH, ionic strength and the dominant ions in

solution, repulsive electrostatic interactions occur at approximately $10 - 20$ nm from the

surface, most often due to the fact that both the microorganism and the surface carry the

same net charge. Since the microorganism and the surface can carry both positive and

negative charges at local sites when the microorganism is around $2 - 10$ nm from the

surface, both repulsive and attractive electrostatic interactions may occur simultaneously.

Furthermore, water adsorbed at the surface can be a potential barrier for attachment, and

the hydrophobic functional groups on the microbial surface may help reduce this barrier

by displacing the water layer. As bacteria approach the surface (< 1 nm), the

hydrodynamic boundary layer and repulsive forces will be overcome by a variety of

chemical interactions, including ligand exchange reactions, ion bridging and van der

Waals forces that facilitate attachment. A number of studies have shown that a thicker

hydrodynamic boundary layer. which the bacteria have to traverse by diffusion before

attachment, will be formed under low linear velocities (Eckert, 2015; Wäsche, Horn, &

Hempel, 2002); conversely, the boundary layer thickness will be compressed at higher

flow rates or shear stress (De Beer *et al*, 1996; Eberl, Picioreanu, Heijnen, & Van

Loosdrecht, 2000; Huang *et al*, 2013; Imayama, Alfredsson, & Lingwood, 2014). The

thicker boundary layer formed under laminar flow conditions may explain the lag in

oocyst attachment to the biofilm surface observed in Figure 3.4.

The experimental data in Figure 3.4 were fitted into a pseudo-second-order model

for *C. parvum* oocyst deposition developed by Luo *et al* (Chapter 2). The model is based

on the discovery that deposition of *C. parvum* oocysts is controlled by calcium and

carboxylate functional group interactions. Both biofilms and oocysts have surface

carboxylate functional groups, and the model assumes that biofilm surfaces have plenty

active binding sites. Calcium enhances the deposition of oocysts by bridging the

carboxylate groups on both the biofilm and oocyst surfaces.

$$\frac{d[RCOO]_t}{dt} = k_1[RCOO]_r^2 = k_1([RCOO]_{eq} - [RCOO]_t)^2 \qquad \textbf{Equation 3.8}$$

where $[RCOO]_t$ is the number of carboxyl active sites bound by oocyst carboxyl

active sites at time t, $[RCOO]_r$ represents the unbound carboxyl active sites on the

biofilm, and $[RCOO]_{eq}$ is the total number of available carboxyl active binding sites at

equilibrium. The driving force $([RCOO]_{eq} - [RCOO]_t)$, is proportional to the available

fraction of active binding sites, and thus the differential equation 1 can be rewritten as

$$\frac{dN_t}{dt} = k_1(N_{eq} - N_t)^2 \qquad \qquad \text{Equation 3.9}$$

where N_t is the number of oocysts attached to biofilm at time t, and N_{eq} is the

number of oocysts attached at equilibrium. Integration of equation 3.9 for the boundary

conditions t = 0 to t = t, and N_t = 0 to N_t = N_t, results in a linear equation:

$$\frac{t}{N_t} = \frac{1}{k_1 N_{eq}^2} + \frac{t}{N_{eq}} \qquad \qquad \text{Equation 3.10}$$

where $k_1 N_{eq}^2$ is the initial deposition rate (#·hr^{-1}) as $\frac{t}{N_t}$ approaches 0. Simple

assumptions in this model include (1) calcium and carboxyl groups are excess, and (2)

detachment of oocysts is negligible compared to attachment of oocysts.

The pseudo-second order model made it possible to calculate the initial deposition

rate constant, $k_1 N_{eq}^2$, from the y-intercept of the plot of $\frac{t}{N_t}$ versus t (Figure 3.5). The

initial deposition rate constant, as well as the number of oocysts attached at equilibrium

(N_{eq}), was then assessed for correlation with wall shear stress to assess the impact of

hydrodynamic forces on *C. parvum* oocyst deposition kinetics. Figure 3.5 shows that the

experimental data obtained under laminar (after the lag phase) and turbulent flow

conditions fit the pseudo-second-order model quite well.
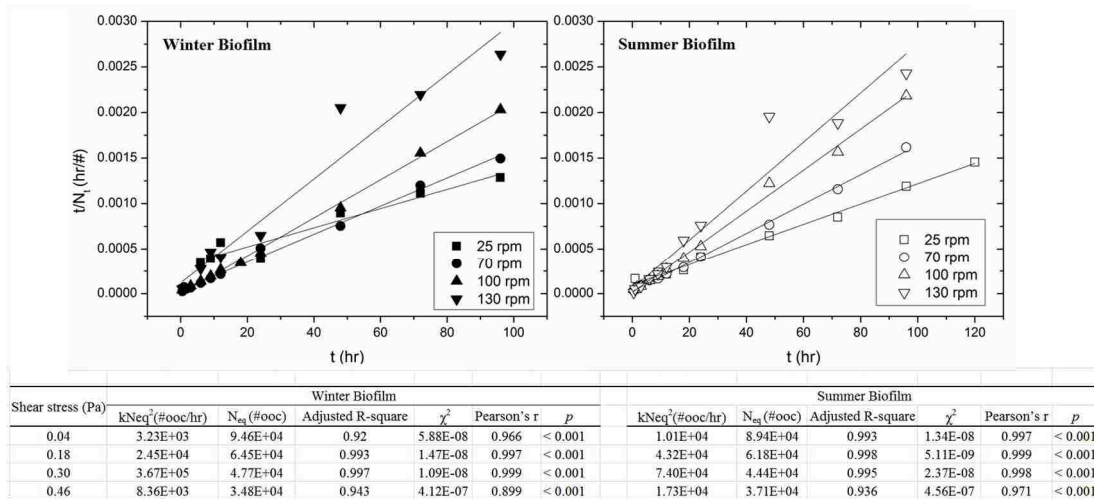
Figure 3. 5. Pseudo-second order kinetic for the deposition of oocysts onto environmental biofilms under various wall shear stress.

Shear stress (Pa)	Winter Biofilm						Summer Biofilm					
	$kNeq^2$(#ooc/hr)	N_{eq} (#ooc)	Adjusted R-square	χ^2	Pearson's r	p	$kNeq^2$(#ooc/hr)	N_{eq} (#ooc)	Adjusted R-square	χ^2	Pearson's r	p
0.04	3.23E+03	9.46E+04	0.92	5.88E-08	0.966	< 0.001	1.01E+04	8.94E+04	0.993	1.34E-08	0.997	< 0.001
0.18	2.45E+04	6.45E+04	0.993	1.47E-08	0.997	< 0.001	4.32E+04	6.18E+04	0.998	5.11E-09	0.999	< 0.001
0.30	3.67E+05	4.77E+04	0.997	1.09E-08	0.999	< 0.001	7.40E+04	4.44E+04	0.995	2.37E-08	0.998	< 0.001
0.46	8.36E+03	3.48E+04	0.943	4.12E-07	0.899	< 0.001	1.73E+04	3.71E+04	0.936	4.56E-07	0.971	< 0.001

The table below the two plots shows the kinetic parameters obtained by the pseudo-second-order model in Equation 3. χ^2 represents the deviation of the theoretical curves from the experimental points; adjusted R-square is the coefficient of multiple determination (R square) divide by the residual degrees of freedom, R square represents the square of the correlation between the response values and the predicated response values.

Oocyst attachment (N_{eq}) was predicted to be high under conditions of higher wall shear stress because of the greater number of oocysts being transported to the biofilm surface; however, we observed a decrease in oocyst attachment with an increase in shear stress (Figure 3.4). This observation may be attributed to (i) the lower contact time between the oocysts and the biofilm surface (Bakker, Van der Plaats, Verkerke, Busscher, & Van der Mei, 2003); (ii) a reduction in available oocyst binding sites after some hours due to attached oocysts occupying those sites (Bakker *et al*, 2003); (iii) the increased shear stress applied onto the biofilm surface; or (iv) the detachment of oocysts promoted by microbial collisions or biofilm sloughing (Meinders & Busscher, 1995).

Figure 3.6 shows that the initial deposition rate constant, kN_{eq}^2, increased with increasing wall shear stress until the shear became too high; in these experiments, the initial deposition rate constant dropped at the highest shear tested (i.e., 0.46 Pa) for both winter and summer biofilm experiments. This drop in the initial deposition rate constant at 0.46 Pa could be attributed to such a short contact time between the oocyst and biofilm surfaces that most of the oocysts had no chance to attach. A lower initial deposition rate constant was found in bioreactors operated under laminar flow, although the number of oocysts attached at equilibrium was higher in these laminar-flow bioreactors. These data show that oocyst attachment in the short- and long-term are impacted differently by shear; higher shear (to a certain limit) may be associated with faster initial oocyst attachment, but lower shear is associated with greater numbers of oocysts attached at equilibrium.
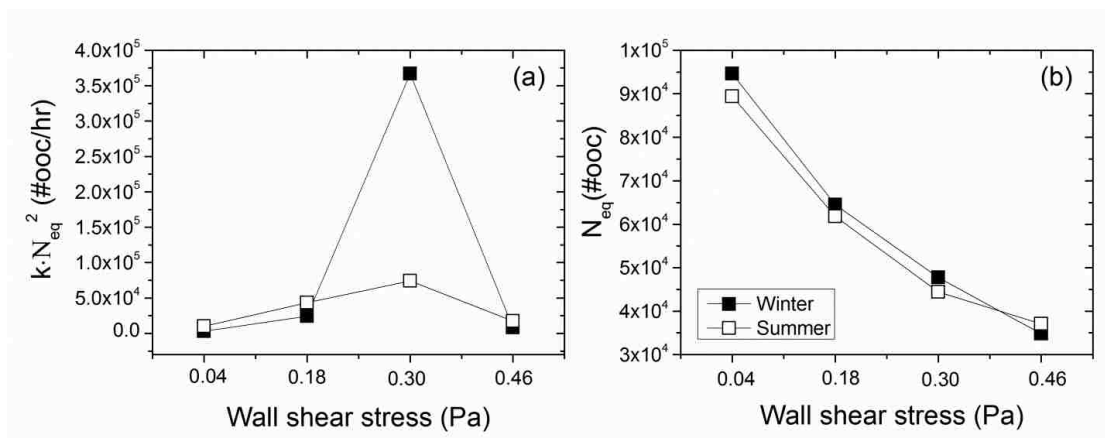
Figure 3. 6. Initial deposition rate constant (a) and total number of oocyst attached to biofilms at equilibrium (b) as a function of wall shear stress in each bioreactor for biofilms collected from different seasons (i.e., winter – closed square; summer – open square).

In industrial processes or environmental systems, biofilms usually develop under a wide range of local hydrodynamic conditions. Depending on location, season, water chemistry, and flow dynamics, biofilms are consequently characterized by different morphology, topography and microbial community compositions. An understanding of the hydrodynamic force-structure-function relationships in microbial biofims is central to interpret and predict *C. parvum* oocyst deposition. The finding that wall shear stress plays a dominant role in oocyst attachment to biofilms may thus have practical implications for removal of *C. parvum* oocysts from water and wastewater treatment plants. Also, hydrodynamic conditions should be considered when choosing sampling areas for the environmental monitoring of *C. parvum* oocysts in streams.

3.6 Acknowledgements

Table S3. 1. Water quality characteristics of bioreactor and stored water

	Mean ± SD (n)									
	Winter					Summer				
Shear stress (Pa)	0.04	0.18	0.3	0.46	Stored	0.04	0.18	0.3	0.46	Stored
pH	7.62 ± 0.58 (12)	7.68 ± 0.52 (14)	7.68 ± 0.52 (18)	7.80 ± 0.52 (15)	7.32 ± 0.48 (12)	7.91 ± 0.25 (6)	8.00 ± 0.21 (7)	8.12 ± 0.12 (7)	8.26 ± 0.24 (6)	8.13 ± 0.40 (4)
Conductivity (μs/cm)	569.44 ± 45.16 (12)	574.05 ± 57.51 (14)	571.67 ± 68.46 (18)	591.64 ± 61.63 (15)	495.92 ± 48.71 (12)	481.33 ± 49.11 (6)	488.24 ± 44.01 (7)	502.95 ± 51.42 (7)	515.50 ± 44.44 (6)	432.17 ± 44.75 (4)
Hardness (mg/L as CaCO3)	127.00 ± 14.65 (12)	132.21 ± 10.24 (14)	130.13 ± 8.06 (18)	132.46 ± 10.61 (15)	101.92 ± 6.88 (12)	119.33 ± 7.23 (6)	125.57 ± 6.21 (7)	134.14 ± 10.48 (7)	132.17 ± 6.91 (6)	103.50 ± 5.92 (4)
Alkalinity (mg/L as CaCO3)	143.08 ± 14.59 (12)	145.89 ± 13.24 (14)	148.38 ± 12.05 (18)	142.77 ± 16.47 (15)	125 ± 10.75 (12)	171.17 ± 15.43 (6)	175.00 ± 6.16 (7)	182.22 ± 6.73 (7)	184.83 ± 12.46 (6)	138.25 ± 6.40 (4)
Phosphorus (mg/L as P)	0.071 ± 0.02 (12)	0.055 ± 0.031 (14)	0.053 ± 0.033 (18)	0.050 ± 0.03 (15)	0.059 ± 0.033 (12)	0.16 ± 0.11 (6)	0.18 ± 0.16 (7)	0.13 ± 0.083 (7)	0.13 ± 0.072 (6)	0.10 ± 0.059 (4)
Nitrate-N (mg/L as NO_3^--N)	2.74 ± 0.65 (12)	2.66 ± 0.90 (14)	2.89 ± 0.78 (18)	3.18 ± 0.71 (15)	2.36 ± 0.56 (12)	1.58 ± 0.85 (6)	2.25 ± 0.72 (7)	1.9 ± 0.88 (7)	2.04 ± 0.94 (6)	3.14 ± 0.31 (4)
Nitrite-N (mg/L as NO_{2-N})	0.030 ± 0.01 (12)	0.045 ± 0.03 (14)	0.051 ± 0.049 (18)	0.052 ± 0.047 (15)	0.008 ± 0.00 (12)	0.017 ± 0.022 (6)	0.037 ± 0.026 (7)	0.046 ± 0.026 (7)	0.046 ± 0.022 (6)	0.0087 ± 0.0015 (4)
Ammonia-N (mg/L as NH_3-N)	0.009 ± 0.02 (12)	0.011 ± 0.02 (14)	0.0083 ± 0.027 (18)	0.0092 ± 0.021 (15)	0.016 ± 0.019 (12)	0.00 ± 0.00 (6)	0.005 ± 0.0090 (7)	0.004 ± 0.0079 (7)	0.006 ± 0.011 (6)	0.013 ± 0.013 (4)
DO (mg/L)	6.33 ± 3.50 (14)	6.27 ± 3.26 (16)	6.91 ± 3.26 (20)	6.56 ± 3.48 (15)	10.24 ± 1.19 (12)	7.74 ± 0.90 (6)	8.06 ± 0.75 (7)	7.96 ± 0.79 (7)	8.48 ± 0.61 (6)	10.33 ± 1.79 (4)
Turbidity (NTU)	1.93 ± 1.68 (12)	1.93 ± 1.68 (14)	14.38 ± 30.96 (18)	2.06 ± 1.81 (15)	0.46 ± 0.21 (12)	2.58 ± 1.43 (6)	5.00 ± 3.79 (7)	5.33 ± 3.95 (7)	6.34 ± 5.93 (6)	0.44 ± 0.16 (4)

Table S3. 2. Summary of biofilm average specific growth rate*

Season	Shear stress (Pa)	Biofilm growth rate (day^{-1})
Winter	0.04	7.37
	0.18	33.82
	0.30	6.56
	0.46	10.92
Summer	0.04	5.14
	0.18	6.80
	0.30	12.45
	0.46	20.64

*Growth rates were calculated by modeling biofilm development after the lag phase and before steady-state as a straight line; the biofilm growth rate (day^{-1}) was taken as the slope of this line.
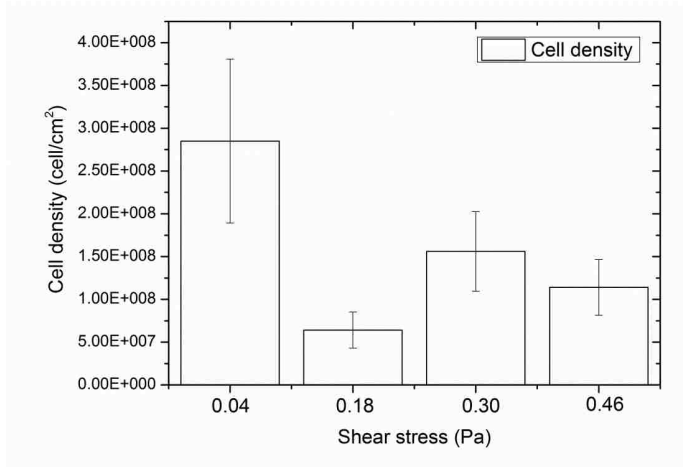
Figure S3. 1. Cell density of mature biofilms as a function of wall shear stress in bioreactors.

Error bars indicate one standard deviation (n=2).

CHAPTER 4

IDENTIFICATION OF *CRYPTOSPORIDIUM PARVUM* OOCYST IN ENVIRONMENTAL BIOFILMS BY IMMUNOGOLD LABELING

4.1 Abstract

Cryptosporidium parvum oocyst is a waterborne parasite, which has a potential to cause Cryptosporidiosis for at risk populations, including infants, the elderly, and immuno-compromised people. We have previously shown that environmental biofilms have the potential to harbor the *C. parvum* oocyst and protect them from the impact of hydrodynamic force to help oocysts survive a longer period. Identification of *Cryptosporidium* in bioilms and the further visualization of the interactions between *Cryptosporidium* and biofilm surfaces pose of interest in our study. Biofilms containing a wide diversity of microorganisms were produced using local stream water on lab-produced polycarbonate coupons within an annular rotating bioreactor. C. parvum oocysts were spiked into the bioreactor with well-established biofilms, and then labeled with monoclonal antibodies and visualized with immunogold conjugates. The focused ion beam scanning electron microscopy (FIB-SEM) enabled the visualization of nano-gold labeled *C. parvum* oocysts, suggesting that immunogold labeling is applicable to *C. parvum* oocyst observations under electron microscopy. Technical aspects of FIB-SEM are explained in detail.

4.2 Introduction

Electron microscopy is considered as an indispensable tool in investigating the intricate structures of the cell and organelle, and also to in studying the cellular biological

processes implicated in the responses to changes in the microenvironment (De Paul *et al*, 2012). The present chapter is intended to describe the main scope and protocols of the immunogold techniques which have been successfully utilized in our lab for the visualization of *Cryptosporidium parvum* oocyst. We aim to target the *C. parvum* oocyst in environmental biofilms to (i) visualize the interactions between *C. parvum* oocyst and biofilm matrix; (ii) investigate the impact of specimen preparation on *C. parvum* oocyst morphology, such as size and shape; (iii) enable the investigation of *C. parvum* oocyst ecology and biofilm structure at the same time.

Since Faulk and Taylor (Faulk & Taylor, 1971) first introduced the colloidal gold as a cell marker for the transmission microscopy, it has been widely used in cell biology (Verkleij, 1992) and microbiology (ERLANDSEN, MACECHKO, KEULEN, & JARROLL, 1996; SOLTYS & GUPTA, 1994). For example, Rogers and Keevil (Rogers & Keevil, 1992) developed a differential interference contrast technique in an episcopic mode, which enable simultaneous visualization of the total biofilm flora and gold-labelled legionellae. By immunogold labeling, Konto-Giorghi *et al* (Konto-Ghiorghi *et al*, 2009) reported that the pilus extends beyond the Streptococcus agalactiae capsule and thus serve as carrier for surface located adhesive cluster of PilA, a structural subunit protein of a pilus.

There are some advantages of particulate gold labels. Firstly, gold is inherently more stable than fluorescein, and not normally present in tissue, thus can be viewed for longer periods and reviewed after storage (Rogers & Keevil, 1992). On the other hand, the immunogold probes give the highest possible spatial resolution, and are able to

provide structural information at the macromolecular level (Powell, Halsey, & Hainfeld, 1998). Powell *et al* (Powell *et al*, 1998) incorporated both a fluorescent label and a 1.4 nm gold cluster compound to collect both fluorescence and electron microscopy data from a single labeling experiment, which could be used to check labeling of specimens before processing for electron microscopy. Therefore, the use of colloidal gold particles in microscopic imaging represents a significant improvement in resolution when using the immunochemistry method.

From its applicability as a probe for transmission electron microscopy, colloidal gold was further developed for a wide variety of microscopy, such as scanning electron microscopy (SEM) (Hermann, Walther, & Müller, 1996), bright-field light microscopy (Lackie, 1996), dark-field and epi-polarization microscopy (De Waele, Renmans, Segers, Jochmans, & Van Camp, 1988). For the application of gold nanoparticles in the bright-field light microscopy, silver could be coupled with the gold to increase the size and contrast of the marker, producing a label visible as black product. This provides an additional amplification step so that the location of immunogold labeling can be seen under the bright-field light microscopy (Lackie, 1996). De Waele *et al* (De Waele *et al*, 1988) used immunogold-silver staining (IGSS) to detect leukocyte cell surface antigens by darkfield and epipolarization microscopy, they reported that the efficiency of IGSS, as detected with darkfield and epipolarization microscopy, was four fold greater than that found with brightfield microscopy or immunofluorescence procedure.

New electron microscopy focused ion beam-SEM (FIB-SEM) has been mostly used on non-biological samples, but recently the FIB-SEM has also been used extensively on biological samples (Heymann *et al*, 2006; Heymann *et al*, 2009; Orlov *et al*, 2015). The

FIB-SEM combines a scanning electron microscopy with a focused ion beam. The images of back scattered electron (BSE) signal and the secondary electron (SE) signal are mixed and compared. The inlens back scattered electron mode built in the microscopy would allow to image the biological sample surface morphology at a significantly high resolution, thus gold particles labeled on surface have a good contrast in BSE images and in the meanwhile SE images show fine surface structures (Hermann *et al*, 1996).

Considering that understanding if the association of *C. parvum* oocysts with the biofilm is purely physical (i.e., only is a function of biofilm topography) or chemical bridging could provide information about oocysts deposition mechanisms to biofilm surface, there is a need to evaluate different microscopy protocols to offer most accurate representation of oocysts attachment. Here, protocols developed for biofilm and *C. parvum* oocyst visualization under electron microscopy were modified step by step. The studies are included two stages, in the first stage, we aim to optimize the electron microscopy analysis in visualization of *C. parvum* oocyst associated biofilms, in the second stage, we applied the immunogold labeling technique in order to localize the *C. parvum* oocyst and further to visualize the connections between oocyst and biofilm surface. In the first stage, the performance of two fixatives in preserving sugar/lipid compounds of the extracellular polyssachride substances (EPS) in biofilms samples was compared in this study. Three different coatings were tried to evaluate which coating protocol not only provided best image quality, but also preserve the morphology of original specimen. Two dehydration protocols (hexamethyldisilazane, HMDS and critical point drying, CPD) and four microscopy techniques (ESEM, VPSEM, Hitachi 4300 SEM and Zeiss 1550 SEM) were also compared to determine which imaging protocol is most

effective in observing thick biofilms morphology with respect to cell deposition details and EPS preservation, the flow chart of the investigation process for the first stage is presented in Figure 4.1. In the second stage, we explored the possibilities of the Zeiss 1550 SEM and FIB-SEM to image the gold colloidal attached to *C. parvum* oocyst surface and protocols used to optimize the image qualities. The dilution factor of the primary and secondary antibody (1:20. 1:40 and 1:100) was investigated to provide a high binding efficiency but use the least amount of antibody.
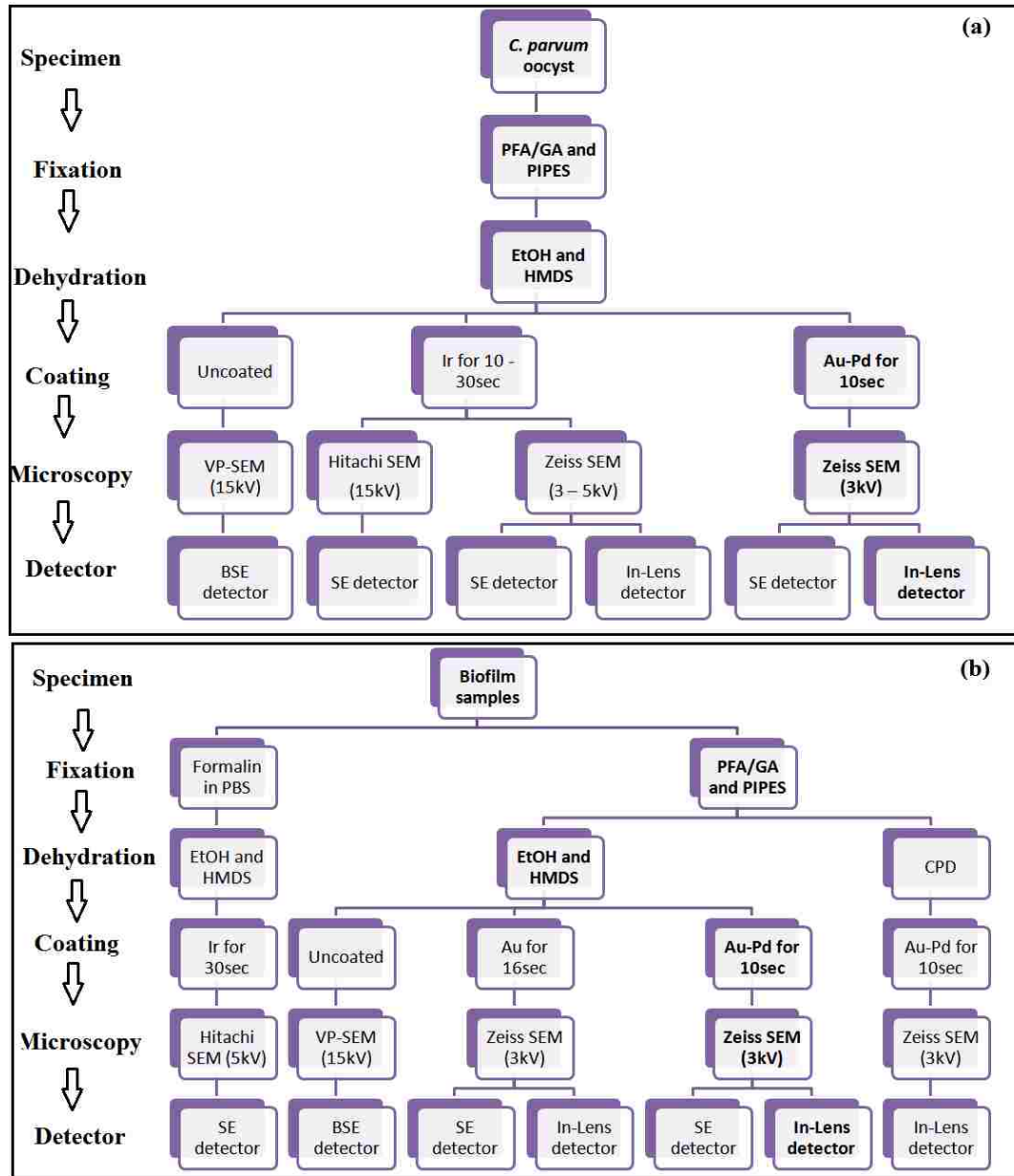
Figure 4. 1 Flow chart of *C. parvum* oocyst (a) and biofilm (b) visualization procedure by scanning electron microscopy in the first stage of the experiment.

Text in bold indicates the final developed protocol used for imaging oocyst and biofilm specimen, respectively. PFA – paraformaldehyde; EtOH – ethanol; GA – glutaraldehyde; SE – secondary electron; BSE – back scattered electron.

4.3 Materials and methods

4.3.1 Biofilm formation and *C. parvum* oocyst deposition

A rotating annular bioreactor, which is composed of a rotating inner drum and a stationary outer cylinder, was used to develop environmental biofilms for the microscopy study. Each bioreactor can house 12 removable polycarbonate coupons. Local stream water along with the rock-harvested biofilms were collected and stored as described by Wolyniak *et al* (Wolyniak *et al*, 2010). A 3 x 108 cells aliquot of the stream rock biofilm culture was introduced into 800 mL of the filtered stream water (0.45 µm retention size) in each bioreactor to improve and accelerate colonization. Biofilms were formed on the surface of polycarbonate coupons (11.2 × 1.1 cm) housing on the inner rotating drum for a period of time (range from 48 – 150 days) to reach steady state. 105 oocysts were spiked into 800 mL prefiltered stream water (0.45 µm retention size) in each bioreactor once biofilms reached to steady-state thickness. The polycarbonate coupon with mature biofilms was then cut into small pieces for electron microscopy analysis.

4.3.2 Immunogold labeling
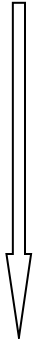
Shortly after harvesting the substrate, specimens were gently rinsed once with phosphate buffered saline (PBS) (with 50 mM glycine). Samples were incubated in 5% fetal bovine serum (FBS) in PBS for 30 min to block any unspecific binding. Following incubation for 120 min with the mouse anti-*Cryptosporidium* immunoglobulin M (IgM) antibody (Waterborne Inc., New Orleans, La) diluted 1:20 in PBS containing 0.5% FBS at 37 °C. After three washes in PBS containing 50 mM glycine (5 min each), the specimens were then covered by immunoglobulin-gold-conjugated anti-mouse IgM (10-

nm or 15-nm-diameter gold particles; Electron Microscopy Sciences, Hatfield, PA) diluted 1:20, 1:40 or 1:100 in PBS. The specimens were then subjected to three washes in PBS containing 50 mM glycine (5 min each).

4.3.3 Specimen preparation for electron microscopy

Conventional protocols used for electron microscopy related to fixation, dehydration, mounting and coating (coating is unnecessary if using Environmental SEM or VP-SEM). Table 4.1 summarizes all methods that have been investigated in our study.

Table 4. 1. Differential procedures of electron microscopy studies to detect *C. parvum* oocyst

Time	Specimen preparation	Treatment		
		# 1	# 2	# 3
	Subject	Biofilm	*C. parvum* oocyst and/or biofilm	*C. parvum* oocyst and/or biofilm
	Immunogold labeling	NA	NA	See Materials and Methods for details
	Fixation	10% formalin in PBS	1% paraformaldehyde (PFA) /1% glutaraldehyde (GA) in 0.05 M PIPES overnight at 4°C. The specimen was then rinsed with 0.01 M PIPES + 0.001M $CaCl_2$ to remove excess fixative. The last rinse takes place overnight at 4°C. In the morning, replace the 0.01 M PIPES (without $CaCl_2$) once prior to dehydration	2.5% glutaraldehyde (GA) in $1 \times$ PBS (pH 7.4) for 60 min
	Dehydration	Specimens were dehydrated through a graded series of ethanol (35, 70, 85, 95 and 100%) followed by a graded series of hexamethyldisilazane HMDS (50 and 100%) or by critical point drying (CPD) with CO_2		
	Coating	Iridium for 30 seconds	Gold; Gold and palladium	Iridium for 10 sec
	Electron microscopy	Hitachi 4300 SEM Voltage was 5 - 15 kV with a working distance of less than 17.2 mm.	Zeiss 1550 SEM Voltage was < 5 kV with a working distance of < 10 mm; Hitachi 4300 SEM in variable pressure (VP) mode, 15 – 30 kV with a working distance of 10 mm; Environmental SEM	Zeiss 1550 SEM Voltage was 5 kV with a working distance of < 10 mm; Focused ion beam – SEM (FIB-SEM), for accelerating voltages of 5 kV, the in lens SE and BSE were used at a working distance of 2 mm
	Element analysis	NA	Energy dispersive X-ray spectroscopy (EDX)	NA

NA – not available.

4.4 Results

As described in the Methods, we first developed preparation protocol to visualize

the *C. parvum* oocyst, followed by preparation protocols for the environmental biofilms.

Based on those results, we developed the immunogold labeling approach to localize the *C.*

parvum oocyst. The optimized staining protocols for *C. parvum* oocysts were then tested

with more complex (i.e., in biofilms spiked with *C. parvum* oocyst). The results are provided in this order.

4.4.1 Treatment 1

We started with a two-week old stream biofilms developed on glass microscopy slide to give us a rough idea about what the environmental biofilms looks like under the scanning electron microscopy after preparation. Figure 4.2(a) shows that complete sample discharging is achieved by iridium film thickness of 10 nm. The fine details of cell surfaces are visible in the image. In this treatment, a 10% neutral buffered formalin, a most widely used fixative for histology and histopathology (James *et al*, 2008; Perloff & Palmer, 2005; Sedghizadeh *et al*, 2008), was applied for biofilm specimen. Cell surface foldings were clearly observed in specimen due to cell shrinkage artifact (Figure 4.2 (b)), suggesting that formalin may not be an appropriate fixative for our study. Using of improper fixative may cause poorly fixed internal structures and induce specimen shrinkage, thus it is necessary to alter strength or type of fixative in the following treatments.
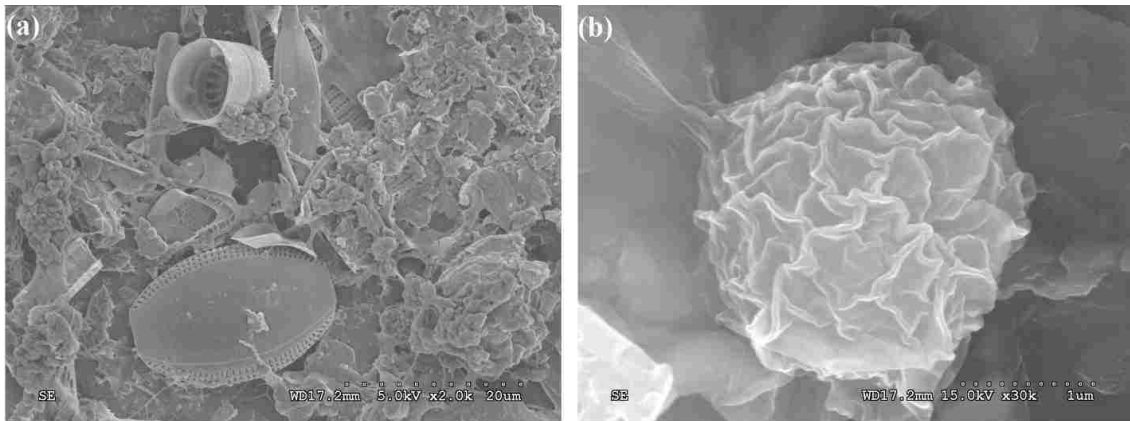
Figure 4. 2. SEM images from treatment 1. SEM imaging acquired with an acceleration voltage of (a) 5 kV and (b) 15 kV, respectively, using SE mode in Hitachi 4300 SEM for environmental biofilms developed on microscope slide. Scale bars indicate 20 μm and 1 μm, respectively.

4.4.2 Treatment 2

Thus, 1% PFA and 1% GA were used as fixative in treatment 2 to stabilize cell morphology and tissue architecture. Additionally, the application of conventional SEM in the treatment 1 cause the callapse and flasking of biofilm specimen due to the high vaccum in coating sputter, thus the VP-SEM was used in the treatment 2 to minimize the deleterious effects during processing. When VP-SEM was applied to the specimens without coating, beam irradiation damages were observed, the cells in specimen were severed or distorted (Figure 4.3 (a – b)). Moreover, the poor signal to noise ration of VP-SEM due to gas in the specimen chamber resulted in obscuring fine cellular features of the specimen (Figure 4.3 (a – b)). The Zeiss 1550 SEM images of both the *C. parvum* oocyst positive control and biofilm specimen with gold-palladium coating operated under inlens mode are shown in Figure 4.3 (c). In contrast to the environmental SEM, cells on those specimens were well preserved with very little morphological distortion, key

identification characteristics of the cells were clearly evident. Figure 4.3 (c) and (d) show images that were acquired with the inlens and conventional Everhart-Thornley (ET) detector, respectively. The inlens detector located at a shorter distance from the sample than a conventional lateral detector, on one side, the collection solid angle for high-energy BSE is larger for the inlens detector than the ET detector, on the other side, the inlens detector is able to collect more secondary electrons than the ET detector, thus resulting in better contrast than ET detector. However, the inlens detector in the Zeiss 1550 SEM only equipped with the SE mode not the BSE mode, thus there was no sufficient BSE signals coming from gold particles on the *C. parvum* oocyst to allow the visualization of individual gold markers even using a high accelerating voltage (*e.g.*, 10 kV). In our study, ethanol bath and HMDS resulted in improved preservation of extracellular matrix in biofilms, whereas CPD drying showed more collapsed hyphae and fibrous structures connected by sheets of EPS (Figure 4.3 (e)).

The first two treatments were used to visualize the morphology of oocyst associated environmental biofilms, but due to the interferences of a number of other microorganisms which have similar features as the oocyst, and due to the distortion of oocyst after processing, the visualization of oocyst in environmental biofilms, and specifically the interaction between oocyst and biofilms was inhibited by using the above treatments. Therefore, the following treatment was mainly focusing on the application of immunogold labeling strategy on identification of oocyst in environmental biofilms.
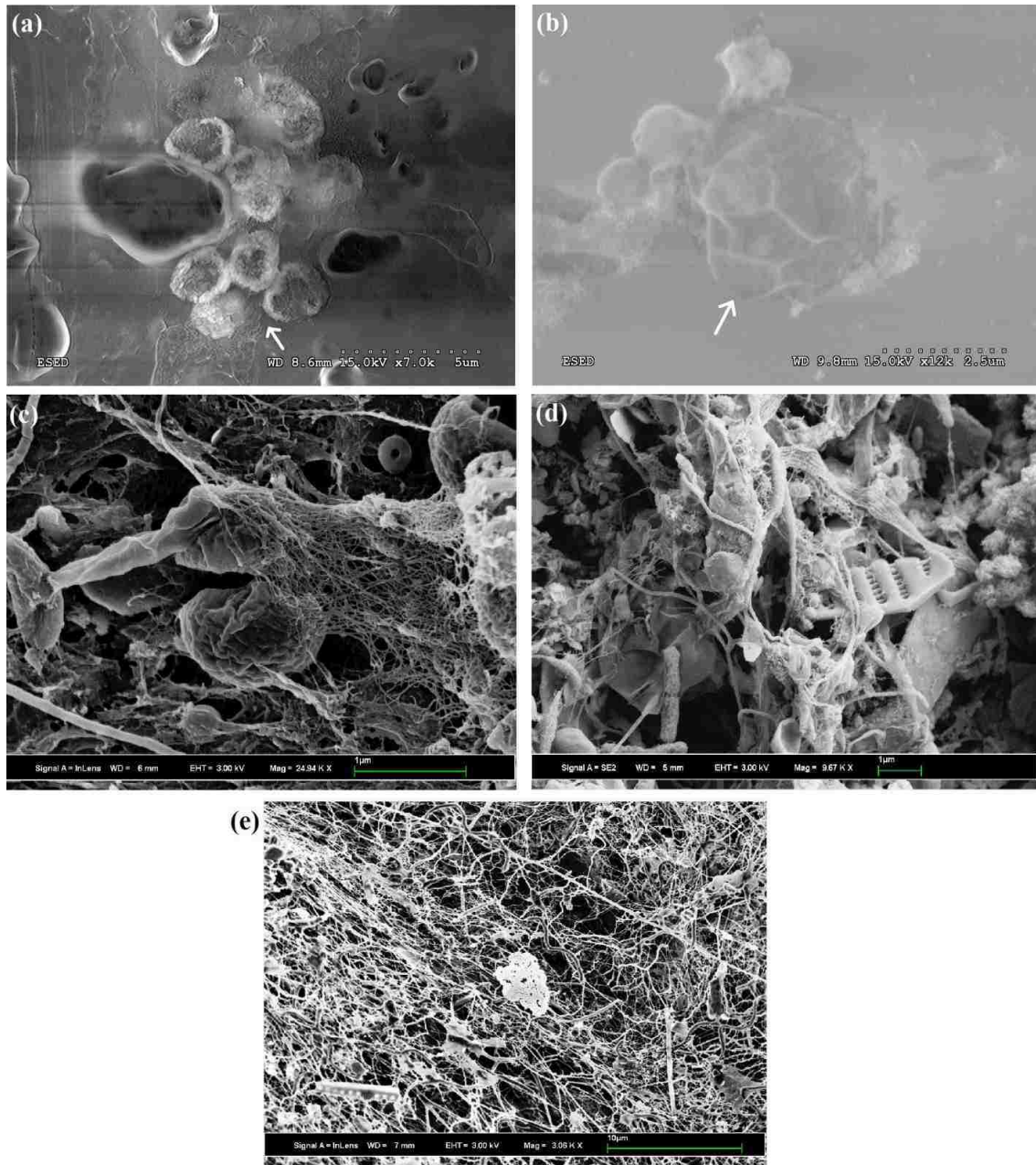
Figure 4. 3. SEM images from treatment 2. Hitachi 4300 VP-SEM images of (a) environmental biofilms; (b) *C. parvum* oocyst positive control without coating. White arrows indicate the cell distortion by beam irradiation damage. Zeiss 1550 SEM imaging with HMDS drying followed by gold-palladium coating obtained with an acceleration voltage of 3 kV, using inlens (c) and ET (d) detectors for environmental biofilms. Zeiss 1550 SEM imaging with CPD drying followed by gold-palladium coating acquired with an acceleration voltage of 3 kV by using inlens detector. Scale bars: a: 5 µm; b: 2.5 µm; c, d: 1 µm; e: 10 µm.

4.4.3 Treatment 3

4.4.3.1 Zeiss 1550 SEM

It has shown that cells observed are similar no matter with or without PFA addition for fixation (graph not shown), thus we used the 2.5% GA alone in treatment 3. Carbon coating was selected here to increase specimen conductivity, moreover, carbon has a low atomic number than gold, thus could provide a good contrast of gold colloidal in BSE images. When imaging the labeled specimen by Zeiss 1550 SEM with or without carbon coating, labeling was not visible with any of the enhancements in primary antibody density, and secondary antibody density or size due to the limitation of resolution. The EDX equipped with the Zeiss 1550 SEM failed to detect a significant signal from the gold on the specimen. This is probably because instead of forming gold clusters, the immunogold markers were dispersed throughout the *C. parvum* oocyst surface, given the low gold density within the scanning region, the intensity measured on the peak of the EDX consisted mainly of background.

The Zeiss 1550 SEM did not allow us to either visualize the individual gold collodials or confirm the presence of gold particles by EDX, therefore new labeling protocol which is able to form gold clusters on oocyst surface, or microscopy which has a better resolution to observe oocyst surface details, was required then. FIB-SEM is combined the inlens detector in the BSE mode, thus was promising on gold colloidal visualization. When imaging labeled sample by FIB-SEM, not only the signals of gold particles but also the morphology of labeled surfaces could be showed under the BSE mode. Optimal labeling conditions for the FIB-SEM were determined by varying the size

and the density of secondary antibody in the procedure. The results are shown in Figure
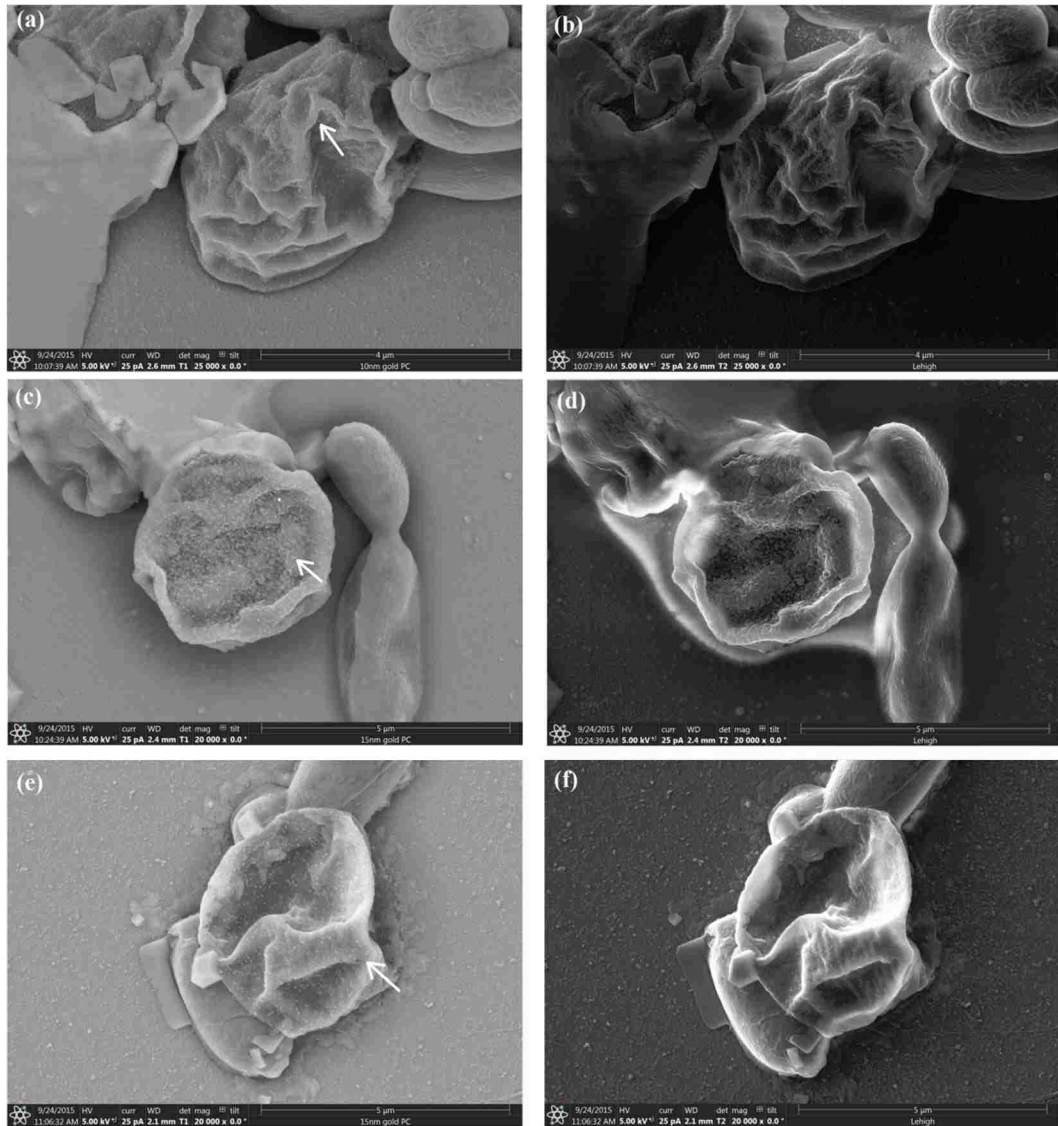
4.4.

Figure 4. 4. FIB-SEM images of the *C. parvum* oocysts with inlens detector (a, c and e) BSE mode (5 kV) and (b, d and f) TE mode (5 kV). The working distance is less than 3 mm. Scale bars: a,b: 4 µm; c – f: 5 µm. The *C. parvum* oocyst was labeled by 1:40 dilution of (a, b) 10 nm and (c, d) 15 nm immunogold, and by 1:20 dilution of (e, f) 15 nm immunogold.

4.4.3.2 FIB-SEM

With an acceleration voltage of 5 kV, working distance of 2-3 mm, the probe currents on the specimens of 25 pA, the 10 or 15 nm gold particles were clearly visible in BSE images of *C. parvum* oocyst positive control when the specimens were coated with a 2-3 nm thick iridium film (Figure 4.4 (a, c, and e)). However, damage by beam irradiation was obvious under a probe current of 50 pA (Figure not shown). In contrast to the *C. parvum* oocysts positive control specimen, which only has a thin layer on microscopy slide, the thickness of the environmental biofilms are not constant over the entire coupon surface. It goes from the region where the biofilms have already well-established reaches its maximum thickness to the minimum one, which corresponds to the region where biofilms were detached by shear forces in flow regime. Thus the density and thickness of biofilms even on the same scanning area may not uniform, therefore, using different coating time for biofilm and *C. parvum* oocyst specimen would be necessary. A substantial charging effect (Figure not shown) was observed with iridium film thicknesses of 5 nm, suggesting that increasing the coating thickness would be necessary to reduce the charging artifact. Moreover, no pits, cracks, or discontinuities was observed when used iridium film for biofilm or *C. parvum* oocyst positive control.

Concentration, as well as particle size of the colloidal gold used was also a factor in this study. Only few markers were located at the surface of the *C.parvum* oocyst when the concentration of the secondary antibody was diluted to 1:100 (Figure not shown). With a dilution of 1:40, the gold markers were numerous and clearly detected by BSE (Figure 4.4 (a, c)). As the density of the secondary antibody increasing from 1:40 to 1:20 dilution, no significant improvement in the immunogold labeling performance was

observed (Figure 4.4 (e)). When SE images and BSE images of the same fields were compared, the appearances of the surface structures in BSE and SE images were quite similar, the BSE images had a higher contrast of gold particles than the SE images (Figure 4.4), suggesting the signals from deeper regions of the sample collected by BSE did not obscure the specimen surface outline (Suzuki, 2002). At high magnification of BSE images for the 10 or 15 nm gold particles alone (Figure 4.5 (a, c)), the gold particle had a good contrast and appeared as bright dots ~ 10 or 15 nm in diameter, whereas the gold particles in their corresponding SE images were less brighter (Figure 4.5 (b, d)). The bright dots in the *C. parvum* oocyst (Figure 4.4) specimen have the similar size and features with those in the gold particle specimen (Figure 4.5). The results suggest that the *C. parvum* oocysts were labeled successfully, and the gold particles attached were able to be detected by the BSE images of FIB-SEM. In general, as the gold particles become smaller, the labeling efficiency will increase and the BSE signal decrease (Heinzmann, Reininger, Autrata, & Höfler, 1994). However, this trend is not evident in our study, no significant difference between specimen labeled by 10 nm and 15 nm gold markers with respect to labeling efficiency. The best combination of coating, resolution and signal-to-noise ratio in our study are 5 kV beam voltage plus -1.5 kV beam receleration at a working distance of less than 3 nm with 1.7 nm (for *C. parvum* oocysts positive specimen) iridium coating.
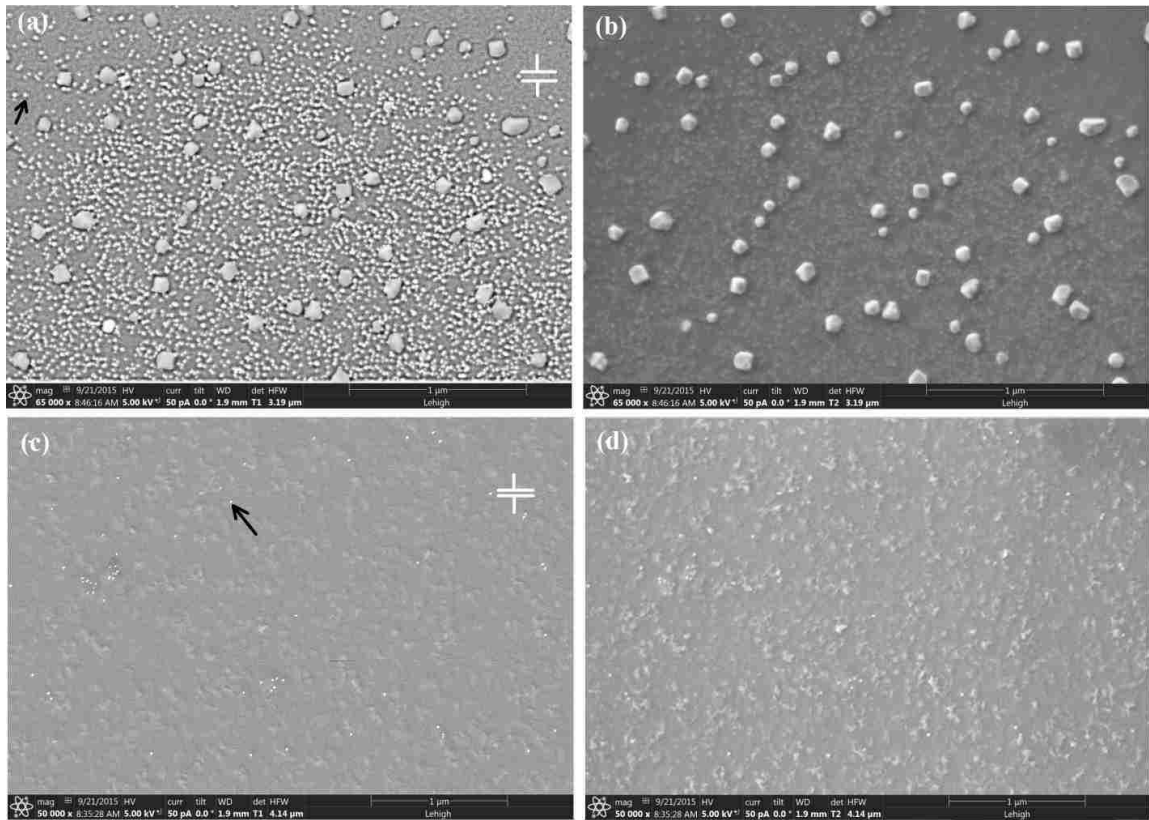
Figure 4. 5. FIB-SEM images of the secondary antibody with (a, b) 10 nm and (c,d) 15 nm gold conjugate acquired with inlens detector (a, c) BSE mode and (b, d) ET mode. Scale bars: 1 μm. Black arrows indicate the gold marker, white scale bars in panel a and c show the size of the gold particle is at 10 and 15 nm, respectively.

4.5 Discussion

Immunoelectron microscopy is one of the best methods used for detecting and localizing proteins in cells and tissues, and furthermore to provide insights into the structure-function associations (De Paul *et al*, 2012). The successful application of immunoelectron microscopy requires an adequate handling of biological samples, including fixation, dehydration, as well as the selection and modification of the electron microscope itself. In this study, we performed immunogold labeling prior to fixation to preserve the antigenicity of the molecules, and to avoid the specimens to be exposed to

harmful or possibly damaging chemicals that can lead to the blocking or loss of target proteins (De Paul *et al*, 2012; Gutièrrez-Mecinas *et al*, 2008).

4.5.1 Fixative

Fixation, a critical step in biological specimen preparation for SEM, is used to stabilize the subcellular components as well as to induce the fast arrest of biological activities with a minimal distortion of the cellular structures (De Paul *et al*, 2012). There is not one fixative suitable for all applications. Small fixative molecules, such as paraformaldehyde (PFA), penetrate more rapidly than larger ones, such as glutaraldehyde (GA), however, the larger ones usually posses more reactive sites and can thus cross-link and stabilize the cellular components more thoroughly (De Paul *et al*, 2012). Therefore, a mixture of GA and PFA could take advantage of the latter which has rapid tissue penetration although the fixation rate is not as rapid as that of GA (Kiernan, 1999). The artifacts which we observed in specimen with formalin fixation did not appear as we used a mixture of PFA and GA fixatives, or GA alone. 10% neutral-buffered formalin is really a 4% formaldehyde solution. It has shown that formaldehyde and glutaraldehyde are responsible for a high quality of fixation due to the fact that they not only react to form cross-links at pH values near neutrality, but also are effective cross-linking reagents at pH value of 8 and greater (Bowes & Cater, 1966). Comparing with the formaldehyde, GA is a stronger protein cross-linker, thus would expect to performance better in preserving cell structures. It has been shown that using the 2.5% GA as fixative is able to give some mechanical strength to the entire biofilm structure so that they can withstand subsequent processing. Thus, in treatment 3, we only used the GA instead of a PFA and GA mixture to reduce the impact of other chemicals on immunolableing.

4.5.2 Dehydration

CPD drying is a general approach to biological SEM, which has been widely used
to dehydrate biological specimen (Araujo *et al*, 2003; Heinzmann *et al*, 1994; Joubert,
Ferreira, Stevens, & Cegelski, 2015). However, disadvantages of this procedure include
cell shrinkage and considerable optimization for specimen type (Araujo *et al*, 2003; Jung,
Joo, Park, & Lee, 2010). Araujo *et al* (Araujo *et al*, 2003) compared the performance of
HMDS and CPD on removing liquids from anaerobic biofilm samples taken from a
fluidized bed reactor. They reported that CPD and HMDS methods had a similar
performance in preserving specimen morphology, but the CPD was time-consuming and
led to specimen shrinkage. They concluded that the surface tension forces generated
during evaporation of HMDS did not have any deleterious effects on the biofilm and
granular sludge samples, and cell envelopes remained intact. In addition, Nation (Nation,
1983) has showed that HMDS was able to cross-link proteins, thus reducing the surface
tension and giving strength to the sample to reduce the collapse and distortion of delicate
specimens during air-drying. In contrast, the vigorous solvent exchange with the cells,
and temperature and pressure changes during CPD drying may lead to shrinkage (Boyde
& Franc, 1981). In line with those researches, the HMDS drying was a superior method
in our study, whereas lots of cracks and filamentous structures were formed in CPD
drying samples due to shrinkage.

4.5.3 Coating materials

Osumi *et al* (Osumi, Yamada, & Nagatani, 1988) have showed that dried, uncoated
biological specimens provide signals without much topographical information since they

develop an increasing charge during the SEM procedure. Therefore, specimen for SEM normally coated with metal, heavy metal or carbon to improve the conductivity. However, ion sputter coating is unable to completely cover the specimens to provide a sufficient charge dissipation from the specimen when it is too thin, on the other hand, thick coating may mask fine structure of the biological specimen, such as immunolabels. Coating time and coating materials are thus likely to be key points during electron microscopy analysis. Carbon has an atomic number much smaller than gold, thus usually provide a good contrast of gold colloidal in BSE images, but due to the poor SE signal and thick coating (usually at 5 nm), the resolution of surface topology has been reduced (Suzuki, 2002) (Figure not shown). Alternatively, by using metal or heavy metal, such as gold, gold-palladium, iridium or platinum, better results could be obtained. However, given the grain size of gold particle, sputtering of gold usually results in obscure the fine surface details (Rodighiero *et al*, 2015) (Figure not shown). In comparison to gold, gold palladium or platinum could be sputtered in much smaller grains, thus could be as effective as gold in both generating enough SE signal and reducing charging problems. However, since the gold or gold palladium has identical or very close atomic number to that of the gold nanoparticles used as markers, these coatings may mask the gold markers. Recently, iridium films have been shown to give excellent fine grain (sub nanometer) film, thus has been considered as an alternative for other metals in immunogold labeling (Fichtman, Shaulov, & Harel, 2013). In our study, the iridium films provide a good contrast and preserve high resolution features in both SE and BSE modes.

4.5.4 Electron microscopy

4.5.4.1 Environmental SEM

SEM is considered as an important tool for high resolution visualization of bacterial biofilms (Walker, Verran, Boyd, & Percival, 2001). Although the TEM has the similar preparation processes as performed for SEM, TEM requires the specimen to be cut into thin layer, and is also not applicable for observing the extent and form of surface-associated growth which is often of interest (Priester *et al*, 2007). Alternatively, in ESEM or VP-SEM, specimens are maintained at a moderate vacuum without a conductive coating, minimizing biofilm dehydration. This aids in preserving the native morphology over conventional SEM (Walker *et al*, 2001). As biofilm flaking and sloughing were experienced during specimen preparation, using VP-SEM or ESEM may better preserve our biofilm specimen. However, these techniques may limit ultrastructural analysis of individual cells and extracellular matrix, minimizing our ability to resolve high-resolution cellular features.

4.5.4.2 Zeiss 1550 SEM

One benefit of the Zeiss 1550 SEM is it is coupled with an energy dispersive X-ray spectroscopy (EDS or EDX) detector, which is a robust tool for elemental analysis in geobiological research. We were trying to take advantage of the EDX to locate and confirm the gold colloidal labeled *C. parvum* and to investigate the performance of immunogold labeling tech, however, since the gold markers were wide spread on the cell surface and the concentration of the gold particles was relatively low, thus caused the misidentification of the gold particles by EDX. Newbury (Newbury, 2009) reported when applying EDX to identify trace elements in the mass fraction range of $0.01 - 0.01$ is likely to lead to the peak identification problem due to a lack of redundancy. Other

researches also reported elemental interferences on EDX spectra from neighboring particles (Hamilton, 2012; Pietrodangelo, Pareti, & Perrino, 2014).

4.5.4.3 FIB-SEM

In comparison to Zeiss 1550 SEM, the combination of Inlens detector with the BSE mode led to better visualization of the gold particles and the specimen surface details with the FIB-SEM as shown in Figure 4.4. Comparing the SE image of immunomarked surface area with the BSE image, we were able to clearly identify immunogold markers in the BSE image because of the significant material contrast between biological matter and the gold label.

In this study, we showed that FIB-SEM makes possible more sensitive detection of immunolabels than conventional SEM, such as Zeiss 1550 SEM and Hitachi 4300 SEM. Other than TEM, this approach is a good alternative for detection of immunogold labeled *C. parvum* oocyst. However, robust, rapid identification of *C. parvum* oocysts in environmental biofilms with highly density and thickness is still limited, but the experimental protocol and the trouble shooting process, which we got through during the past a year are still valuable and useful for visualization of the interaction between oocyst and bioflms in our future study.

4.6 Acknowledgements

CHAPTER 5

CONCLUSIONS AND FUTURE RESEARCH

In this study, we observed that attachment of *C. parvum* oocysts to biofilm surfaces was mediated by calcium. Additionally, we developed a pseudo-second-order kinetic model for oocyst attachment to biofilms and investigated correlations between the model parameters and environmental conditions (including water conductivity, hardness, alkalinity, light exposure, and wall shear stress) and biofilm properties (including dry mass, organic mass, protein content, mean biofilm thickness and roughness, and chlorophyll a content). Attachment of *C. parvum* oocysts to biofilms was independent of water conductivity and alkalinity, but the removal of magnesium and calcium from water inhibited the attachment of the oocysts to biofilms. Oocyst deposition efficiency was enhanced by the addition of calcium, as well as a mixture of calcium and magnesium, to the water, whereas the addition of magnesium alone did not enhance oocyst attachment. These observations suggest that calcium is the predominant factor affecting oocyst deposition on biofilms. Increasing wall shear stress negatively affected the attachment of oocysts to biofilms grown in different seasons, suggesting the wall shear stress controlled the kinetics of oocyst attachment despite different biofilm characteristics. Biofilm smoothness and the increased drag force between biofilms and oocysts seemed to discourage the attachment of the oocysts at higher shear stresses.

Although a strong correlation between oocyst binding and biofilm surface roughness was reported by Wolyniak *et al* (2012) previously, this correlation was not evident in the current study. Biofilms with similar roughness developed under a given

wall shear stress condition in our first experiment (Chapter 2), and it is possible that the range of biofilm roughness achieved in the study was too narrow to observe any meaningful relationship between roughness and oocyst attachment. In the second experiment (Chapter 3), biofilm smoothness did inhibit oocyst attachment, but this impact on oocyst attachment was less significant than the influence of wall shear stress.

This work focused on modeling the kinetics of *C. parvum* attachment to biofilms, which is a significant step in the understanding of *C. parvum* oocyst fate and transport in the environment. Understanding the mechanisms of oocyst attachment to biofilms under different environmental conditions will be critical to the development and manufacturing of a biomimetic surface to detect oocysts in the environment; this understanding will also enable predictions of oocyst deposition under various flow regimes. However, environmental changes, including fluxuations in hydrodynamic shear force, pH and temperature, may occur after oocysts attach to biofilms and alter fate and transport predictions based on the current work. Several key issues have not been investigated here and remain a challenge for future research:

- The detachment of oocysts and biomass from biofilm matrices is a natural process that happens throughout a biofilm's lifetime. The detachment process is actually an important mechanism that helps a biofilm adapt to environmental changes, such as an increase in shear stress, a depletion of nutrients, a change of temperature, or a pH shift. The release of oocysts from detached biomass may lead to more significant oocyst dispersal and disease transmission in the environment. Therefore, a comprehensive study is needed to better understand

how shear stress variations impact not only attachment, but also detachment and re-attachment, of oocysts to biofilms.

- *C. parvum* oocyst viability and infectivity after the attachment to, and detachment from, biofilms is also of great importance to understand if oocysts attached to biofilms still pose a threat to public health. Thus, a more in-depth study of oocyst viability and infectivity after attachment and detachment is required.

- In environmental biofilms, there can exist a high diversity of microbial species with morphology similar to *C. parvum* oocysts, making it difficult to distinguish *C. parvum* oocysts from the general microbial population. The current study has shown that FIB-SEM and immunogold labeling are appropriate approaches to improving confidence in *C. parvum* oocyst identification. Double labeling (i.e., the simultaneous localization of wall antigens on the oocyst surface with two gold complexes of different gold particle sizes) may be helpful in improving the efficiency of the labeling and may thus permit precise identification of *C. parvum* oocysts attached to environmental biofilms. Efficient immunolabeling will enable future research into the specific interactions between biofilm exopolymeric substances and *C. parvum* oocysts.

REFERENCES

Amann, Rudolf I, Binder, Brian J, Olson, Robert J, Chisholm, Sallie W, Devereux, Richard, & Stahl, David A. (1990). Combination of 16S rRNA-targeted oligonucleotide probes with flow cytometry for analyzing mixed microbial populations. *Applied and environmental microbiology, 56*(6), 1919-1925.

Amirtharajah, Appiah, & O'melia, Charles R. (1990). Coagulation processes: destabilization, mixing, and flocculation. *MCGRAW-HILL, INC.,(USA). 1194*, 1990.

Araujo, Juliana C, Téran, Francisco C, Oliveira, Roberto A, Nour, Edson AA, Montenegro, Martha AP, Campos, José R, & Vazoller, Rosana F. (2003). Comparison of hexamethyldisilazane and critical point drying treatments for SEM analysis of anaerobic biofilms and granular sludge. *Journal of electron microscopy, 52*(4), 429-433.

Azeredo, Joana, Visser, J, & Oliveira, Rosário. (1999). Exopolymers in bacterial adhesion: interpretation in terms of DLVO and XDLVO theories. *Colloids and Surfaces B: Biointerfaces, 14*(1), 141-148.

Babaeyan-Koopaei, K, Ervine, DA, Carling, PA, & Cao, Z. (2002). Velocity and turbulence measurements for two overbank flow events in River Severn. *Journal of Hydraulic Engineering, 128*(10), 891-900.

Bakker, DP, Van der Plaats, A, Verkerke, GJ, Busscher, HJ, & Van der Mei, HC. (2003). Comparison of velocity profiles for different flow chamber designs used in studies of microbial adhesion to surfaces. *Applied and environmental microbiology, 69*(10), 6280-6287.

Battin, Tom J, Kaplan, Louis A, Newbold, J Denis, Cheng, Xianhao, & Hansen, Claude. (2003). Effects of current velocity on the nascent architecture of stream microbial biofilms. *Applied and Environmental Microbiology, 69*(9), 5443-5452.

Bowes, JH, & Cater, CW. (1966). The reaction of glutaraldehyde with proteins and other biological materials*. *Journal of the Royal Microscopical Society, 85*(2), 193-200.

Boyde, Alan, & Franc, Frantisek. (1981). Freeze-drying shrinkage of glutaraldehyde fixed liver. *Journal of microscopy, 122*(1), 75-86.

Braissant, Olivier, Decho, Alan W, Dupraz, Christophe, Glunk, Christina, Przekop, Kristen M, & Visscher, Pieter T. (2007). Exopolymeric substances of sulfate-reducing bacteria: Interactions with calcium at alkaline pH and implication for formation of carbonate minerals. *Geobiology, 5*(4), 401-411.

Braissant, Olivier, Decho, Alan W, Przekop, Kristen M, Gallagher, Kimberley L, Glunk, Christina, Dupraz, Christophe, & Visscher, Pieter T. (2009). Characteristics and turnover of exopolymeric substances in a hypersaline microbial mat. *FEMS microbiology ecology, 67*(2), 293-307.

Bruce, Beau B, Blass, Mitchell A, Blumberg, Henry M, Lennox, Jeffrey L, del Rio, Carlos, & Horsburgh, C Robert. (2000). Risk of *Cryptosporidium* parvum transmission between hospital roommates. *Clinical infectious diseases, 31*(4), 947-950.

Bruner, GW. (2008). River Analysis System Hydraulic reference manual. *Do Defense, Davis*.

Brush, Charles F, Walter, Michael F, Anguish, Lynne J, & Ghiorse, William C. (1998). Influence of pretreatment and experimental conditions on electrophoretic mobility

and hydrophobicity of *Cryptosporidium* parvum oocysts. *Applied and Environmental Microbiology, 64*(11), 4439-4445.

Butkus, Michael A, Bays, J Timothy, & Labare, Michael P. (2003). Influence of surface characteristics on the stability of *Cryptosporidium* parvum oocysts. *Applied and environmental microbiology, 69*(7), 3819-3825.

Characklis, WG. (1990). Biofilms: a basis for an interdisciplinary approach. 3–15. WG Characklis and KC Marshall (ed.) Biofilms: Wiley-Interscience, New York.

Chatterjee, Anirban, Banerjee, Sulagna, Steffen, Martin, O'Connor, Roberta M, Ward, Honorine D, Robbins, Phillips W, & Samuelson, John. (2010). Evidence for mucin-like glycoproteins that tether sporozoites of *Cryptosporidium* parvum to the inner surface of the oocyst wall. *Eukaryotic cell, 9*(1), 84-96.

Chen, Shulin, Ling, Jian, & Blancheton, Jean-Paul. (2006). Nitrification kinetics of biofilm as affected by water quality factors. *Aquacultural engineering, 34*(3), 179-197.

Chénier, Martin R, Beaumier, Danielle, Roy, Réal, Driscoll, Brian T, Lawrence, John R, & Greer, Charles W. (2003). Impact of seasonal variations and nutrient inputs on nitrogen cycling and degradation of hexadecane by replicated river biofilms. *Applied and environmental microbiology, 69*(9), 5170-5177.

Dai, Xiaojun, & Hozalski, Raymond M. (2002). Effect of NOM and biofilm on the removal of *Cryptosporidium* parvum oocysts in rapid filters. *Water Research, 36*(14), 3523-3532.

De Beer, Dirk, Stoodley, Paul, & Lewandowski, Zbigniew. (1996). Liquid flow and mass transport in heterogeneous biofilms. *Water Research, 30*(11), 2761-2765.

De Kerchove, Alexis J, & Elimelech, Menachem. (2008). Calcium and magnesium cations enhance the adhesion of motile and nonmotile Pseudomonas aeruginosa on alginate films. *Langmuir, 24*(7), 3392-3399.

De Paul, Ana L, Torres, Alicia I, Quintar, Amado A, Maldonado, Cristina A, Mukdsi, Jorge H, Petiti, Juan P, & Gutiérrez, Silvina. (2012). *Immunoelectron microscopy: a reliable tool for the analysis of cellular processes*: INTECH Open Access Publisher.

De Waele, M, Renmans, W, Segers, E, Jochmans, K, & Van Camp, B. (1988). Sensitive detection of immunogold-silver staining with darkfield and epi-polarization microscopy. *Journal of Histochemistry & Cytochemistry, 36*(6), 679-683.

DiCesare, EA Wolyniak, Hargreaves, BR, & Jellison, KL. (2012). Biofilm roughness determines *Cryptosporidium* parvum retention in environmental biofilms. *Applied and environmental microbiology, 78*(12), 4187-4193.

Donnelly, JK, & Stentiford, EI. (1997). The *Cryptosporidium* problem in water and food supplies. *LWT-Food Science and Technology, 30*(2), 111-120.

Drozd, C, & Schwartzbrod, J. (1996). Hydrophobic and electrostatic cell surface properties of *Cryptosporidium* parvum. *Applied and Environmental Microbiology, 62*(4), 1227-1232.

Dupraz, Christophe, & Visscher, Pieter T. (2005). Microbial lithification in marine stromatolites and hypersaline mats. *Trends in microbiology, 13*(9), 429-438.

Eberl, HJ, Picioreanu, C, Heijnen, JJ, & Van Loosdrecht, MCM. (2000). A three-dimensional numerical study on the correlation of spatial structure, hydrodynamic

conditions, and mass transfer and conversion in biofilms. *Chemical Engineering Science, 55*(24), 6209-6222.

Eckert, RB. (2015). Emphasis on biofilms can improve mitigation of microbiologically influenced corrosion in oil and gas industry. *Corrosion Engineering, Science and Technology, 50*(3), 163-168.

Ehsan, Amimul, Geurden, Thomas, Casaert, Stijn, Paulussen, Jef, De Coster, Lut, Schoemaker, Toon, . . . Claerebout, Edwin. (2015). Occurrence and potential health risk of *Cryptosporidium* and Giardia in different water catchments in Belgium. *Environmental monitoring and assessment, 187*(2), 1-12.

ERLANDSEN, STANLEY L, MACECHKO, PAUL T, KEULEN, HARRY VAN, & JARROLL, EDWARD L. (1996). Formation of the Giardia cyst wall: studies on extracellular assembly using immunogold labeling and high resolution field emission SEM. *Journal of Eukaryotic Microbiology, 43*(5), 416-430.

Falkentoft, CM, Harremoes, P, & Mosbaek, H. (1999). The significance of zonation in a denitrifying, phosphorus removing biofilm. *Water Research, 33*(15), 3303-3310.

Faulk, W Page, & Taylor, G Malcolm. (1971). Communication to the editors: an immunocolloid method for the electron microscope. *Immunochemistry, 8*(11), 1081-1083.

Fayer, Ronald, Speer, CA, & Dubey, JP. (1990). General biology of *Cryptosporidium*. *Cryptosporidiosis of man and animals.*, 1-29.

Feng, Qian, Xiao, Yubing, Wang, Xiao, Li, Jun, Wu, Yangfang, Xue, Zhaoxia, . . . Oleyiblo, James Oloche. (2015). The influences of shear stress on Extracellular Polymeric Substances of activated sludge. *Desalination and Water Treatment*, 1-8.

Fichtman, Boris, Shaulov, Lihi, & Harel, Amnon. (2013). Imaging metazoan nuclear pore complexes by field emission scanning electron microscopy. *Methods in cell biology, 122*, 41-58.

Finnemore, John E, & Franzini, Joseph B. (2002). *Fluid mechanics*: McGraw-Hill.

Fletcher, Madilyn. (1996). DIVERSITY OF SURFACES AND ADHESION STRATEGIES. *Bacterial adhesion: molecular and ecological diversity, 19*, 1.

Fokoua, Georges, Gabillet, Céline, & Colin, Catherine. (2013). *Experimental study of bubble-drag interaction in a Taylor-Couette flow.* Paper presented at the 8th International Conference on Multiphase Flow (ICMF 2013), Jeju, Korea, May 26-31.

Fonseca, AP, & Sousa, JC. (2007). Effect of shear stress on growth, adhesion and biofilm formation of Pseudomonas aeruginosa with antibiotic-induced morphological changes. *International journal of antimicrobial agents, 30*(3), 236-241.

Gao, Xiaodong, & Chorover, Jon. (2009). In-situ monitoring of *Cryptosporidium* parvum oocyst surface adhesion using ATR-FTIR spectroscopy. *Colloids and Surfaces B: Biointerfaces, 71*(2), 169-176.

Gao, Xiaodong, Metge, David W, Ray, Chittaranjan, Harvey, Ronald W, & Chorover, Jon. (2009). Surface complexation of carboxylate adheres *Cryptosporidium* parvum Oocysts to the hematite− water interface. *Environmental science & technology, 43*(19), 7423-7429.

Gomez-Bautista, M, Ortega-Mora, LM, Tabares, E, Lopez-Rodas, V, & Costas, E. (2000). Detection of infectious *Cryptosporidium* parvum oocysts in mussels (Mytilus

galloprovincialis) and cockles (Cerastoderma edule). *Applied and environmental microbiology, 66*(5), 1866-1870.

Gutièrrez-Mecinas, M, Blasco-Ibáñez, JM, Nàcher, J, Varea, E, Martínez-Guijarro, FJ, & Crespo, C. (2008). Distribution of the A3 subunit of the cyclic nucleotide–gated ion channels in the main olfactory bulb of the rat. *Neuroscience, 153*(4), 1164-1176.

Habimana, Olivier, Meyrand, Mickael, Meylheuc, Thierry, Kulakauskas, Saulius, & Briandet, Romain. (2009). Genetic features of resident biofilms determine attachment of Listeria monocytogenes. *Applied and environmental microbiology, 75*(24), 7814-7821.

Hamilton, Anita. (2012). *The Formation and Characterisation of a Polypyrrole Based Sensor for the Detection of Urea.* National University of Ireland Maynooth.

Harris, J Robin, & Petry, Franz. (1999). *Cryptosporidium* parvum: structural components of the oocyst wall. *The Journal of parasitology*, 839-849.

Heinzmann, U, Reininger, A, Autrata, R, & Höfler, H. (1994). Imaging of immunolabeled membrane receptors in uncoated SEM specimens. *Scanning, 16*(4), 241-245.

Henderson, Francis Martin. (1996). *Open channel flow*: Macmillan.

Hermann, Ren, Walther, Paul, & Müller, M. (1996). Immunogold labeling in scanning electron microscopy. *Histochemistry and cell biology, 106*(1), 31-39.

Heymann, Jurgen AW, Hayles, Mike, Gestmann, Ingo, Giannuzzi, Lucille A, Lich, Ben, & Subramaniam, Sriram. (2006). Site-specific 3D imaging of cells and tissues with a dual beam microscope. *Journal of structural biology, 155*(1), 63-73.

Heymann, Jurgen AW, Shi, Dan, Kim, Sang, Bliss, Donald, Milne, Jacqueline LS, &
Subramaniam, Sriram. (2009). 3D imaging of mammalian cells with ion-abrasion
scanning electron microscopy. *Journal of structural biology, 166*(1), 1-7.

Howsam, P. (1995). A question of scale and slime. *Water and Wastewater Treatment*, 39-
47.

Huang, Z, McLamore, ES, Chuang, HS, Zhang, W, Wereley, Steven, Leon, JLC, &
Banks, MK. (2013). Shear-induced detachment of biofilms from hollow fiber
silicone membranes. *Biotechnology and bioengineering, 110*(2), 525-534.

Imayama, Shintaro, Alfredsson, P Henrik, & Lingwood, Rebecca J. (2014). On the
laminar–turbulent transition of the rotating-disk flow: the role of absolute
instability. *Journal of Fluid Mechanics, 745*, 132-163.

Iriberri, Juan, Ayo, Begoña, Unanue, Marian, Barcina, Isabel, & Egea, Luis. (1993).
Channeling of bacterioplanktonic production toward phagotrophic flagellates and
ciliates under different seasonal conditions in a river. *Microbial ecology, 26*(2),
111-124.

Iyer, Venkatesh Shankar, Majumdar, Udayan, Waskar, Morris, & Dagaonkar, Manoj V.
(2013). Aggregation kinetics of *Cryptosporidium* parvum oocysts. *Journal of
Environmental Chemical Engineering, 1*(3), 504-509.

James, Garth A, Swogger, Ellen, Wolcott, Randall, Secor, Patrick, Sestrich, Jennifer,
Costerton, John W, & Stewart, Philip S. (2008). Biofilms in chronic wounds.
Wound Repair and regeneration, 16(1), 37-44.

Janjaroen, Dao, Liu, Yuanyuan, Kuhlenschmidt, Mark S, Kuhlenschmidt, Theresa B, &
Nguyen, Thanh H. (2010). Role of divalent cations on deposition of

Cryptosporidium parvum oocysts on natural organic matter surfaces.
Environmental science & technology, 44(12), 4519-4524.

Joubert, Lydia-Marie, Ferreira, Jose AG, Stevens, David A, & Cegelski, Lynette. (2015).
Aspergillus fumigatus biofilms: a comparison of processing techniques for
scanning electron microscopy of fungal mycelium and extracellular matrix.
Microscopy and Microanalysis, 21(S3), 935-936.

Jung, Seung Won, Joo, Hyoung Min, Park, Joon Sang, & Lee, Jin Hwan. (2010).
Development of a rapid and effective method for preparing delicate
dinoflagellates for scanning electron microscopy. *Journal of applied phycology,
22*(3), 313-317.

Kalinichev, AG, & Kirkpatrick, RJ. (2007). Molecular dynamics simulation of cationic
complexation with natural organic matter. *European Journal of Soil Science,
58*(4), 909-917.

Karaman, Marilyn E, Pashley, Richard M, Bustamante, Heriberto, & Shanker, S Raj.
(1999). Microelectrophoresis of *Cryptosporidium* parvum oocysts in aqueous
solutions of inorganic and surfactant cations. *Colloids and Surfaces A:
Physicochemical and Engineering Aspects, 146*(1), 217-225.

Kiernan, John Alan. (1999). Histological and histochemical methods: theory and practice.
Shock, 12(6), 479.

Kim, Hyunjung N, Walker, Sharon L, & Bradford, Scott A. (2010). Coupled factors
influencing the transport and retention of *Cryptosporidium* parvum oocysts in
saturated porous media. *water research, 44*(4), 1213-1223.

Konto-Ghiorghi, Yoan, Mairey, Emilie, Mallet, Adeline, Duménil, Guillaume, Caliot, Elise, Trieu-Cuot, Patrick, & Dramsi, Shaynoor. (2009). Dual role for pilus in adherence to epithelial cells and biofilm formation in Streptococcus agalactiae. *PLoS Pathog, 5*(5), e1000422-e1000422.

Kuznar, Zachary A, & Elimelech, Menachem. (2004). Adhesion kinetics of viable *Cryptosporidium* parvum oocysts to quartz surfaces. *Environmental science & technology, 38*(24), 6839-6845.

Lackie, Peter M. (1996). Immunogold silver staining for light microscopy. *Histochemistry and cell biology, 106*(1), 9-17.

Lawrence, JR, Chenier, MR, Roy, R, Beaumier, D, Fortin, N, Swerhone, GDW, . . . Greer, CW. (2004). Microscale and molecular assessment of impacts of nickel, nutrients, and oxygen level on structure and function of river biofilm communities. *Applied and Environmental microbiology, 70*(7), 4326-4339.

Leme, AF Paes, Koo, H, Bellato, CM, Bedi, G, & Cury, JA. (2006). The role of sucrose in cariogenic dental biofilm formation—new insight. *Journal of dental research, 85*(10), 878-887.

Li, Zhaoxu, Lei, Hengyi, & Lou, In Chio. (2012). Combined effects of flow rate and light on characteristics of biofilms grown on three-dimensional elastic carriers. *Desalination and Water Treatment, 45*(1-3), 241-249.

Liu, Yu, & Tay, Joo-Hwa. (2002). The essential role of hydrodynamic shear force in the formation of biofilm and granular sludge. *Water Research, 36*(7), 1653-1665.

Liu, Yuanyuan, Janjaroen, Dao, Kuhlenschmidt, Mark S, Kuhlenschmidt, Theresa B, & Nguyen, Thanh H. (2009). Deposition of *Cryptosporidium* parvum oocysts on

natural organic matter surfaces: microscopic evidence for secondary minimum deposition in a radial stagnation point flow cell. *Langmuir, 25*(3), 1594-1605.

Luo, Xia, Jellison, Kristen L, Huynh, Kevin, & Widmer, Giovanni. (2015). Impact of Bioreactor Environment and Recovery Method on the Profile of Bacterial Populations from Water Distribution Systems. *PloS one, 10*(7), e0133427.

Lynch, RJM, & Ten Cate, JM. (2006). Effect of calcium glycerophosphate on demineralization in an in vitro biofilm model. *Caries research, 40*(2), 142-147.

Mawdsley, Jane L, Bardgett, Richard D, Merry, Roger J, Pain, Brian F, & Theodorou, Michael K. (1995). Pathogens in livestock waste, their potential for movement through soil and environmental pollution. *Applied Soil Ecology, 2*(1), 1-15.

McClaine, Jennifer W, & Ford, Roseanne M. (2002). Reversal of flagellar rotation is important in initial attachment of Escherichia coli to glass in a dynamic system with high-and low-ionic-strength buffers. *Applied and Environmental Microbiology, 68*(3), 1280-1289.

Medema, GJ, Bahar, M, & Schets, FM. (1997). Survival of *Cryptosporidium* parvum, Escherichia coli, faecal enterococci and Clostridium perfringens in river water: influence of temperature and autochthonous microorganisms. *Water Science and Technology, 35*(11), 249-252.

Meinders, JM, & Busscher, HJ. (1995). Influence of interparticle interactions on blocked areas and desorption during particle deposition to glass in a parallel plate flow chamber. *Langmuir, 11*(1), 327-333.

Nation, James L. (1983). A new method using hexamethyldisilazane for preparation of

soft insect tissues for scanning electron microscopy. *Biotechnic & Histochemistry,*

58(6), 347-351.

Nelson, Yarrow M, Lion, Leonard W, Shuler, Michael L, & Ghiorse, William C. (1999).

Lead binding to metal oxide and organic phases of natural aquatic biofilms.

Limnology and Oceanography, 44(7), 1715-1729.

Neu, Thomas R. (1996). Significance of bacterial surface-active compounds in

interaction of bacteria with interfaces. *Microbiological reviews, 60*(1), 151.

Neu, Thomas R, & Marshall, Kevin C. (1990). Bacterial polymers: physicochemical

aspects of their interactions at interfaces. *Journal of biomaterials applications,*

5(2), 107-133.

Newbury, Dale E. (2009). Mistakes encountered during automatic peak identification of

minor and trace constituents in electron-excited energy dispersive X-ray

microanalysisThis article is a US government work and, as such, is in the public

domain in the United States of America. *Scanning, 31*(3), 91.

Nielsen, Per Halkjær, Jahn, Andreas, & Palmgren, Rikke. (1997). Conceptual model for

production and composition of exopolymers in biofilms. *Water Science and*

Technology, 36(1), 11-19.

Orlov, Igor, Schertel, Andreas, Zuber, Guy, Klaholz, Bruno, Drillien, Robert, Weiss,

Etienne, . . . Spehner, Danièle. (2015). Live cell immunogold labelling of RNA

polymerase II. *Scientific reports, 5*.

Osumi, M, Yamada, N, & Nagatani, T. (1988). *High-resolution, low-voltage SEM of cell*

wall regeneration of yeast Schizosaccharomyces pombe protoplasts. Paper

presented at the Proceedings... annual meeting, Electron Microscopy Society of America (USA).

Pereira, Maria Olivia, Kuehn, Martin, Wuertz, Stefan, Neu, Thomas, & Melo, Luis F. (2002). Effect of flow regime on the architecture of a Pseudomonas fluorescens biofilm.

Perloff, Joel R, & Palmer, James N. (2005). Evidence of bacterial biofilms in a rabbit model of sinusitis. *American journal of rhinology, 19*(1), 1-6.

Peyton, Brent M. (1996). Effects of shear stress and substrate loading rate on Pseudomonas aeruginosa biofilm thickness and density. *Water Research, 30*(1), 29-36.

Pietrodangelo, A, Pareti, S, & Perrino, C. (2014). Improved identification of transition metals in airborne aerosols by SEM–EDX combined backscattered and secondary electron microanalysis. *Environmental Science and Pollution Research, 21*(6), 4023-4031.

Porter, Karen G, & Feig, Yvette S. (1980). The use of DAPI for identifying and counting aquatic microflora1. *Limnology and oceanography, 25*(5), 943-948.

Powell, Richard D, Halsey, Carol MR, & Hainfeld, James F. (1998). Combined fluorescent and gold immunoprobes: reagents and methods for correlative light and electron microscopy. *Microscopy research and technique, 42*(1), 2-12.

Priester, John H, Horst, Allison M, Van De Werfhorst, Laurie C, Saleta, José L, Mertes, Leal AK, & Holden, Patricia A. (2007). Enhanced visualization of microbial biofilms by staining and environmental scanning electron microscopy. *Journal of microbiological methods, 68*(3), 577-587.

Purevdorj, B, Costerton, JW, & Stoodley, P. (2002). Influence of hydrodynamics and cell
     signaling on the structure and behavior of Pseudomonas aeruginosa biofilms.
     Applied and environmental microbiology, 68(9), 4457-4464.

Ribot, Miquel, von Schiller, Daniel, Peipoch, Marc, Sabater, Francesc, Grimm, Nancy B,
     & Martí, Eugènia. (2013). Influence of nitrate and ammonium availability on
     uptake kinetics of stream biofilms. *Freshwater Science, 32*(4), 1155-1167.

Rijnaarts, Huub HM, Norde, Willem, Bouwer, Edward J, Lyklema, Johannes, & Zehnder,
     Alexander JB. (1993). Bacterial adhesion under static and dynamic conditions.
     Applied and Environmental Microbiology, 59(10), 3255-3265.

Rijnaarts, Huub HM, Norde, Willem, Bouwer, Edward J, Lyklema, Johannes, & Zehnder,
     Alexander JB. (1995). Reversibility and mechanism of bacterial adhesion.
     Colloids and Surfaces B: Biointerfaces, 4(1), 5-22.

Robertson, LJ, Campbell, AT, & Smith, HV. (1993). Induction of folds or sutures on the
     walls of *Cryptosporidium* parvum oocysts and their importance as a diagnostic
     feature. *Applied and environmental microbiology, 59*(8), 2638-2641.

Rodighiero, Simona, Torre, Bruno, Sogne, Elisa, Ruffilli, Roberta, Cagnoli, Cinzia,
     Francolini, Maura, . . . Falqui, Andrea. (2015). Correlative scanning electron and
     confocal microscopy imaging of labeled cells coated by indium-tin-oxide.
     Microscopy research and technique.

Roefer, Peggy A, Monscvitz, JT, & Rexing, David J. (1996). The Las Vegas.

Rogers, J, & Keevil, CW. (1992). Immunogold and fluorescein immunolabelling of
     Legionella pneumophila within an aquatic biofilm visualized by using episcopic

differential interference contrast microscopy. *Applied and Environmental Microbiology, 58*(7), 2326-2330.

Romaní, Anna M, Borrego, Carles M, Díaz-Villanueva, Verónica, Freixa, Anna, Gich, Frederic, & Ylla, Irene. (2014). Shifts in microbial community structure and function in light-and dark-grown biofilms driven by warming. *Environmental microbiology, 16*(8), 2550-2567.

Ruecker, Norma J, Braithwaite, Shannon L, Topp, Edward, Edge, Thomas, Lapen, David R, Wilkes, Graham, . . . Neumann, Norman F. (2007). Tracking host sources of *Cryptosporidium* spp. in raw water for improved health risk assessment. *Applied and environmental microbiology, 73*(12), 3945-3957.

Samuelson, John, Bushkin, G Guy, Chatterjee, Aparajita, & Robbins, Phillips W. (2013). Strategies to discover the structural components of cyst and oocyst walls. *Eukaryotic cell, 12*(12), 1578-1587.

Schmidt, JEE, & Ahring, Birgitte Kiær. (1994). Extracellular polymers in granular sludge from different upflow anaerobic sludge blanket (UASB) reactors. *Applied Microbiology and Biotechnology, 42*(2-3), 457-462.

Searcy, Kristin E, Packman, Aaron I, Atwill, Edward R, & Harter, Thomas. (2006). Deposition of *Cryptosporidium* oocysts in streambeds. *Applied and environmental microbiology, 72*(3), 1810-1816.

Sedghizadeh, Parish P, Kumar, Satish KS, Gorur, Amita, Schaudinn, Christoph, Shuler, Charles F, & Costerton, J William. (2008). Identification of microbial biofilms in osteonecrosis of the jaws secondary to bisphosphonate therapy. *Journal of Oral and Maxillofacial Surgery, 66*(4), 767-775.

Shiraishi, Fumito, Bissett, Andrew, de Beer, Dirk, Reimer, Andreas, & Arp, Gernot.
(2008). Photosynthesis, respiration and exopolymer calcium-binding in biofilm
calcification (Westerhöfer and Deinschwanger Creek, Germany).
Geomicrobiology Journal, 25(2), 83-94.

Smith, HV. (1992). *Cryptosporidium* and water: a review. *Water and Environment
Journal, 6*(5), 443-451.

SOLTYS, BOHDAN J, & GUPTA, RADHEY S. (1994). Immunoelectron Microscopy of
Giardia lamblia Cytoskeleton Using Antibody to Acetylated α-Tubulin. *Journal of
Eukaryotic Microbiology, 41*(6), 625-632.

Stoodley, P, Cargo, R, Rupp, CJ, Wilson, S, & Klapper, I. (2002). Biofilm material
properties as related to shear-induced deformation and detachment phenomena.
Journal of Industrial Microbiology and Biotechnology, 29(6), 361-367.

Stoodley, Paul, Dodds, I, Boyle, JD, & Lappin-Scott, HM. (1999). Influence of
hydrodynamics and nutrients on biofilm structure. *Journal of applied
microbiology, 85*, 19S-28S.

Sussman, Max, Denyer, SP, & Gorman, SP. (1993). *Microbial biofilms: formation and
control*: Blackwell Scientific Publication.

Sutherland, Ian W. (2001). Biofilm exopolysaccharides: a strong and sticky framework.
Microbiology, 147(1), 3-9.

Suzuki, E. (2002). High-resolution scanning electron microscopy of immunogold-labelled
cells by the use of thin plasma coating of osmium. *Journal of Microscopy, 208*(3),
153-157.

Te Chow, Ven. (1959). Open channel hydraulics.

Teunis, PFM, Medema, GJ, Kruidenier, L, & Havelaar, AH. (1997). Assessment of the risk of infection by *Cryptosporidium* or Giardia in drinking water from a surface water source. *Water Research, 31*(6), 1333-1346.

Thielman, Nathan M, & Guerrant, Richard L. (2004). Acute infectious diarrhea. *New England Journal of Medicine, 350*(1), 38-47.

Tsuneda, Satoshi, Aikawa, Hirotoshi, Hayashi, Hiroshi, Yuasa, Atsushi, & Hirata, Akira. (2003). Extracellular polymeric substances responsible for bacterial adhesion onto solid surface. *FEMS microbiology letters, 223*(2), 287-292.

Tufenkji, Nathalie, Dixon, David R, Considine, Robert, & Drummond, Calum J. (2006). Multi-scale *Cryptosporidium*/sand interactions in water treatment. *Water research, 40*(18), 3315-3331.

Tzipori, Saul, & Griffiths, Jeffrey K. (1998). Natural history and biology of *Cryptosporidium* parvum. *Adv Parasitol, 40*, 5-36.

van Loosdrecht, Mark CM, Lyklema, Johannes, Norde, Willem, & Zehnder, Alexander JB. (1989). Bacterial adhesion: a physicochemical approach. *Microbial Ecology, 17*(1), 1-15.

Van Loosdrecht, MCM, Heijnen, JJ, Eberl, H, Kreft, J, & Picioreanu, C. (2002). Mathematical modelling of biofilm structures. *Antonie van Leeuwenhoek, 81*(1-4), 245-256.

Verkleij, AJ. (1992). Immunogold labeling in cell biology. *Micron and Microscopica Acta, 23*(1), 127-128.

Vunjak-Novakovic, Gordana, Obradovic, Bojana, Martin, Ivan, Bursac, Predrag M, Langer, Robert, & Freed, Lisa E. (1998). Dynamic cell seeding of polymer scaffolds for cartilage tissue engineering. *Biotechnology progress, 14*(2), 193-202.

Walker, James T, Verran, Joanne, Boyd, Robert D, & Percival, Steven. (2001). [16] Microscopy methods to investigate structure of potable water biofilms. *Methods in enzymology, 337*, 243-255.

Walters, Evelyn, Schwarzwälder, Kordula, Rutschmann, Peter, Müller, Elisabeth, & Horn, Harald. (2014). Influence of resuspension on the fate of fecal indicator bacteria in large-scale flumes mimicking an oligotrophic river. *Water research, 48*, 466-477.

Wäsche, Stefan, Horn, Harald, & Hempel, Dietmar C. (2002). Influence of growth conditions on biofilm development and mass transfer at the bulk/biofilm interface. *Water Research, 36*(19), 4775-4784.

Wendt, F. (1933). Turbulent flow between two rotating coaxial cylinders. *Ing. Arch, 4*, 577-595.

Wentland, Eric J, Stewart, Philip S, Huang, Ching-Tsan, & McFeters, Gordon A. (1996). Spatial variations in growth rate within Klebsiellapneumoniae colonies and biofilm. *Biotechnology progress, 12*(3), 316-321.

Wolyniak, EA, Hargreaves, BR, & Jellison, KL. (2009). Retention and release of *Cryptosporidium* parvum oocysts by experimental biofilms composed of a natural stream microbial community. *Applied and environmental microbiology, 75*(13), 4624-4626.

Wolyniak, EA, Hargreaves, BR, & Jellison, KL. (2010). Seasonal retention and release of *Cryptosporidium* parvum oocysts by environmental biofilms in the laboratory. *Applied and environmental microbiology, 76*(4), 1021-1027.

Wu, Jianfeng, & Xi, Chuanwu. (2009). Evaluation of different methods for extracting extracellular DNA from the biofilm matrix. *Applied and environmental microbiology, 75*(16), 5390-5395.

Ylla, Irene, Borrego, Carles, Romaní, Anna M, & Sabater, Sergi. (2009). Availability of glucose and light modulates the structure and function of a microbial biofilm. *FEMS microbiology ecology, 69*(1), 27-42.

Yuan, Baoling, Pham, Mai, & Nguyen, Thanh H. (2008). Deposition kinetics of bacteriophage MS2 on a silica surface coated with natural organic matter in a radial stagnation point flow cell. *Environmental science & technology, 42*(20), 7628-7633.

Yun, Mi-Ae, Yeon, Kyung-Min, Park, Jong-Sang, Lee, Chung-Hak, Chun, Jongsik, & Lim, Dong Joon. (2006). Characterization of biofilm structure and its effect on membrane permeability in MBR for dye wastewater treatment. *Water research, 40*(1), 45-52.

Zobell, Claude E. (1943). The effect of solid surfaces upon bacterial activity. *Journal of bacteriology, 46*(1), 39.

Xia Luo, Ph.D.

Mobile: 610-762-8693

E-mail: xil410@lehigh.edu; 411427792@qq.com

Add: Department of Civil & Environmental Engineering

Lehigh University

1 West Packer Avenue

Bethlehem, PA, 18015

Basic Information

- Place of birth   Qujing, Yunnan Province, China
- Date of birth   January 3rd, 1986
- Name of parents   Father   Yongqing Luo
                                      Mother   Xiuzhen Miao

Education Background

- 08/2010-12/2015   Ph.D. in Environmental Engineering from ***Lehigh University***, PA, US

    Dissertation: Characterization of *Cryptosporidium parvum* oocyst attachment to environmental biofilm surfaces
    Advisor: Dr. Kristen L. Jellison
    Co-advisor: Dr. Sabrina Jedlicka
- 09/2005-07/2009 B.Sc. in Environmental Science from ***Qingdao University of Science & Technology,*** Qingdao, Shandong Province, China

Research Interests

- Waterborne pathogen removal for water and wastewater treatment
- Biofiltration and biofilm systems for drinking water treatment, disinfection, and drinking water distribution systems
- Fate and transport of antibiotic resistant bacteria in surface environment and watershed

Professional Experience

- 08/2010 – 12/2015   Research Assistant in *Lehigh University*
  - Biomimetic Biofilm Surfaces for in-situ Detection of Waterborne Contaminants
    - Characterization of biofilm surfaces to identify kinetic mechanisms and specific parameters necessary for *Cryptosporidium* adhesion via both biological and materials science analytical tools
    - Localization of *Cryptosporidium parvum* oocyst by immunolabeling technique
  - Assessing Performance of Biofilm Sampling Approaches
    - Evaluating the similarity of biofilm grows in rotating annular bioreactor and water distribution systems of two utilities (Department of Water and Sewer Resources in Bethlehem, PA, USA & Golden state Water Company in California, CA, USA)
    - Comparing the recovery of two bacterial indicators (*E. coli*, *Mycobacterium smegmatis*) from the reactor biofilms sampled by bead beating, scraping, sonication, and stomaching.
    - Identifying whether biofilms sampled from more easily accessible locations in the distribution system can represent biofilms growing in water mains.
    - Providing utilities with optimum protocols for sampling biofilms from surface with the best possible recovery of biofilm-associated microorganisms.
    - Establishing clear biofilm sampling guidelines
    - Evaluating the interaction of bacteria with biofilm
  - Investigation into the Effects of Manufacturing Variables on the Microbiological Efficiency of Ceramic Pot Filter Material

- - Evaluated the influence of production variables (burn-out material, burn-out material processing, filter mixture ratio as well as clay)on flow rate, microbiological removal efficiency (LRV & Percentage of removal), pH and porosity
    - Provided recommendation for consistent production and quality control for filter manufacturing

- 08/2012 – 05/2015   Teaching Assistant in *Lehigh University*
    - Assisted in teaching 1 undergraduate course sizes of up to 80 students for two years (i.e., 2014 - 2015). Topic: <u>Introduction to Environmental Engineering</u>
    - Assisted in teaching 2 graduate level courses ranging in size from 30 - 40 students. Topics included: <u>Modeling Flow and Contaminant Transport in Water</u>, and <u>Water & Wastewater Treatment Facilities</u>
    - Assisted in teaching Introduction to Engineering Practice for the Southeast University (SEU) faculty members from China for 4 years. Topic: <u>Safe Drinking Water for Developing Countries</u>
    - Prepared course materials including laboratory experiments and homework
    - Led weekly laboratory for groups of 20 - 30 students
    - Supervised students in homework, graded exams and weekly quizzes

Awards & Honors

- 01/2014   The Dean's Scholarship of Lehigh University
- 06/2013   The Pennsylvania Water Environment Association (PWEA) Student Research Award
- 06/2012   The P.C. Rossin Doctoral Fellowship of Lehigh University
- 07/2009   Excellent Graduation Design of Qingdao University of Science and Technology
- 10/2008   The Culture & Sports Excellent Award, Social Practice Award
- 09/2007   The Second Place of "Safe Campus" Cartoon Contest
- 06/2007   Outstanding Student of Qingdao University of Science and Technology
- 2005 - 2007 The Third Class Scholarship of Qingdao University of Science and Technology

Research Skills

- Laboratory skills:
    - Bacteriology: Maintain and purify bacteria and cell culture, growth and maintenance of cell lines
    - Biochemistry/Genetics: Infectivity assay
    - Molecular techniques: Polymerase chain reaction (PCR), gel electrophoresis, Fluorescence in-situ hybridization (FISH), immunomagnetic separation (IMS), immunofluorescence assay (IFA), immunogold labeling
    - Spectrophotometers: UV, atomic absorption, FTIR , LEIS
    - Column: ion exchange resins, HPLC
    - Water quality analysis: pH, conductivity, alkalinity, hardness, TOC, TN, nutrients (NO_3^--N, NH_3-N,NO_2^--N, P), inorganic elements, BOD_5, COD_{Cr}
- Microscopy: Atomic Force Microscopy (AFM), Optical Microscopy, Scanning Confocal Laser Microscopy (SCLM), Scanning Electron Microscopy (SEM) (including Variable pressure (VP)-SEM and Environmental SEM), Transmission Electron Microscopy (TEM), and Focused Ion Beam - Scanning Electron Microscopy (FIB - SEM)
- Basic computer software: Microsoft excel, Microsoft word, End Note, Power Point, Adobe Acrobat, Adobe Photoshop
- Specialized software: SPSS, Image J, COMSTAT, LSM 510 Image Browser (image analysis software for SCLM), Matlab
- Language: Fluency in English. Have a reasonable understanding of Spanish
- Interests: Traveled through the United States; squash ball; traditional Chinese painting and calligraphy; musical instruments (Ba Wu and Cucurbit Flute etc.)

Journal Publications

1. **Luo, X.**, Jellison, K. L., Huynh, K., & Widmer, G. (2015). Impact of Bioreactor Environment and Recovery Method on the Profile of Bacterial Populations from Water Distribution Systems. *PloS one*, *10*(7), e0133427. (IF = 3.70)
2. **Luo, X.**, Jedlicka S., & Jellison, K. L. (under review). Pseudo-second Order Calcium-mediated *Cryptosporidium* parvum oocyst Attachment to Environmental Biofilms.

3. **<u>Luo, X.</u>**, Jedlicka S., & Jellison, K. L. (under review). Role of Wall Shear Stress on *Cryptosporidium* parvum oocyst Adhesion Kinetics to Environmental Biofilms.
4. Rayner J., **<u>Luo, X.</u>**, Schubert, J., Lennon, P., Jellison, K. L., & Lantagne, D. (under review). The Effects of Manufacturing Variables on Ceramic Water Filter Efficiency for Drinking Water Treatment in Developing Countries.

Conferences

1. **<u>Luo, X.</u>**, Jedlicka S., & Jellison, K. L., (2015). Role of shear stress on *Cryptosporidium* parvum oocyst attachment to environmental biofilms. New England Graduate Student Water Symposium annual conference, MA, US.
2. **<u>Luo, X.</u>**, Huynh, K., Widmer, G., & Jellison, K. L., (2014). Comparing the Performance of Four Sampling Approaches for Recovering Escherichia coli and Mycobacterium smegmatis from Drinking Water Biofilms. The Pennsylvania Section of the American Water Works Association (AWWA) annual conference, PA, US.
3. **<u>Luo, X.</u>**, Jellison, K. L., & Widmer, G. (2013). Evaluation of Formation and Recovery of Biofilms in Drinking Water Distribution Systems. Pennsylvania Water Environment Association (PWEA) annual conference, PA, US.